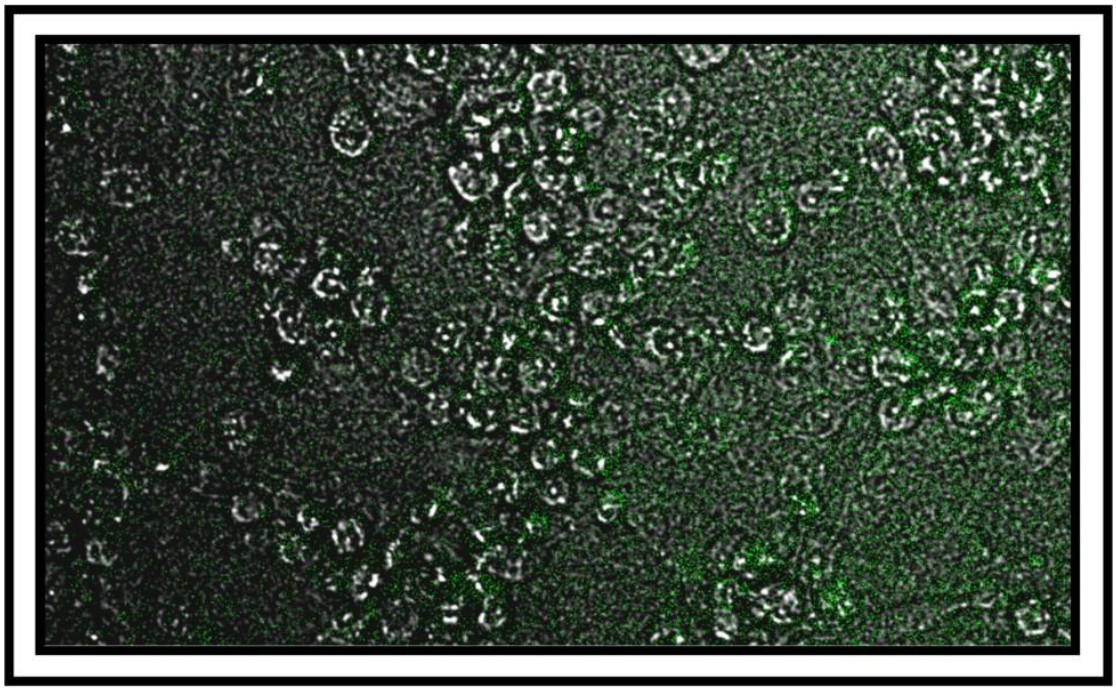

# Optimizing Polymeric Nanoparticle-Based mRNA Gene Delivery Materials

## Aiming to Control Cellular Glycosylation

Master thesis report in Biotechnology

Yifan Gu

DEPARTMENT OF LIFE SCIENCES—

CHALMERS UNIVERSITY OF TECHNOLOGY
Gothenburg, Sweden 2025
www.chalmers.se

MASTER THESIS REPORT 2025

# Polymeric Nanoparticle-Based mRNA Gene Delivery Materials

Yifan Gu


CHALMERS
UNIVERSITY OF TECHNOLOGY

Department of Life Sciences
Stubelius Lab
CHALMERS UNIVERSITY OF TECHNOLOGY
Gothenburg, Sweden 2025

Optimizing Polymeric Nanoparticle-Based mRNA Gene Delivery Materials- Aiming to Control Cellular Glycosylation

YIFAN GU



Supervisor: Alexandra Stubelius, Department of Life Sciences; Gaurav Goyal, CEO of Nanolyze AB
Examiner: Alexandra Stubelius, Department of Life Sciences

Master thesis report 2025
Department of Life Sciences
Chalmers University of Technology
SE-412 96 Gothenburg
Sweden
Telephone +46 31 772 1000

Cover: GFP expression in macrophage incubated with GFP loaded PAMAM under confocal microscopy

Typeset in LaTeX
Gothenburg, Sweden 2025

Optimizing Polymeric Nanoparticle-Based mRNA Gene Delivery Materials- Aiming to Control Cellular Glycosylation

YIFAN GU
Department of Life Sciences
Chalmers University of Technology

# Abstract

The ability to modulate cellular glycosylation through gene expression holds significant promise for advancing immunotherapies and precision medicine. In this thesis, we developed and optimized poly(lactic-co-glycolic acid) (PLGA)-based nanoparticles for mRNA delivery, aiming to establish a biocompatible platform for targeted glycosylation control. Messenger RNA was first condensed using poly(amidoamine) (PAMAM) dendrimers and then encapsulated into PLGA nanoparticles (NPs) using a modified double emulsion technique. The resulting mRNA-loaded NPs exhibited sizes ranging from 160–220 nm with favorable positive surface charge, and mRNA/PAMAM cargo loading of 20% regardless of the mRNA type. Confocal imaging confirmed successful intracellular delivery and protein expression in macrophage cells, while in vitro experiments indicated improved protection of mRNA from degradation and enhanced transfection stability compared to mRNA/PAMAM complexes alone. Collectively, this work presents a robust and scalable polymeric platform for mRNA delivery and demonstrates its potential in immune targeted applications. These findings offer a promising basis for future efforts to regulate glycosylation pathways via mRNA delivery.

Keywords: Nanoparticles, mRNA, Gene delivery, PLGA, PAMAM, Emulsion, Protein Corona.

# Acknowledgements

I'd like to thank my supervisor Prof. Dr. Alexandra Stubelius and Dr. Gaurav Goyal for providing me the opportunity to get involved in research and for their guidance and supervision. I also want to thank Dr. Ratish Nair for his help in chemical synthesis and suggestions in the project; thank Fan Jia and Loise Råberg for their help in cell culture and confocal microscopy; thank Hanna Mårtensson for her help in gel electrophoresis and giving me mRNA; thank Hamza Yakubu and Hugo Barbosa for supportive information. And thank every collegue working in Chalmers who helped me.

Yifan Gu, Gothenburg, 06-2025

# Contents

# List of Figures

# List of Tables

# 1 Introduction

## 1.1 Background

Messenger RNA (mRNA) serves as the intermediary molecule that conveys genetic information from DNA to ribosomes, directing protein synthesis. Over the past few decades, mRNA has emerged as a promising therapeutic agent due to its ability to induce the expression of functional proteins. Therapeutic applications include: (1) altering cellular behavior by expressing growth factors, and (2) initiating immune responses by encoding immune-stimulating proteins [2]. Compared to DNA-based therapies, mRNA therapy offers greater genetic safety, as it avoids the risk of genomic integration[3]. Moreover, since mRNA functions directly in the cytosol, it can be used to express virtually any protein inside the cell, broadening its application in fields such as immunotherapy [4].

Despite its potential, mRNA-based genetic therapy faces significant challenges due to the intrinsic properties of mRNA: (1) Size — Naked mRNA molecules are small enough (hydrodynamic diameter < 5.5 nm) to be rapidly filtered and eliminated by the kidneys [5]. (2) Negative charge — mRNA is highly negatively charged, which causes electrostatic repulsion from the negatively charged cell membrane (-40 to -80 mV), hindering cellular uptake [6]. (3) Instability — As a single-stranded nucleic acid, mRNA is highly susceptible to degradation by extracellular ribonucleases abundant in the bloodstream [7][8].

To overcome these limitations, cationic (amine-containing) biomaterials have been developed to serve as delivery carriers. These materials protect mRNA from degradation, facilitate cellular uptake by neutralizing electrostatic repulsion, and enable intracellular release. Various platforms have been explored, including lipid nanoparticles (LNPs), protamine-based NPs, and cationic polymeric NPs. Among them, LNPs are the most established and widely used. Following the protocol by McKenzie et al., LNPs can achieve particle sizes around 100 nm and high mRNA loading efficiencies ( 90%) [9]. However, their clinical translation has been limited by the toxicity of their starting materials [10]. Additionally, ester groups in LNPs can lead to premature degradation in certain tissues, compromising both delivery efficiency and protein expression [11].

Protamine, a naturally occurring cationic protein, demonstrates strong mRNA condensation and has shown enhanced transfection efficiency. Nevertheless, it may induce severe immune responses upon partial degradation [12]. On the other hand, polymer-based NPs, such as dendrimers, polyethylenimine (PEI), and chitosan-

coated PLGA, also feature high amine content, which often results in poor biocompatibility. Despite this drawback, their tunable surface chemistry presents an opportunity for improving biocompatibility, offering significant potential for safe and effective mRNA delivery.

Another critical factor influencing the success of nanoparticle-based mRNA delivery is the formation of a protein corona (PC) during systemic circulation. The PC can drastically alter the physicochemical properties of NPs, impacting their biodistribution, cellular uptake, and therapeutic efficacy. For instance, opsonization, where serum proteins adsorb onto the NP surface, can mask targeting ligands and reduce the effectiveness of targeted delivery strategies [13]. Understanding and controlling PC formation is thus essential for advancing the safety and precision of nanoparticle-based gene therapies.

## 1.2 Aim of the study

This project aims to utilize PLGA as a carrier for mRNA gene delivery and explore two NP formulation methods (nanoprecipitation and double emulsion) to achieve immune cell-targeted particle sizes and optimal drug encapsulation. To enhance NP functionality, surface modifications are to investigate by using PEG, PEI, and mPEG-PEI, where PEGylation extending systemic circulation time and PEI providing a positive surface charge to promote immune cell uptake. In the long term, the project seeks to enable controlled modulation of cellular glycosylation and deepen our understanding of PC formation in diverse biological microenviron- ments.

## 1.3 Goals

To protect mRNA from enzymatic degradation, PAMAM dendrimer-based condensation was employed. Various PLGA formulation techniques, such as nanoprecipitation and double emulsion, were evaluated for their ability to encapsulate PAMAM and reduce its cytotoxicity. The targeted particle sizes for effective delivery are approximately 10 nm for mRNA–dendrimer complexes and 170 nm for dendrimer-loaded PLGA NPs.

Following formulation, the NPs were assessed for biocompatibility, gene delivery efficiency, and interactions with serum proteins, which influence biological behavior and targeting capacity.

The long-term objective is to use these NPs for the delivery of ST6Gal I mRNA into immune cells. Upon expression, ST6Gal I will promote $\alpha$2-6 sialylation on the surface of $CD4^+$ T cells, thereby enhancing their activation and inducing the release of proinflammatory cytokines.

## 1.4 Limitations

Despite the promising results, several limitations remain in this study. First, the size

of cargo-loaded NPs could be further reduced to improve cellular uptake and tissue penetration. The mRNA loading efficiency also requires enhancement to increase therapeutic efficacy. Additionally, more precise quantification methods are needed to accurately determine the amount of mRNA encapsulated within the NPs (e.g. $^{31}P$ NMR). The mRNA release profile was not comprehensively characterized, limiting understanding of intracellular release dynamics. The resolution of confocal microscopy was insufficient to fully visualize subcellular localization and distribution. Moreover, the interactions between NPs and a broader range of serum proteins (e.g., fibrinogen, glycoproteins) were not explored, which may affect circulation time, biodistribution, and immune recognition in vivo. And the primary goal of the thesis, visualizing protein adsorption onto NPs by using the nanolyze system, was unable to be achieved due to instrument technical issues. Lastly, due to the time limitation, the long term goal of modulating cellular glycosylation was not reached.

# 2

# Theory

## 2.1 mRNA gene delivery

mRNA can rapidly induce protein expression as long as it is delivered into the cytoplasm, without requiring integration into the host genome. This eliminates the risk of insertional mutagenesis and reduces off-target effects, making mRNA a safer alternative to DNA-based therapies. As a result, mRNA has found broad applications in vaccines and cancer immunotherapy [14].

However, several barriers must be overcome for mRNA therapies to become clinically viable. Due to its single-stranded structure, mRNA is highly susceptible to degradation by extracellular nucleases. Additionally, the strong electrostatic repulsion between the negatively charged mRNA and the negatively charged cell membrane hinders cellular uptake [14]. Naked mRNA is also rapidly cleared by renal filtration, further limiting its therapeutic efficacy.

To address these challenges, various cationic biomaterials have been developed to enhance mRNA delivery, including LNPs, protamine-based NPs, and polymeric NPs. While these systems may offer advantages such as efficient mRNA condensation, favorable particle size, or improved delivery efficiency, their high content of amine groups often leads to cytotoxicity and poor biocompatibility. This has posed a significant hurdle to the development of safe and effective nanoparticle-based mRNA delivery systems. Nevertheless, the structural tunability of polymeric NPs offers a potential path to improved biocompatibility, making them a promising platform for mRNA delivery.

For example, Bae et al. designed a PAMAM dendrimer modified with ornithine to deliver mRNA encoding apoptin, achieving mRNA loading but resulting in relatively large particles (300–500 nm) [15]. Similarly, Joubert's group developed positively charged mRNA–PAMAM dendriplexes that improved cellular uptake and protected mRNA from degradation [16]. However, these dendriplexes still require further optimization, as their delivery and transfection efficiencies re- main suboptimal. Moreover, their performance is significantly impaired in the pres- ence of serum, which limits their applicability in vivo.

One potential strategy to address these issues is to encapsulate or embed the dendriplex within a larger NP to better control size and surface properties. Among polymeric carriers, PEI [17] and PLGA [18] have been widely explored for gene delivery. PEI has been extensively studied due to its strong mRNA condensation and delivery efficiency [19, 20]. However, high-molecular-weight PEI is highly

cytotoxic, and modifications, suchas PEGylation, or conjugation with amino acids or targeting ligands, are often required to mitigate toxicity [21]. In contrast, PLGA offers superior biocompatibility, biodegradability, and ease of formulation, making it an attractive alternative for mRNA delivery [18].

### 2.1.1 Modifying glycosylation as a new target for mRNA delivery

Glycans are carbonhydrates formed by few or many monosaccharides, such as iduronic acid (IdoA), mannose (Man), glucuronic acid (GlcA), xylose (Xyl), fucose (Fuc), N-acetylgalactosamine (GalNAc), N-acetylglucosamine (GlcNAc), glucose (Glc), galactose (Gal) and sialic acid (Neu5Ac)[22]. Glycoproteins are proteins containing oligosaccharide (sugar) chains that covalently bind to specific amino acid residues on proteins. This process is conducted by a post-translational modification (PTM) named glycosylation. Glycans and glycoproteins play essential roles in selectin-glycan interaction that regulates NP-cell interaction, cell adhesion and immune response[22][23]. For example, the Siglecs (sialic acid-binding immunoglobulin-like lectins) are essential glycoproteins on surface of immune cells. They bind to sialic acid-containing glycans, followed by regulating innate and adaptive immune responses. Also, the Siglecs were reported highly associated to immune evasion by altering glycosylation[23]. Besides immune response, glycosylation has impact on stability of NPs and NP-cell interaction. Wan et.al confirmed that cell adhesion and internalization of NPs were improved after removing the glycans from proteins adsorbed on the surface of NPs[24]. And glycosylation applied on the NP surface proteins can prolong NP circulation time and enhance antitumor efficacy [25].

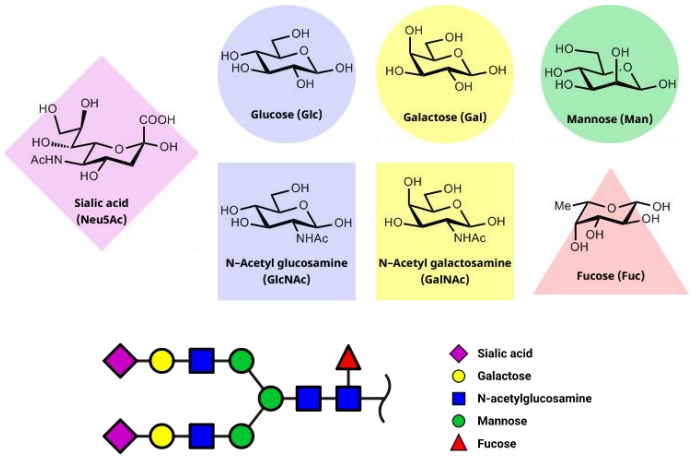


**Figure 2.1:** The structures of glycans and glycan constituents

## 2.2 Material choice

### 2.2.1 PLGA

Poly(lactic-co-glycolic acid) (PLGA), a copolymer of D,L-lactic acid and glycolic acid, has demonstrated great potential in targeted, precise drug delivery therapies due to its favorable biocompatibility, mechanical strength, and versatile surface

functionalization capabilities. Moreover, the half-life and biodegradability of PLGA can be tuned by adjusting its molecular weight or the lactic-to-glycolic acid ratio.[26]

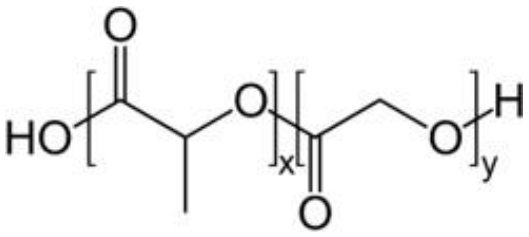


**Figure 2.2:** PLGA structure

### 2.2.2 PEI and PEGylation

Polyethylenimine (PEI) is a synthetic polymer widely used for nucleic acid condensation and transfection due to its high cationic charge density.[27] However, cytotoxicity, as well as transfection efficiency, of PEI is highly related to molecular weight and molecular structure; branched PEI with larger molecular weight has higher transfection efficiency but also increased cytotoxicity.[28] It was reported that PEGylation would improve its biocompatibility by reducing the concentration of amino groups. [29]

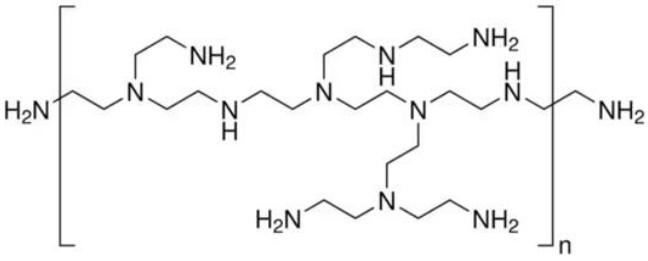


**Figure 2.3:** PEI structure

In this project, we conducted PEGylation on branched PEI with high molecular weight to not only reduce its cytotoxicity but also to improve the colloidal stability of the NPs during formulation.

### 2.2.3 The cargo – mRNA-PAMAM

Poly(amidoamine) (PAMAM) is a hyperbranched polymer composed of an ethylenediamine core and repetitive internal amidoamine branching units. Its numerous terminal amine groups confer a high cationic charge density and offer versatile sites for functionalization. PAMAM exists in multiple generations (G0 to G10), with higher generations exhibiting increased molecular weight and a greater number of surface amine groups. While commonly employed in nucleic acid condensation, higher generation of PAMAM tends to exhibit increased cytotoxicity and reduced circulation time due to the abundance of primary amines. Additionally, the cell viability of macrophage when incubated with PAMAM reveals significant PAMAM concentration dependence: higher concentration of PAMAM leads to lower cell

viability[30]. The cytotoxicity of PAMAM to macrophages can be explained that the interaction between positively charged PAMAM and negatively charged cell membrane leads to formation of nanopores on cell membrane, resulting in leakage and cell death [31]. Thus, strategies such as surface modification or encapsulation are often necessary to mitigate cytotoxicity.

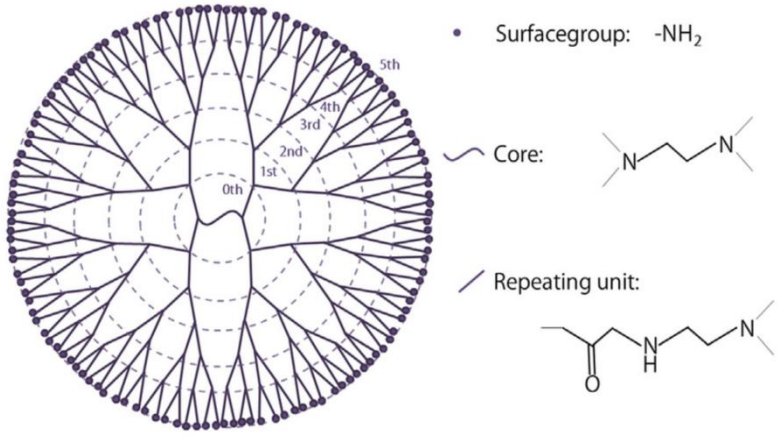


**Figure 2.4:** PAMAM G5 structure.[78]

PAMAM dendrimers have been widely reported for their excellent DNA and RNA condensation capabilities and have been applied in various therapeutic contexts [32][33][34][15]. For example, Rajasekaran et.al. developed PEGylated PAMAM to condense and deliver siRNA that encoded for astrocyte elevated gene-1 (AEG-1) and all-trans retinoic acid (ATRA) for treatment of hepatocellular carcinoma [33]. Bae et.al. modified PAMAM with Ornithine to incorporate apoptin-coded RNA to induce cell death [15]. Li et.al. coated PAMAM with anti-EGFR (epidermal growth factor receptor) antibody to achieve tumor cell targeting, after DNA condensation [32]. In another study, PAMAM polymers of various generations were surface-modified to enhance fusogenic properties and reduce toxicity while preserving mRNA condensation capacity [35]. However, all these systems resulted in complexes with sizes ranging from 200 nm to 300 nm, which are suboptimal for efficient delivery to immune cells due to limited cellular uptake and tissue penetration.

In this project, we employed PAMAM G5 to condense and protect mRNA (Poly-A, mCherry and GFP). To control the particle size, we replaced traditional bulk mixing and incubation with a stirring-assisted method during formulation, which produced mRNA/PAMAM complexes ranging from 6–10 nm. These condensed complexes were then encapsulated into PLGA NPs using a double emulsion technique.

## 2.3 Nanoparticle synthesis

### 2.3.1 Nanoprecipitation

Nanoprecipitation has been a widely used method for loading hydrophobic drug molecules since its introduction in 1989. The process consists of four main steps: polymer supersaturation, nucleation, nuclei growth, and coagulation. When a polymer solution in an organic solvent is introduced into an aqueous phase, the diffusion

of the organic solvent into the water induces polymer supersaturation and the formation of nuclei. These primary nuclei continue to grow until thermodynamic stability is reached. Beyond this point, further increases in particle size occur primarily through collision-induced coagulation.[36]

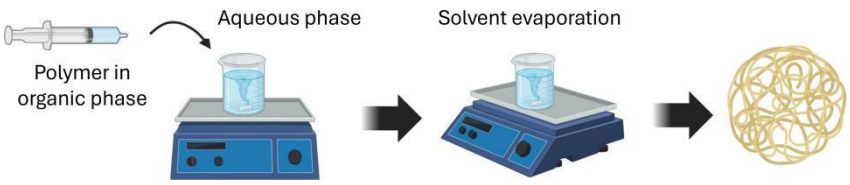


**Figure 2.5:** General diagram for nanoprecipitation formulation. (made in Biorender)

Several formulation parameters influence NP sizes, including the choice of organic solvent, ionic strength of the aqueous phase, polymer concentration, injection rate of the organic phase, agitation rate of the aqueous phase, temperature, and solvent evaporation conditions. Huang et.al. and Hernández-Giottonini et.al. had demonstrated that only solvent evaporation, polymer concentration, the type of organic solvent, and ionic strength were found to significantly affect the size of the resulting NPs.[37][38] Notably, all four factors are linked to a single critical parameter; the diffusion coefficient of the organic solvent in water. A high salt concentration, high polymer concentration, and use of a solvent with a low diffusion coefficient collectively lead to a lower overall diffusion rate of the organic phase, ultimately resulting in larger NPs.[37]

### 2.3.2 Single and double emulsion

In contrast to nanoprecipitation, O/W emulsion technique can enhance the encapsulation efficiency of hydrophilic molecules into PLGA NPs. The steps of emulsion are seen in Figure 2.6 – emulsifying a polymer solution in an organic solvent with an aqueous surfactant solution using sonication, followed by solvent evaporation. To produce smaller NPs, Mainardes et.al. optimized the formulation conditions, such as using lower polymer concentrations, higher surfactant concentrations, increased sonication power, extended sonication time, and accelerated solvent evaporation.[39] These factors collectively facilitate better dispersion of the polymer phase into the aqueous phase and improve colloidal stability. Specifically, a lower polymer concentration reduces the viscosity of the organic phase, allowing for finer droplet formation. Higher surfactant concentrations stabilize the emulsion through hydrogen bonding, reducing droplet coalescence. Rapid solvent evaporation further aids in solidifying NPs before droplet collapse or aggregation occurs.[40][41][39]

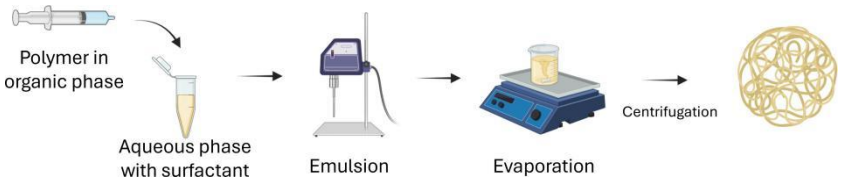


**Figure 2.6:** General diagram for emulsion formulation. (made in Biorender)

In the double emulsion technique, the final NP size is primarily determined by the droplet size in the primary emulsion and the concentration of the encapsulated hydrophilic drug. Notably, the factors that control particle size in single emulsions apply to both emulsification steps in the double emulsion method. Therefore, to obtain small PLGA NPs, a lower polymer concentration is recommended, as it reduces organic phase viscosity and promotes effective dispersion of the inter- nal aqueous phase into the organic phase. Additionally, studies have shown that using a lower drug concentration in the internal aqueous phase leads to improved encapsulation efficiency, narrower particle size distribution (PDI), and smaller over- all particle size. This is attributed to a reduced osmotic pressure gradient, which minimizes droplet rupture and exchange between the internal and external aqueous phases.[42][43][44]

## 2.4 Protein corona

NPs are exposed to multiple blood cells and serum proteins when they circulating in bloodstream[1]. The PC is a layer of proteins adsorbed onto the surface of NPs when the particles are applied in drug delivery. Albumin is the most abundant protein in serum, while fibrinogen and immunoglobulins are in low concentration[45][46]. With these proteins adsorbed onto a NP surface, the size and surface charge of the NP will be affected, followed by altering of NP internalization, circulation time and NP-cell interaction[1]. For example, Monopoli et.al found that binding of fibrinogen triggers phagocytosis clearing NPs from bloodstream, while binding with albumin helps NPs obtain prolonged circulation time[47]. Additionally, Fleischer et.al confirmed that after protein binding, cationic NPs obtained negative surface charge and anionic NPs became less negative. And different binding sites on protein were used in cationic and anionic NPs, which accordingly had positive and negative impact on cellular binding and internalization of NPs[1].

In the formation of PCs, the Vroman effect plays an essential role: the proteins in low-concentration but with higher affinity to NP will replace part of those proteins in higher amount but having lower affinity to NP. Therefore, albumin has been reported dominant in PCs on NPs, while fibrinogen and immunoglobulins have also been observed on the surface of NPs[47]. The balance between kinetic and thermodynamic makes the PC divided into hard corona (HC, which binds to NP surface tightly) and soft corona (SC, which loosely binds to NP or protein in HC)[48]. Additionally, it is reported that the PC formation might depend on temperature, NP-PC contacting time, NP's size, charge and stability, together with protein types and properties[49].

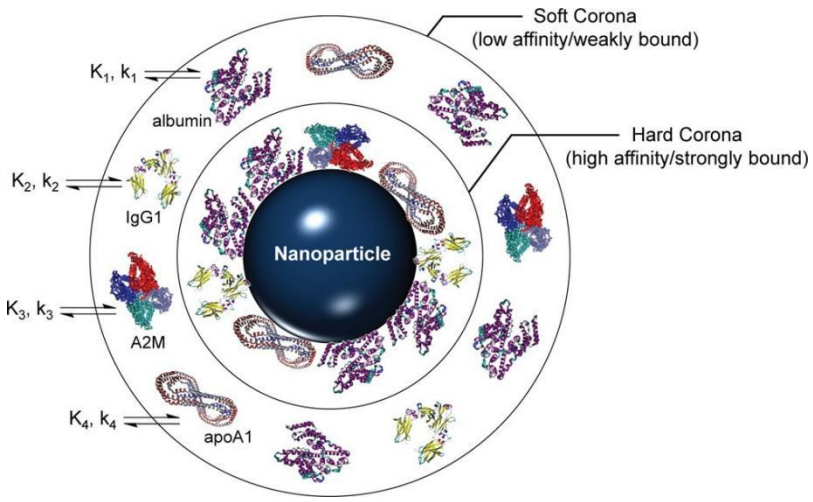


**Figure 2.7:** Hard corona (HC) and soft (SC) corona formed on the surface of NPs[1]

Currently, the instruments used and methods employed for investigating NP-PC interactions are indirect: centrifugation has been used to seperate PC from NP, followed by gel electrophoresis or size exclusion chromatography (SEC) to determine protein types after measuring molecular weight and size[1][48][46]. The adsorption kinetic and binding affinity were investigated via fluorescence correlation spectroscopy (FCS) which requires a fluorescent label, isothermal titration calorimetry (ITC) which destroys the sample by heating, or surface plasmon resonance (SPR) in which special sensor chips with gold surface and NP-surface linkage are required [48]. Recently, new analytical technologies are developed such as Evanescent Field Sensing (Nanolyze system) which brings together microscopy and scattering light detection. With the scattering light intensity captured in microscopy, it allows analysis of NP-PC interaction in label-free and on a single-particle level.

## 2.5 Particle analysis

### 2.5.1 Dynamic light scattering (DLS)

Dynamic Light Scattering (DLS) is a technique used to measure the size distribution of small particles in suspension or polymers in solution. It works by illuminating the sample with a laser and detecting the scattering of light caused by the Brownian motion of particles. As the particles move, the intensity of scattered light fluctuates over time. These fluctuations are analyzed to determine the diffusion coefficient of the particles. Using the Stokes–Einstein equation, the diffusion coefficient is then converted into a hydrodynamic diameter, which reflects the hydrodynamic particle size [50].

### 2.5.2 Fourier Transform Infrared Spectroscopy (FTIR)

Fourier Transform Infrared Spectroscopy (FTIR) is an non-destructive analytical technique used to identify functional groups and molecular structures based on

their vibrational transitions. When infrared (IR) light passes through a sample, specific wavelengths are absorbed by the sample's molecules, causing them to vibrate (stretching, bending, etc.). Each type of chemical bond absorbs IR radiation at characteristic frequencies, producing a unique absorption spectrum. FTIR measures the intensity of transmitted or reflected IR light as a function of wavelength, creating a spectrum that acts like a molecular fingerprint [51].

### 2.5.3 Proton Nuclear Magnetic Resonance ($^1$H NMR)

Proton Nuclear Magnetic Resonance ($^1$H NMR) spectroscopy is a technique used to determine the structure and environment of hydrogen atoms in a molecule. It works by placing a sample in a strong magnetic field, which causes the nuclei of hydrogen atoms (protons) to align with or against the field. When exposed to a specific radiofrequency, these protons absorb energy and flip their spin states. The absorbed energy is detected and translated into a spectrum, where each peak corresponds to a distinct hydrogen environment. The position of the peaks (chemical shift) reveals information about the electronic surroundings of each proton, while the splitting patterns (spin-spin coupling) provide insights into neighboring hydrogen atoms. The area under each peak (integration) indicates the number of protons in that environment [52].

### 2.5.4 UV-Vis spectrometry

Ultraviolet–Visible (UV-Vis) spectroscopy is a technique used to analyze how molecules absorb light in the ultraviolet (200–400 nm) and visible (400–700 nm) regions of the electromagnetic spectrum. When light passes through a sample, electrons in certain chemical bonds can absorb specific wavelengths and become excited from a lower to a higher energy state. The resulting absorption spectrum shows how much light is absorbed at each wavelength. The position and intensity of absorption peaks provide information about the electronic structure of the molecule, especially the presence of conjugated systems or chromophores. The absorbance is typically proportional to concentration, allowing quantitative analysis using the Beer–Lambert law [53].

### 2.5.5 Evanescent light scattering (Nanolyze system)

The Nanolyze system is an advanced analytical tool that uses evanescent field light scattering to detect and monitor individual NPs in real time. When light is directed through a specialized glass chip at a specific angle, it creates an evanescent field — a localized electromagnetic field that penetrates only a few hundred nanometers into the sample above the surface. NPs that enter this field scatter the light, and this scattering is detected by a highly sensitive optical microscope. As molecules like proteins bind to the NP surface (e.g., forming a PC), the particle's size and refractive index change, which alters the scattering intensity. These changes are recorded over time, allowing for label-free, single-particle-level analysis of dynamic interactions like protein adsorption or surface modification. Unlike bulk techniques such as DLS, Nanolyze provides time-resolved, individual particle data without requiring ensemble averaging or separation steps. This makes it especially useful for studying fast kinetics and surface interactions in complex environments [35].

# 3

# Material and methods

## 3.1 Synthesis of PLGA NP via nanoprecipitation and emulsion

### 3.1.1 Activation of mPEG and mPEG-PEI conjugation

To maximize yield, the synthesis procedure and catalyst were optimized based on the protocol by Zhao et al.[54]. Specifically, 0.4 mmol of mPEG (purchased from Sigma-Aldrich, US, MW 5000 g/mol and 20,000 g/mol) was dissolved in 20 mL of DCM (purchased from Sigma-Aldrich, US, MW 84.93 g/mol) and purged with nitrogen to remove moisture and oxygen. Subsequently, 0.1 mmol of triethylamine (TEA) (purchased from Sigma-Aldrich, US, MW 137.65 g/mol) was added to the mPEG solution. Separately, 0.1 mmol of 4-nitrophenyl chloroformate (4-NPC) (purchased from Sigma-Aldrich, US, MW 201.56 g/mol) was dissolved in 10 mL of DCM. After stirring for 10 minutes, the mPEG solution was added dropwise to the 4-NPC solution. The reaction mixture was concentrated by evaporation to a final volume of 10 mL, and the residue was precipitated dropwise into an excess of cold diethyl ether (purchased from Sigma-Aldrich, US, MW 74.12 g/mol). The precipitation process was repeated twice. The final product was collected and dried under vacuum. Characterization and confirmation of the product were conducted using FTIR (Perkin Elmer, US) and NMR spectroscopy.

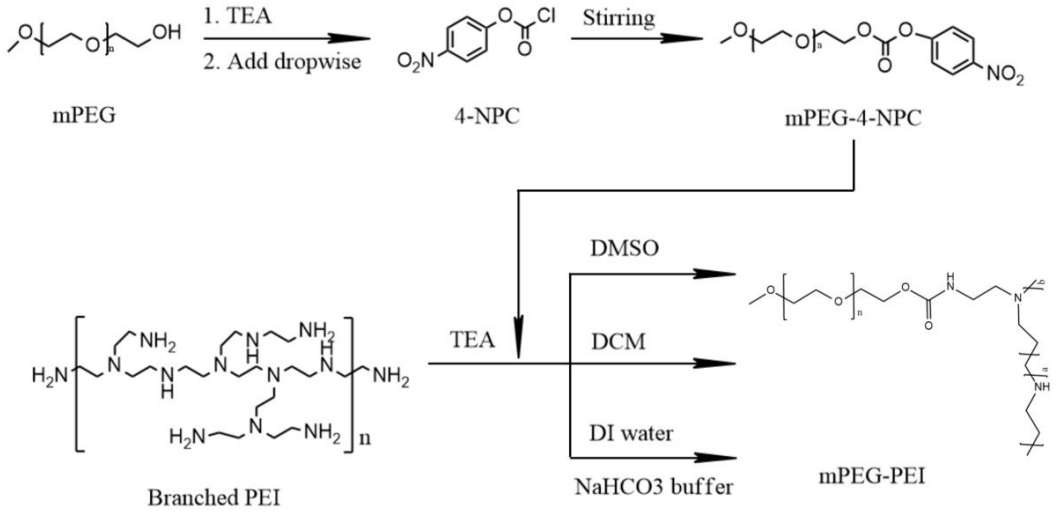


**Figure 3.1:** Schemes of mPEG acitivation and PEI PEGylation

To achieve PEGylation on PEI, three methods were investigated. Specifically,

activated mPEG and purified branched PEI (purchased from Sigma-Aldrich, US, MW 800 g/mol, 1200 g/mol and 2000 g/mol, 50 wt% in water solution) were dissolved separately in DMSO (purchased from Sigma-Aldrich, US, MW 78.13 g/mol) in the first method. TEA was added to the PEI solution for deprotonation. The mPEG solution was then added dropwise into the PEI solution under stirring, and the reaction was allowed to proceed for 48 hours. The mixture was dialyzed against deionized (DI) water using a PES membrane with a molecular weight cut-off (MWCO) of 1000 Da for 72 hours to remove DMSO. Subsequently, the product was washed three times with DI water in a 3 kDa filtration centrifuge tube to remove excess PEI. The final product was obtained after lyophilization[55][56] (CoolSafe, ScanVac Control AB, Sweden). The second method was modified based on previous one. Here, mPEG was dissolved in DCM, while PEI was initially dissolved in methanol and then added up to half volumn of mPEG solution by DCM, followed by adding TEA. mPEG solution was introduced dropwise into the PEI solution, followed by stirring at room temperature for 48 hours. The mixture was added dropwise into excess cold diethyl ether to induce precipitation. This precipitation process was repeated twice, using DCM to dissolve the precipitates each time. Finally, the precipitate was recrystallized in ethyl acetate and dried under a ventilation hood[57]. Conducted in an aqueous environment, the last method used DI water to dissolve mPEG, while PEI was dissolved in sodium bicarbonate buffer (pH 10). The mPEG solution was added dropwise into the PEI solution under continuous stirring for 48 hours. The product was washed three times with DI water using a 3 kDa filtration centrifuge tube and then lyophilized[58]. The products from these methods were characterized by FTIR and $^{1}$H NMR.

### 3.1.2 Synthesis of blank PLGA NP via nanoprecipitation

The established method for PLGA nanoprecipitation utilizes acetone (purchased from Sigma-Aldrich, US, MW 58.08 g/mol) as the organic phase and an aqueous solution containing a surfactant as the aqueous phase[59]. To protect mRNA from degradation and ensure PLGA solubility, citrate buffer (pH 6)[60] and phenol-chloroform[61] (purchased from Sigma-Aldrich, US, a 25:24:1 (v/v) mixture of phenol, chloroform and isoamyl alcohol) were explored as potential alternatives for the aqueous and organic phases, respectively. To evaluate the applicability of these alternatives, three comparative experiments were conducted: one replacing water with citrate buffer, another substituting acetone with phenol-chloroform, and a third replacing both. Throughout these experiments, key parameters influencing nanoparticle size were kept consistent, including the agitation speed, concentration of PLGA, the molecular weight and composition of the surfactant, and the organic-to-aqueous phase ratio. Take the third experiment as an example, the method was followed as below:

17 mg/mL PLGA (purchased from Sigma-Aldrich, US, MW 7,000-17,000 g/mol) solution in phenol-chloroform was firstly prepared. The aqueous phase was prepared by dissovling PEG(20k) (purchased from Sigma-Aldrich, US, MW 8,000 g/mol and 20,000 g/mol) and mPEG(20k)-PEI(2k) (in 10:1 molar ratio) in citrate buffer pH 6, followed by magnetic stirring at 400 rpm under room temperature. PLGA solution was injected into the aqueous phase dorpwise in a ratio of 2 mL of PLGA per 100 mL aqueous phase. After stirring under RT for 24 h, the

solution was filtered with 300mL Milli-Q water by 300K tengential flow filtration (Sigma-Aldrich, US). Then the solution was transferred into 30K filter centrifugal tube and centrifuged under 4700 rpm for 30 min, followed by washing with MilliQ water and centrifugation twice. 200 $\mu$l of PLGA NP water solution was collected and frozen for 24 h. 60 $\mu$l of NP solution was diluted into 1.5 mL and characterized under DLS (Zetasizer Ultra, Malvern Panalytical, England) for its size and zeta potential.

Based on the results of the previous experiments, the method utilizing citrate buffer (pH 6) was selected for subsequent studies. Key parameters such as agitation speed, temperature, PLGA concentration, and the molecular weight and composition of the surfactant were systematically investigated to optimize NP size. Guided by literature findings[37], the agitation speed was increased from 400 rpm to 700 rpm, the reaction temperature was raised to 45°C, and the PLGA concentration was reduced from 17 mg/mL to 8.5 mg/mL. Additionally, various surfactants, including mPEG (MW 20k or 2k)-PEI(MW 2k or 1200 or 800), PEG (MW 20k or 2k), were evaluated.

### 3.1.3 Synthesis of blank PLGA NP via emulsion

A well-established emulsion method using 5% PVA (purchased from Sigma-Aldrich, US, MW 89,000-98,000 g/mol) solution as an emulsion stabilizer successfully produced minimal-sized PLGA NPs[38][40]. Since PEG contains hydroxyl groups capable of forming hydrogen bonds in water, it was hypothesized that PEG could also function as a surfactant. Consequently, a 5% PEG (purchased from Sigma-Aldrich, US, MW 8,000 g/mol) solution was employed as the emulsion stabilizer.

To impart a positive surface charge, 2.5% PEI with varying molecular weights (2k, 1200, and 800 g/mol) was blended with PEG. Based on the performance of PEI across different molecular weights, PEI-2k was selected for subsequent experiments. Concentrations of 0.5%, 1.5%, and 2.5% PEI-2k were tested to evaluate the influence of PEI molecular weight on particle size and zeta potential.

To remove excess PEI from the NP surface and concentrate the particles, filtration centrifugation was applied after each trial. Changes in particle size and surface charge before and after concentration were carefully monitored. For example, the method used with 2.5% PEI-2k is described as follows:

15 mg of PLGA were dissolved in 1 mL of DCM to prepare the organic phase. Simultaneously, 250 mg of PEG (20k) and 250 mg of PEI-2k (50 wt% aqueous solution) were dissolved in Milli-Q water through sonication for 30 minutes, followed by filtration using a 0.22 $\mu$m syringe filter. After combining the organic phase with the aqueous phase, the mixture was sonicated using a 6 mm probe at 60% power for 12 minutes (VCX-750 sonicator, Sonics & Materials, Inc. U.S.), resulting in a milk-like emulsified solution. This solution was then evaporated under 50 mPa for 12 minutes to remove the organic solvent. Subsequently, the solution was filtered with 300 mL of Milli-Q water using a 300K tangential flow filtration system. The filtrate was then transferred to a 30K centrifugal filter tube and centrifuged at 4700 rpm for 30 minutes. The NP samples, both before and after concentration, were characterized for particle size and zeta potential using DLS.

Alternatively, the influence of PEGylated PEI on particle size and surface charge was also investigated. mPEG-PEI synthesized previously was mixed with PEG in molar ratio of 1:1, 1:5, 1:10 and 1:30. The mixture was dissolved in DI water to prepare 5% of PEG solution as emulsion stablizer. Synthesis method followed the one above.

## 3.2 Formation of a Protein Corona

The interaction between PLGA NPs and the PCs was initially studied using bovine serum albumin (BSA) (purchased from Sigma-Aldrich, US, lyophilized powder), the most abundant protein in serum and a well-established model for investigating NP–protein interactions. [62][63][64] In human serum, the albumin concentration ranges from approximately 35–50 g/L (35–50 mg/mL). Given its molecular weight of 66.5 kDa and an approximate hydro- dynamic diameter of 20 nm, a 100 kDa molecular weight cutoff (MWCO) centrifugal filter was used to remove unbound proteins. Protein adsorption onto the NP surface occurs rapidly, typically reaching saturation within seconds. To capture the early kinetics of this interaction, incubation times of 0.5, 1.5, 2.5, 3.5, 4.5, 5.0, 9.5, 12, 16, 22, and 30 minutes were selected. Both blank NPs and BSA were dispersed in 10 mM HEPES buffer to mimic physiological conditions. Initial characterization was performed using DLS for bulk population measurements, followed by single-particle analysis using the Nanolyze system.

To prepare the protein solution, 105 mg of BSA was dissolved in 3 mL of 10 mM HEPES buffer, yielding a 30 mg/mL BSA solution. Separately, 4 mg of PLGA NPs were dispersed in 4 mL of 10 mM HEPES buffer to make a 1 mg/mL NP solution. For each incubation, 0.5 mL of BSA solution was mixed with 0.5 mL of NP solution in a 1.5 mL centrifuge tube. Incubations were conducted for 0.5, 1.5, 2.5, 3.5, 4.5, 5.0, 9.5, 12, 16, 22, and 30 minutes. After incubation, samples were centrifuged at 4,500 rpm for 15 minutes using a 100K MWCO centrifugal filter to separate free BSA. The samples were then washed by replenishing with HEPES buffer up to 1 mL and centrifuged again. This washing step was repeated three times. The collected NPs were analyzed by DLS to measure hydrodynamic size and zeta potential. Samples were subsequently stored at –20°C for later analysis using the Nanolyze system.

In addition to DLS, the interaction between BSA and PLGA NPs was analyzed using the Nanolyze platform, which enables real-time, single-particle light scattering measurements under controlled liquid exchange. Blank PLGA NPs (100 nm) were first introduced into the sensor channel, and their baseline scattering intensity was recorded. Next, a BSA solution was pumped through the system, and changes in the scattering intensity of individual NPs were monitored to evaluate protein adsorption. Furthermore, pre-incubated BSA–NP complexes were also analyzed to compare scattering signatures after corona formation.

## 3.3 Synthesis of mRNA–PAMAM Complexes and Encapsulation into PLGA Nanoparticles

Synthesis of mRNA/PAMAM was conducted in two methods – incubation[16] and stirring. The model Poly-A mRNA (purchased from Sigma-Aldrich, US, lyophilized powder) was employed for mRNA-PAMAM optimization. Subsequently, GFP (purchased from Sigma-Aldrich, US, liquid, MW ~28 kDa) and mCherry mRNA (without cap protection, home made) were used to evaluate gene delivery efficiency.

### 3.3.1 mRNA/PAMAM formulation by incubation technique

The incubation method for forming mRNA–PAMAM dendriplexes was adapted from the previous researches' protocols.[16][15][32][33] A 200 $\mu$g/mL mRNA solution was prepared in 50 mM citrate buffer (pH 6), as this pH has been reported to provide optimal mRNA stability.[65] PAMAM G5 (purchased from Sigma-Aldrich, US, 5 wt% in methanol, density 0.797 g/mL at 25 °C) was diluted to 0.05 mg/mL using the same buffer. A total of 2000 $\mu$L of PAMAM solution was mixed with the mRNA solution to achieve an N:P molar ratio of 12:1, a ratio previously shown to yield high mRNA loading (>85%) and reduced particle size. The size and zeta potential of the resulting complexes were characterized by DLS. However, incubation often led to oversized particles. Therefore, an alternative stirring-based method was explored.

### 3.3.2 mRNA/PAMAM formulation by stirring technique

In the stirring method, PAMAM G5 (0.05 mg/mL) and mRNA solutions (400 ng/$\mu$L of Poly-A, GFP, or mCherry mRNA) were prepared in 50 mM citrate buffer at pH 6. The mRNA solution was pipette slowly into the PAMAM solution under constant stirring at 500 rpm. Formulations were prepared at mRNA:PAMAM weight ratios of 1:25, 1:50, and 1:100 (corresponding to molar ratios of approximately 1:3, 1:6, and 1:12). Stirring continued for 24 and 48 hours, respectively. The resulting complexes (50 $\mu$g/mL) were characterized for particle size via DLS. Due to the low particle concentration and buffer conditions, zeta potential measurements were not applicable. To verify successful mRNA condensation into PAMAM, FTIR and UV–Vis spectroscopy were employed.

### 3.3.3 Encapsulation into PLGA via Double Emulsion

mRNA/PAMAM complexes were encapsulated into PLGA NPs using a water/oil/water (w/o/w) double emulsion method based on established protocols.[66] For the primary emulsion, the mRNA/PAMAM complex solution was suspended to a PLGA/DCM solution (5 mg/mL and 15 mg/mL PLGA concentrations were tested), with an aqueous to organic phase ratio of 5:1. The mixture was sonicated at 40% amplitude on ice for 5 minutes.[41] The resulting primary emulsion was then emulsified into an aqueous surfactant solution (o/w ratio of 1:5) via sonication at 75% power on ice for 12 minutes. Solvent evaporation was performed using a rotary evaporator at 70 mPa for 8 minutes. The NPs were purified by filtration through 300 mL of deionized water using a 300K T-flow filter.

## 3.4 Quantification of mRNA Content and Encapsulation Efficiency

The mRNA content (Poly-A, GFP, and mCherry) in the mRNA/PAMAM complexes was initially quantified using a Nanodrop spectrophotometer immediately after formulation. In parallel, UV–Vis spectroscopy was employed to measure the absorbance at 260 nm, a characteristic peak for nucleic acids.[67] Since both methods detect total mRNA, including free and condensed mRNA within the dendriplexes, agarose gel electrophoresis was used to assess whether unbound mRNA remained in solution following complexation. By comparing sample absorbance values with a pre-established calibration curve (mRNA concentration vs. absorbance at 260 nm), the mRNA content in the formulation could be quantitatively determined.

The mRNA loading and encapsulation efficiency (EE) were calculated using the following equations:[68]

$$Loading(\%) = \frac{Aount\ of\ mRNA\ (\mu g/ml)}{Amount\ of\ NP\ (\mu g/ml)} \times 100 \tag{3.1}$$

$$EE(\%) = \frac{W_{(Initial\ mRNA)} - W_{(Entrapped\ mRNA)}}{W_{(Initial\ mRNA)}} \times 100 \tag{3.2}$$

Alternatively, for comparative analysis, the encapsulation efficiency of mRNA within PLGA NPs can be determined by extracting mRNA from lysed NPs[69][70] and post-formulation mRNA quantification using Nanolyze system. However, due to time constraints, the two approaches were not carried out.

## 3.5 Cytotoxicity Assessment of mRNA/PAMAM-PLGA Nanoparticles

The cytotoxicity of mRNA/PAMAM-PLGA NPs (Poly-A-loaded NPs, 169 nm and 229 nm), along with blank PLGA NPs (100 nm), was evaluated using the resazurin assay.[71] According to protocols established in previous work from our lab, L929 fibroblast cells were cultured in Dulbecco's Modified Eagle Medium (DMEM) (purchased from Sigma-Aldrich, US) supplemented with 10% fetal bovine serum (FBS). Cells were seeded into 96-well plates at a density of $2 \times 10^4$ cells/180 $\mu$l per well and incubated for 24 h at 37 °C in a 5% $CO_2$ atmosphere.

Following incubation, 20 $\mu$L of NP solutions at serial concentrations (4500, 2250, 1125, 562.5, 281.25, and 140.625 $\mu$g/mL) were added to the wells, resulting in final NP concentrations in the culture medium. 1% of Triton-X100 in dPBS was introduced to kill the cell and used as positive control. Each concentration was tested in quadruplicate. After 24 h of exposure, 20 $\mu$L of resazurin solution was added to each well, followed by an additional 4 h incubation period. Fluorescence intensity, indicative of cell metabolic activity, was measured using a plate reader at an excitation wavelength of 550 nm and emission wavelength of 590 nm. All experiments were conducted in triplicate to ensure reproducibility.

The relative cell viability was calculated as follows (where $OD_{sample}$ was that obtained in the presence of NPs, $OD_{control}$ was that obtained in the absence of NPs and

$OD_{background}$ was that obtained in the absence of NPs and cells.):

$$cellviability(\%) = \frac{OD_{(sample)} - OD_{(background)}}{OD_{(control)} - OD_{(background)}} \times 100\ (\%) \quad (3.3)$$

## 3.6 Cellular Uptake Efficiency of Rhodamine-B Labeled PLGA Nanoparticles

Cellular uptake efficiency was assessed using Rhodamine-B-labeled PLGA NPs and the L929 fibroblast cell line. The fluorescently labeled NPs were synthesized by incorporating Rhodamine-B-conjugated PLGA (MW 24–30 kDa) (purchased from Sigma-Aldrich, US) into a blend with unlabeled PLGA (MW 7–17 kDa) at a molar ratio of 1:99, following the emulsion protocol described in Section 3.1.3. The resulting fluorescent NPs exhibited size and surface charge properties comparable to those of unlabeled blank NPs.

L929 fibroblast cells were cultured in Dulbecco's Modified Eagle Medium (DMEM) supplemented with 10% fetal bovine serum (FBS). Cells were seeded into a 96-well plate at a density of $2 \times 10^4$ cells/180 $\mu$l per well in 180 $\mu$L of medium and incubated for 24 h at 37 °C in a humidified 5% $CO_2$ environment. Following incubation, 20 $\mu$L of Rhodamine-B-labeled NP suspension (2250 $\mu$g/mL) was added to each well and incubated for an additional 24 h under the same conditions.

After incubation, cells were washed three times with Dulbecco's phosphate-buffered saline (dPBS) to remove uninternalized NPs. Each well was then filled with 200 $\mu$L of dPBS, and fluorescence intensity was measured using a plate reader with excitation at 545 nm and emission at 566 nm. All measurements were performed in triplicate.

The relative cell uptake was calculated as intensity variation; $\Delta I/I_0$ (where $I_{sample}$ was that obtained in the presence of NPs, $I_{control}$ was that obtained in the absence of NPs and $I_{background}$ was that obtained in the absence of NPs and cells):

$$\Delta I/I_0(\%) = \frac{I_{(sample)} - I_{(control)}}{I_{(control)} - I_{(background)}} \times 100\ (\%) \quad (3.4)$$

## 3.7 Evaluation of Gene Delivery Efficiency

To compare the gene delivery efficiency of bare mRNA/PAMAM complexes and PLGA NP-encapsulated cargo in immune cells, the RAW 264.7 macrophage cell line was used. Cells were cultured in DMEM supplemented with 10% fetal bovine serum (FBS) and seeded in 96-well plates at a density of $2 \times 10^4$ cells/180 $\mu$l per well, followed by incubation for 24 h at 37 °C in a humidified atmosphere containing 5% $CO_2$. Subsequently, 20 $\mu$L of mRNA/PAMAM solution (GFP and mCherry at

concentrations of 25, 12.5, and 6.25 $\mu$g/mL) or NP suspension (2250, 1125, and 562.5 $\mu$g/mL) was added to each well. The final concentrations of mRNA/PAMAM complexes in wells were 2.5, 1.25, and 0.625 $\mu$g/mL. And the final concentrations of cargo loaded NPs in wells were 225, 1125, and 56.25 $\mu$g/mL. Notably, the cells were not washed before mRNA/PAMAM complexes and cargo loaded PLGA NPs were added. The samples were then incubated for 24, 48, and 72 h. Each concentration was performed in quadruplicate and all experiments were performed in triplicate.

For samples treated with GFP/PAMAM or GFP/PAMAM-PLGA NPs, fluorescence intensity was measured using a plate reader at an excitation wavelength of 485 nm and an emission wavelength of 520 nm. For samples treated with mCherry/PAMAM or mCherry/PAMAM-PLGA NPs, cells were washed three times with dPBS to eliminate background signal caused by the pink color of the culture medium, followed by fluorescence measurement (excitation at 575 nm, emission at 616 nm). All experiments were performed in triplicate.

The relative delivery efficiency was calculated as intensity variation; $\Delta I/I_0$ (where $I_{sample}$ was that obtained in the presence of NPs, $I_{control}$ was that obtained in the absence of NPs and $I_{background}$ was that obtained in the absence of NPs and cells):

$$\Delta I/I_0(\%) = \frac{I_{(sample)} - I_{(control)}}{I_{(control)} - I_{(background)}} \times 100\ (\%) \qquad (3.5)$$

Furthermore, for comparion analysis, the gene delivery efficiencies of GFP and mCherry in cargo (GFP and mCherry loaded PAMAM) and cargo loaded PLGA NPs (GFP/PAMAM-PLGA and mCherry/PAMAM-PLGA) were visualized by confocal microscopy. The cargo samples (2.5 $\mu$g/mL) and cargo loaded PLGA NPs (225 $\mu$g/mL) were incubated with RAW 264.7 macrophages for 72 hours at 37 °C in a humidified atmosphere containing 5% $CO_2$, followed by taking images both in bright field and fluorescent modes (excitation at 485 nm and 575 nm for GFP and mCherry respectively).

# 4

# Results

## 4.1 PLGA NP Synthesis via nanoprecipitation and emulsion

### 4.1.1 Activation of mPEG and mPEG-PEI conjugation

To enhance mPEG activation and improve yield, modifications were made to a previously reported activation method[54]. In this approach, TEA was used to deprotonate mPEG under a nitrogen atmosphere. The deprotonated mPEG was then added dropwise into an excess amount of 4-NPC to ensure complete consumption of the reagent. Initially, the reaction was allowed to proceed for 24 hours, and the resulting product was characterized using FT-IR and $^{1}$H NMR spectroscopy.

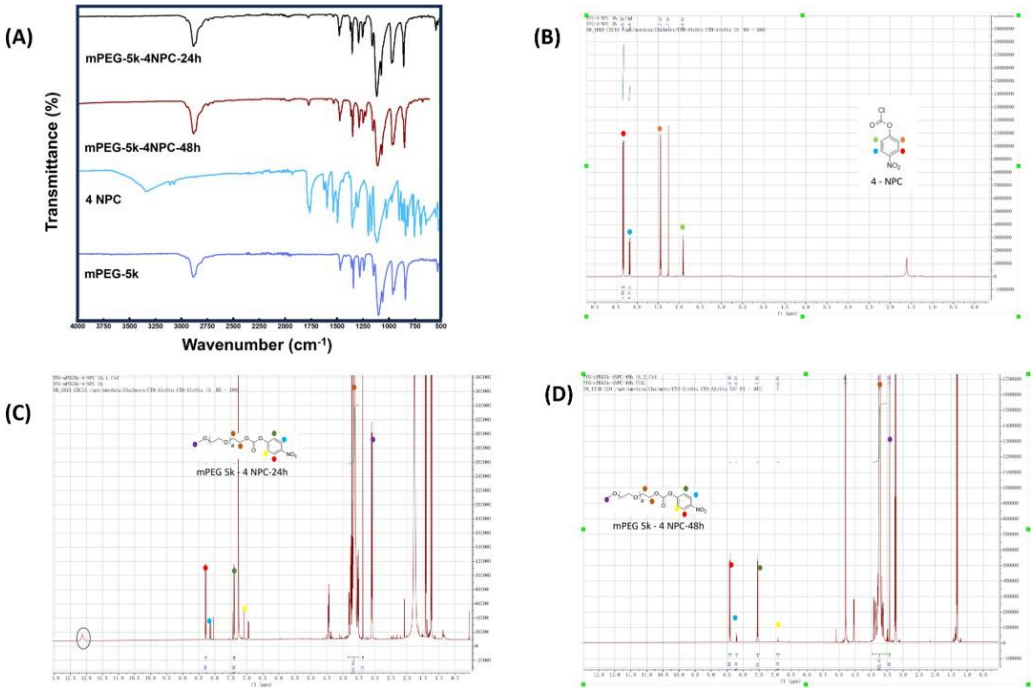


**Figure 4.1:** (a) FTIR from mPEG5k, 4 nitrophynol chloroformate (4 NPC), activated mPEG5k which the reaction went for 24h, and the activated mPEG5k which the reaction went for 48h. (b) $^{1}$H NMR chacterizing peaks for pure 4 NPC. (c) $^{1}$H NMR chacterizing peaks for activated mPEG5k which the reaction went for 24h. (d) $^{1}$H NMR chacterizing peaks for activated mPEG5k which the reaction went for 48h.

As shown in Figure 4.1 (a), the characteristic -C=O stretch at 1764 $cm^{-1}$ in the sample "mPEG-4-NPC-24h" was faintly detectable, indicating the successful bonding of 4-NPC to mPEG. However, the extent of reaction completion was uncertain. Further analysis using $^{1}H$ NMR (Figure 4.1 (c)) revealed an additional singlet corresponding to the -OH group of mPEG, confirming that the reaction was incomplete.

To address this, the reaction time was extended to 48 hours. In the FT-IR spectrum of the 48-hour sample (Figure 4.1 (a)), the intensity of the -C=O stretch was notably higher than in the 24-hour sample. Moreover, $^{1}H$ NMR analysis of the 48-hour sample (Figure 4.1 (d)) showed no singlet for the free -OH group, and the signal intensity for 4-NPC was approximately six times stronger compared to the 24-hour sample. These results indicate that the reaction reached completion after 48 hours, with the yield calculated to be 91.1%. Therefore, mPEG5k and mPEG20k in the following experiments were activated by this way.

To optimize the conjugation of PEI to mPEG and maximize yield, three methods were investigated. In the first method, the reaction was carried out in DMSO, followed by dialysis against water to remove the solvent and filtration centrifugation to eliminate excess PEI. The second method utilized DCM and methanol as solvents, with purification achieved through precipitation in diethyl ether. In the third method, the reaction was performed in a basic aqueous environment (pH 10), followed by filtration centrifugation. For the first method, the effects of varying reaction times (24 hours and 48 hours) and different PEI forms (50% wt aqueous PEI and lyophilized PEI) on product quality were also evaluated.

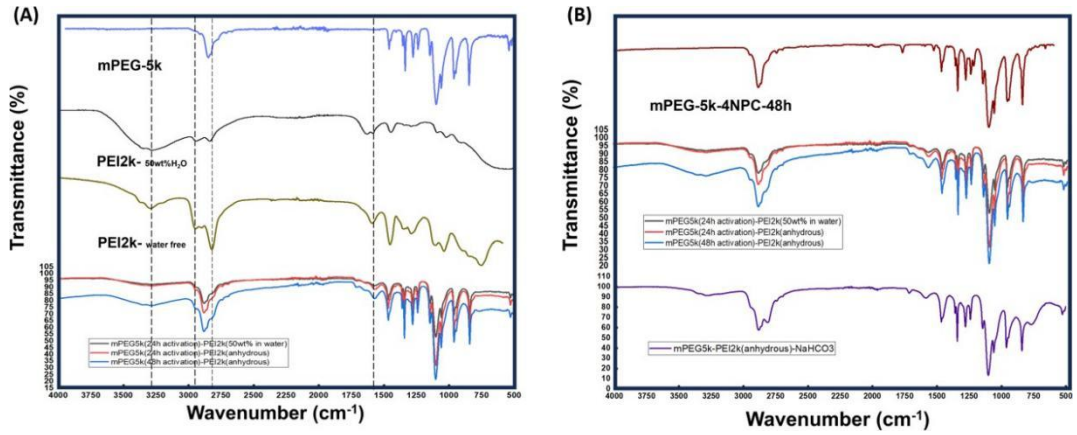


**Figure 4.2:** (a) FTIR from mPEG5k, PEI2k in 50%wt water, anhydrous PEI2k, and mPEG5k-PEI2k synthesized by first method in different reaction time (24 h and 48 h) and PEI2k types (in water solution and lyophilized one). (b) FTIR from activated mPEG5k, mPEG5k-PEI2k synthesized by first method in different reaction time (24 h and 48 h) and PEI2k types (in water solution and lyophilized one), and mPEG-PEI synthesized by third method.

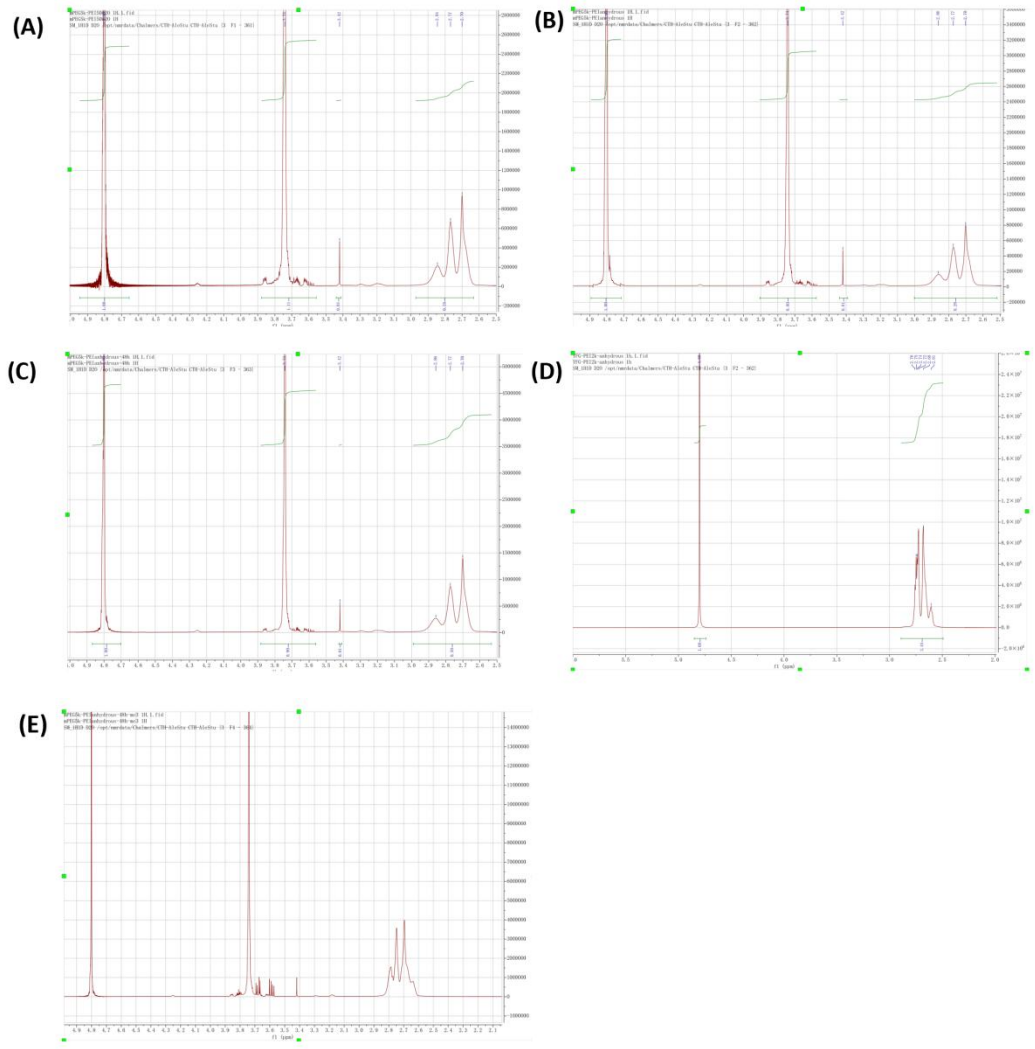


**Figure 4.3:** $^{1}$H NMR data for (a) mPEG5k-PEI2k with PEI2k in 50%wt water solution and reacted for 24 h, method 1; (b) mPEG5k-PEI2k with anhydrous PEI2k and reacted for 24 h, method 1; (c) mPEG5k-PEI2k with anhydrous PEI2k and reacted for 48 h, method 1; (d) anhydrous PEI2k; and (e) mPEG5k-PEI2k with anhydrous PEI2k and reacted for 48 h, by third method.

As a result, the first method demonstrated the best performance among the protocols. The use of anhydrous PEI significantly improved the yield of mPEG-PEI, as did the extension of reaction time to 48 hours. As shown in Figure 4.2 (a), the three mPEG samples synthesized using method 1 were successfully conjugated with PEI. However, the IR signal intensities varied across samples with different PEI types and reaction times. The sample prepared using anhydrous PEI and a reaction time of 48 hours exhibited the highest signal intensity, which was further confirmed by $^{1}$H NMR.

The results from method 2 were excluded due to its poor yield. PEI and mPEG were both insoluble in diethyl ether, and the excess PEI used in the reaction caused the product to aggregate and co-precipitate with the sticky PEI. As a result, the

product could not be effectively extracted from the mixture.

For method 3, the IR spectrum in Figure 4.2 (b) suggested that PEI was not completely removed during purification. This was confirmed by $^{1}$H NMR (Figure 4.3), where the mPEG-PEI samples synthesized by method 3 displayed four characteristic PEI peaks, similar to those seen in the pure PEI sample. In contrast, the mPEG-PEI samples synthesized by method 1, with successful PEGylation and complete removal of excess PEI, showed only three characteristic PEI peaks.

| Method Applied | PEI2k used | Reaction time (h) | Yield (%) |
|---|---|---|---|
| Method 1 | 50%wt in water | 24 | 22.32 |
| Method 1 | Anhydrous | 24 | 29.89 |
| Method 1 | Anhydrous | 48 | 24.22 |
| Method 2 | Anhydrous | 48 | 0 |
| Method 3 | Anhydrous | 48 | 39.15 |

**Table 4.1:** mPEG5k-PEI2k yield from three methods, with different reaction time and PEI type.

Based on the yields presented in Table 4.1, method 1 was identified as the optimal conjugation protocol. The best results were achieved using anhydrous PEI and a reaction time of 48 hours. Therefore, the subsequent mPEG20k activation and the synthesis of mPEG5k-PEI1200, mPEG5k-PEI800, and mPEG20k-PEI2k were performed under these optimized condition

### 4.1.2 Synthesize blank PLGA NP via nanoprecipitation

To protect mRNA from degradation, modifications were made to a well-established method for PLGA nanoprecipitation[59]. Three experiments were conducted to evaluate the feasibility of replacing acetone and water with phenol-chloroform and citrate buffer (pH 6): (1) acetone and water were replaced with phenol-chloroform and citrate buffer, respectively; (2) phenol-chloroform was used as the organic phase; and (3) citrate buffer (pH 6) was used as the aqueous phase. The resulting particle sizes are presented in Figures 4.4 (a), 4.4 (b), and 4.4 (c).

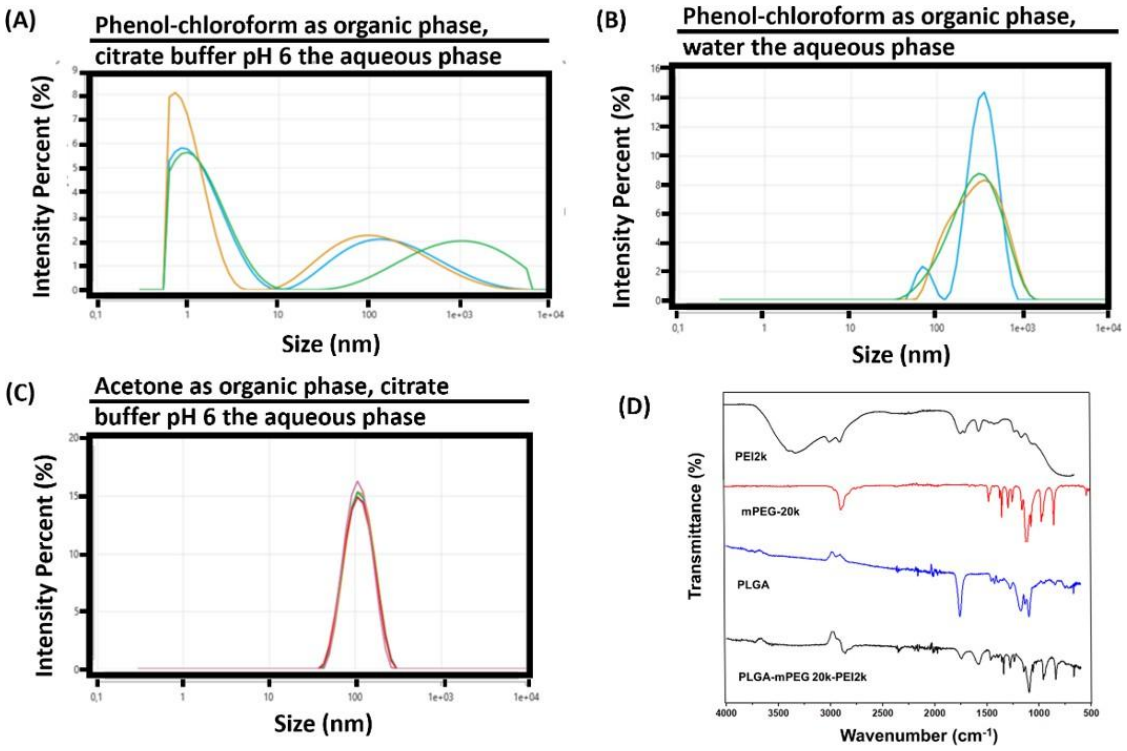


**Figure 4.4:** DLS data of particle average sizes and PDI. (a) Phenol-chloroform was used as organic phase, and citrate buffer pH 6 the aqueous phase. (b) Phenol-chloroform was used as organic phase, and water the aqueous phase. Mean particle size is 360 nm, and PDI 0.56. (c) Acetone was used as organic phase, and citrate buffer pH 6 the aqueous phase. Mean particle size is 108 nm, and PDI 0.12. And (d) FT-IR diagram of PEI2k (50 wt% in $H_2O$), mPEG20k, PLGA, and the freeze dried NP sample B in table 4.2.

Among the methods tested, the approach where acetone was added dropwise into citrate buffer (pH 6) produced stable NPs with a suitable size (108 nm) and narrow size distribution (PDI = 0.12). In contrast, replacing acetone with phenol-chloroform led to significant particle aggregation, resulting in an average particle size of 360 nm and a high polydispersity. When both phases were replaced with phenol-chloroform and citrate buffer, NPs failed to form. Based on these results, the method involving acetone and citrate buffer (pH 6) was selected for subsequent experiments.

As previously described, NP size during nanoprecipitation is influenced by multiple parameters, primarily through their effect on the diffusion coefficient of the organic solvent in water in the presence of the polymer[37]. A lower diffusion coefficient reduces the solvent's diffusion rate into water, leading to larger particle sizes and broader size distributions. This principle provides a potential explanation for the varying outcomes of the phase replacement experiments. According to literature, phenol has a smaller diffusion coefficient compared to acetone[72], while chloroform is virtually insoluble in water[73]. Consequently, phenol-chloroform diffuses significantly slower than acetone, resulting in larger particle sizes. These findings support the proposed hypothesis, but the potential influence of pH on particle size warrants further investigation. For example, the pH of citrate buffer can be adjusted to be acidic, neutral and basic, followed by NP formulation tests via nanoprecipitation.

The 108 nm control NPs from the previous step exhibited a stable and suit- able size for drug delivery. However, their negative surface charge posed a challenge for cell membrane penetration, thereby reducing delivery efficiency. To address this issue, PEI2k-conjugated mPEG was introduced as a surfactant by mixing it with PEG in an initial molar ratio of 1:10 in the aqueous phase.

| Sample | Ratio of PEG and mPEG | PLGA concentration (mg/ml) | Temperature | Size (nm) | PDI | Zeta potential (mV) |
|---|---|---|---|---|---|---|
| A.mPEG20k, PEG20k | 1:10 | 17 | RT | 108 | 0.12 | -58.79 |
| B.mPEG20k-PEI2k, PEG20k | 1:10 | 17 | RT | 200 | 0.05 | 0.66 |
| C.mPEG20k-PEI2k, PEG2k | 1:30 | 17 | RT | 200 | 0.07 | 1.42 |
| D.mPEG20k-PEI2k, PEG2k | 1:30 | 8.5 | 45℃ | 230 | 0.10 | 0.63 |
| E.mPEG2k-PEI2k, PEG2k | 1:10 | 17 | RT | 300 | 0.23 | 0 |

**Table 4.2:** PLGA NP synthesized by nanoprecipitation within variant circumstance: temperature, PLGA concentration, and the molecular weight and composition of the surfactant

As shown in Table 4.2, the addition of mPEG20k-PEI2k significantly increased the surface charge of sample B to 0.66 mV, compared to -58.79 mV for the control particles. However, the particle size also increased from 108 nm (control) to 200 nm in sample B. The increase in particle size can be attributed to changes in the organic solvent's diffusion coefficient caused by the presence of PEI. Branched PEI is sparingly soluble in organic solvents, such as acetone, and its dissolution in the aqueous phase hinders acetone diffusion, resulting in larger particles. Additionally, the acidic environment of the citrate buffer protonates PEI, increasing its positive charge and causing electrostatic repulsion, which further contributes to particle size enlargement.

In sample C, the molecular weight of PEG was reduced to 2k g/mol to enhance the influence of PEI. To maintain a sufficient volume of the 1% PEG aqueous phase, the molar ratio of mPEG-PEI to PEG was adjusted to 1:30, with the expectation of reducing NP size. However, the effect of PEI dominance offset the reduced molar ratio, resulting in a particle size comparable to sample B but with an even more positive surface charge.

For sample D, lower PLGA concentration and higher reaction temperature were

applied in an attempt to decrease particle size. Contrary to expectations, the resulting NPs remained large and exhibited reduced zeta potential. This unexpected outcome may be due to the influence of temperature on both PLGA solubility in acetone and the acetone evaporation rate. While higher temperatures increase PLGA solubility, promoting smaller particle formation, they also accelerate acetone evaporation, which can lead to larger particles. In sample D, with molecular weight reduction of both mPEG and PEG into 2k g/mol, the effect of PEI became dominant and supported the previous hypothesis: diffusion coefficient of acetone in water in presence of PEI became smaller and repulsion force increased when PEI was more dominant, resulting in 300 nm of size. To verify the hypothesis, future experiments can employ DLS (by analyzing scattered light) or Voltammetry (by analyzing the current response) to measure diffusion coefficient of acetone in water with different concentrations of PEI dissolved, and compare the resulted NP sizes with the corresponding diffusion coefficients.

### 4.1.3 Synthesize blank PLGA NP via emulsion

Since nanoprecipitation primarily loads hydrophobic cargo, an emulsion-based synthesis method, which allows for hydrophilic drug (like mRNA) encapsulation within the particles, was investigated. The formation and size of NPs using the emulsion technique depend on several factors, including surfactant concentration, PLGA concentration, sonication power, sonication time, and the evaporation method. These parameters collectively influence the size and stability of the emulsion droplets[41][39]. To study the effects of PEI addition and its molecular weight on the particle size and surface charge of emulsion-derived NPs, the following parameters were kept constant: 15 mg/mL PLGA in DCM, 5 wt% PEG20k in water, sonication power of 60% for 12 minutes, and evaporation under reduced pressure.

| Sample | PEG20k concentration (wt%) | PEI molecular weight (D) | PEI concentration (wt%) | Size (nm) | PDI | Zeta potential (mV) |
|---|---|---|---|---|---|---|
| A. | 5% | - | - | 108 | 0.13 | -5.00 |
| B. | 5% | 2000 | 2.5% | 500 | 0.30 | +43 |
| C. | 5% | 1200 | 2.5% | 500 | 0.60 | +38 |
| D. | 5% | 800 | 2.5% | 200 | 1 | +23 |
| B.Washed | 5% | 2000 | 2.5% | 200 | 0.40 | +38 |
| C.Washed | 5% | 1200 | 2.5% | 300 | 0.60 | +60 |
| D.Washed | 5% | 800 | 2.5% | 108 | 1 | +64 |

**Table 4.3:** PLGA NPs synthesized by emulsion with variant PEI molecular weights (2000 g/mol, 1200 g/mol and 800 g/mol), and the same batch after being washed by 30k filtration tube.

As shown in Table 4.3, the control sample (Sample A) without PEI achieved results comparable to those obtained through nanoprecipitation, producing NPs with a stable and suitable size (108 nm) but a higher surface charge (-5 mV compared to -58.79 mV). The success of Sample A demonstrated the feasibility of using PEG

as a surfactant.

In Samples B, C, and D, 2.5 wt% of PEI with varying molecular weights (2000, 1200, and 800 g/mol, respectively) was incorporated. It was anticipated that Sample B (PEI2k) would show a moderate size increase compared to the control, with particle size decreasing as PEI molecular weight decreased. However, while all samples (B, C, and D) achieved stable positive zeta potentials and their surface charge decreased as PEI molecular weight decreased, the particle sizes were excessively large, rendering them unsuitable for drug delivery.

The size enlargement can be explained by the interplay of electrostatic attraction and repulsion. Electrostatic attraction between negatively charged PLGA-PEG and protonated PEI likely caused significant aggregation of PLGA-PEG-PEI complexes. However, the repulsion from branched PEI2k helped maintain relatively uniform interparticle distances, resulting in a particle size of 500 nm for Sample B, with a PDI of 0.3. As the molecular weight of PEI decreased, repulsion forces weakened, becoming insufficient to counteract the attraction forces. This imbalance led to the formation of multiple particle populations, as evidenced by the increasing PDI values from Sample B to Sample D.

To further investigate the effect of PEI concentration on particle size and surface charge, Samples E, F, and G were prepared with 2.5 wt%, 1.5 wt%, and 0.5 wt% of PEI2k, respectively.

| Sample | PEG20k concentration (wt%) | PEI molecular weight (D) | PEI concentration (wt%) | Size (nm) | PDI | Zeta potential (mV) |
|---|---|---|---|---|---|---|
| E. | 5% | 2000 | 2.5% | 500 | 0.30 | +43 |
| F. | 5% | 2000 | 1.5% | 525 | 0.30 | +40 |
| G. | 5% | 2000 | 0.5% | 200 | 1 | -21, +38 |
| E.Washed | 5% | 2000 | 2.5% | 200 | 0.40 | +38 |
| F.Washed | 5% | 2000 | 1.5% | 390 | 0.52 | +70 |
| G.Washed | 5% | 2000 | 0.5% | 4, 200 | 1 | -21, +28 |

**Table 4.4:** PLGA NPs synthesized by emulsion with variant PEI2k con- centration (0.5 wt%, 1.5 wt% and 2.5 wt%), and the same batch after being washed by 30k filtration tube.

Samples E and F showed comparable results, with particle sizes around 500 nm, a PDI of 0.3, and a surface charge of approximately +40 mV. This suggests that both 2.5 wt% and 1.5 wt% of PEI2k achieved a similar electrostatic balance. In contrast, Sample G, with only 0.5 wt% PEI2k, formed multiple particle populations, resulting in a high PDI of 1. Additionally, the presence of both a negative and a positive peak in the zeta potential measurements for Sample G indicates the possible coexistence of separate PEI particles and PLGA-PEG particles. However, this hypothesis requires further characterization to confirm. For example, scanning electron microscopy (SEM) and energy dispersive X-ray analysis (EDX) can be applied to visualize and discern PEI particles and PLGA-PEG particles, to evaluate the hypothesis.

Interestingly, after being washed using a 30k molecular weight cutoff filtration centrifuge at 4700 rpm, Samples C, D, F, and G exhibited reduced particle sizes, increased surface charges, and slightly elevated PDI values. Conversely, Sample B and E showed a slight decrease in surface charge after centrifugation. This behavior can be attributed to the separation of aggregates during the filtration process, which increased the PDI. For Samples B and E, the high PEI concentration and large PEI molecular weight likely saturated the particle surfaces, leaving no free PEI to adsorb during centrifugation. In contrast, for Samples C, D, F, and G, free PEI in the system was condensed and adsorbed onto the particle surfaces, leading to an increase in surface charge. Future experiments could employ sonication to further disaggregate the particles and refine these findings.

To balance the strong electrostatic forces introduced by branched PEI and to obtain NPs of appropriate size, PEGylation of PEI was performed. Table 4.5 summarizes the optimization of formulation parameters, including PLGA molecular weight, the type of PEGylated PEI, and the percentage of surfactants.

The initial formulation used high molecular weight PLGA (24 kDa) to compare with the previously tested sample A. This resulted in particles that were approximately 30% larger. Additionally, NPs prepared with 24 kDa PLGA and mPEG5k- PEI2k exhibited acceptable surface charge but showed a broad size distribution with multiple populations. This was attributed to the increased viscosity of the organic phase caused by the higher PLGA molecular weight, which hindered efficient dispersion into the aqueous phase. As a result, subsequent optimization employed PLGA with a lower molecular weight (7–17 kDa).

| PLGA MW | Type of mPEG-PEI | mPEG-PEI Concentration (wt%) | PEG8k concentration (wt%) | Size (nm) | PDI | Zeta potential (mV) |
|---|---|---|---|---|---|---|
| 24k | / | / | 5% | 131 | 0.24 | +5 |
| 24k | mPEG5k-PEI2k | 3% | 2% | 225* | 0.29 | +14 |
| | | | Optimization 1 | | | |
| 7-17k | mPEG5k-PEI2k | 5% | 0 | 125* | 0.29 | +26 |
| 7-17k | mPEG5k-PEI2k | 3% | 2% | 108 | 0.32 | +24 |
| 7-17k | mPEG5k-PEI2k | 1% | 4% | 182 | 0.25 | +20 |
| | | | Optimization 2 | | | |
| 7-17k | mPEG5k-PEI1200 | 3% | 2% | 93 | 0.25 | +23 |
| 7-17k | mPEG5k-PEI800k | 3% | 2% | 50, 140 | 0.25 | +20 |
| 7-17k | mPEG20k-PEI2k | 3% | 2% | 100 | 0.21 | +13 |
| | | | Repeat | | | |
| 7-17k | mPEG20k-PEI2k | 3% | 2% | 111 | 0.12 | +7.5 |
| 7-17k | mPEG20k-PEI2k | 3% | 2% | 125 | 0.25 | +7.3 |

**Table 4.5:** PLGA NPs synthesized by emulsion with variant surfactant and surfactant concentrations.

In the first optimization stage, the effect of different ratios of mPEG-PEI and PEG8k was evaluated while keeping the PLGA molecular weight and surfactant

type constant. Formulations containing either only mPEG5k-PEI2k or a low amount of it resulted in broad or large particle size distributions. However, the combination of 3 wt% mPEG5k-PEI2k and 2 wt% PEG8k yielded NPs with favorable size and uniformity. It can be explained that at this ratio, a balance between electrostatic attraction and repulsion among PEI, PEG, and PLGA was achieved. Nevertheless, all three samples displayed surface charges exceeding +20 mV due to the dominant influence of PEI, which is suboptimal for immune-cell-targeted drug delivery. Therefore, further refinement of the PEG-to-PEI ratio was necessary.

In the second optimization phase, different PEGylated PEI (mPEG5k-PEI1200, mPEG5k-PEI800, and mPEG20k-PEI2k) were tested to identify the most suitable surfactant. Notably, NPs prepared with lower PEI molecular weight or reduced PEI contribution exhibited smaller sizes. Among the formulations, mPEG20k-PEI2k produced NPs that met both size (~100 nm) and surface charge (+13 mV) criteria. This suggests that when the molecular weight ratio of mPEG to PEI reaches approximately 10:1, the disruptive effects of PEI on NP size and surface charge can be significantly minimized. The resulting formulation was reproduced twice, consistently yielding favorable NP characteristics, thus demonstrating its robustness and reproducibility.

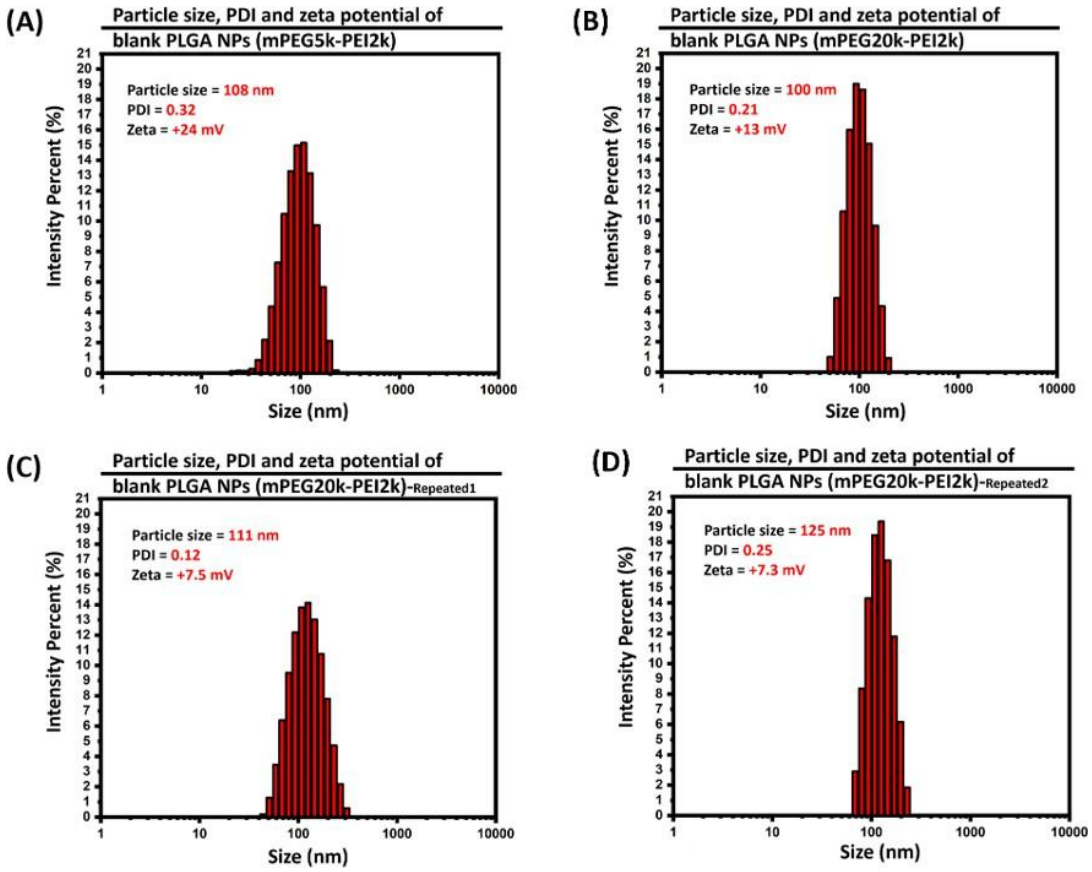


**Figure 4.5:** DLS data of particle size and PDI. (a) Blank PLGA NPs synthesized by emulsion with surfactant of mPEG5k-PEI2k. (b) Blank PLGA NPs synthesized by emulsion with surfactant of mPEG20k-PEI2k. (c) Repeated Blank PLGA NPs 1 with the same protocol as sample (b). And (d) Repeated Blank PLGA NPs 2 with

the same protocol as sample (b).

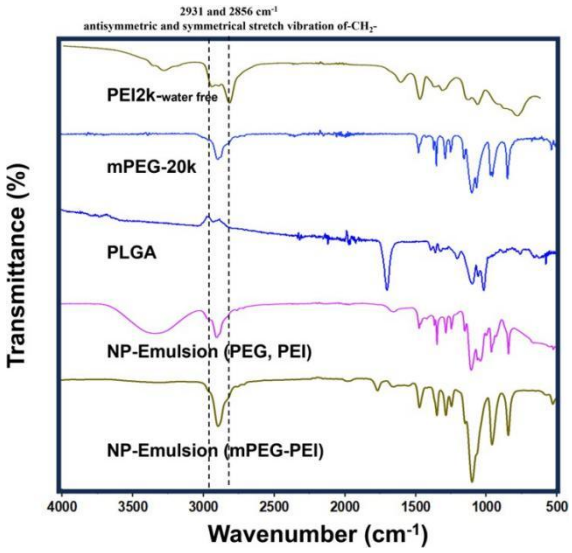


**Figure 4.6:** FTIR for emulsion blank PLGA NPs

As shown in Figure 4.5, the DLS profiles of blank PLGA NPs (favorable size and zeta potential) prepared by the emulsion method were compared. Although particles synthesized with mPEG5k-PEI2k achieved the desired mean diameter, they displayed a broad, non-uniform size distribution. By contrast, NPs formulated with mPEG20k-PEI2k (and their replicate batch) exhibited both the target size and a much narrower, monomodal distribution. These three batches represent the optimized blank PLGA formulations obtained via the emulsion route.

To verify NP composition, FTIR spectroscopy was performed on starting materials (anhydrous PEI2k, mPEG20k, and PLGA 7–17 kDa) and on the formulated particles (Sample E from Section 4.1.3 and the final emulsion formulation), as shown in Figure 4.6. Comparative analysis of the bands at 2931 $cm^{-1}$ and 2856 $cm^{-1}$, the antisymmetric and symmetric –CH2– stretching vibrations characteristic of PEI [74], confirms successful incorporation of PEI in both NP samples. However, Sample E displays markedly stronger –CH2– peaks, indicating an excess of PEI relative to PEG, whereas the final formulation shows a balanced contribution from PEG and PEI. This spectral evidence corroborates the earlier observation that the higher PEI content in Sample E led to broader particle sizes, while the optimized PEG-to-PEI ratio in the final formulation yielded a more uniform NP population.

## 4.2 Molecular interaction between PLGA NPs and albumin

The interaction between the PLGA NPs and PC formation was initially investigated using DLS, starting with BSA as a model protein. The blank PLGA NPs were formulated by emulsion technique, which had favorable size and surface charge of 100 nm and +13 mV respectively (seen in Table 4.5). Blank PLGA NPs (1 mg/mL in HEPES buffer) were incubated with 30 mg/mL BSA (also in HEPES buffer) for defined time intervals. After incubation, the mixtures were centrifuged and washed to remove unbound BSA. Given that PC formation occurs within seconds, incubation times were selected as follows: 0.5, 1.5, 2.5, 3.5, 4.5, 5.0, 9.5, 12, 16, 22, and 30 minutes.

DLS data were presented in multiple formats (Figure 4.7): Panels (a) shows the time dependent size changes of PLGA NPs incubated with BSA as a 2D color map . Panel (B) illustrates the percentage size change relative to the original blank PLGA NPs ( 100 nm). And Panel (C) reveals the dynamic change of zeta potential when NP was incubated with BSA.

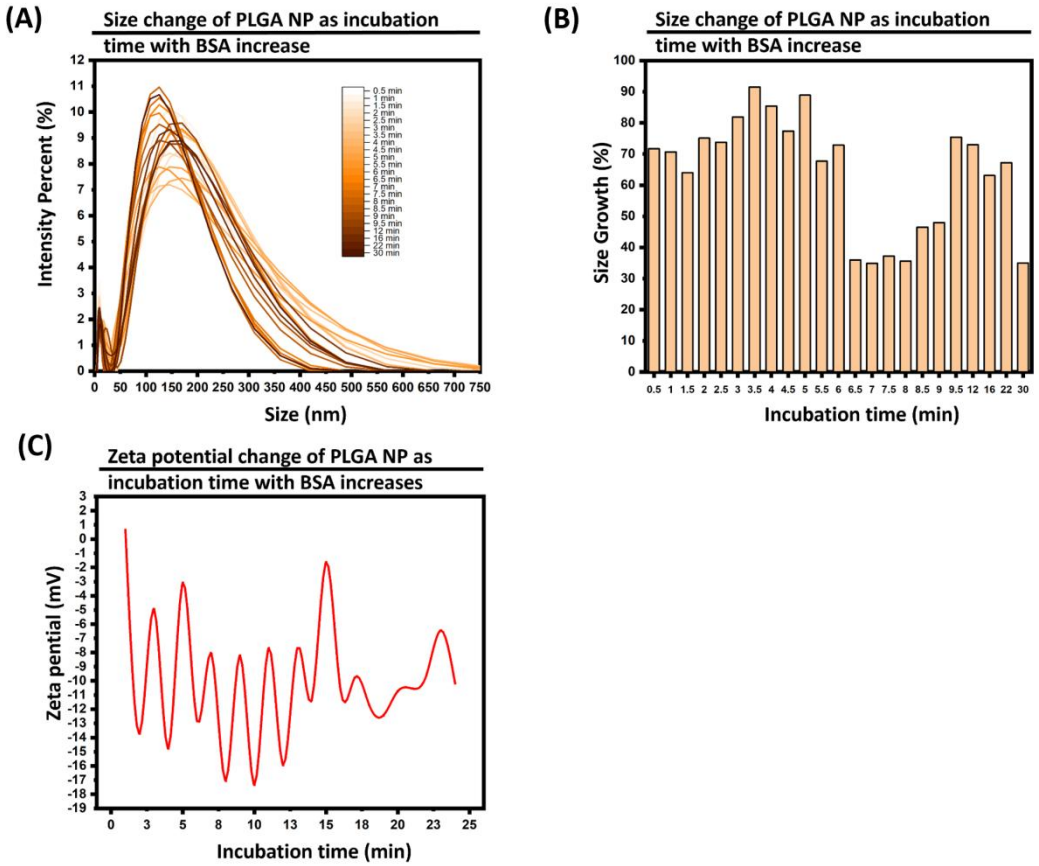


**Figure 4.7:** Molecular interaction between PLGA NPs and bovine serum albumin. (a) Size change versus incubation time, in line diagram. (b) Size growth

($\Delta S/S0 \times 100$) versus incubation time, in histogram. (c) Zeta potential change versus incubation time, in line diagram.

From the results, a 70% size increase was observed within the first 6 minutes, indicating rapid BSA adsorption. After 6 minutes, the size changes became oscillatory, with a brief decrease (6–9 minutes), followed by an increase up to 22 minutes and another decrease at 30 minutes. These observations align with previous reports indicating that PCs formation reaches saturation within seconds [62]. However, according to the Vroman effect, proteins with lower affinity but higher abundance (such as BSA) are gradually replaced by lower abundance, higher-affinity proteins over time [47]. The zeta potential variation shown in panel (d) also reflected this dynamic equilibrium; as more BSA adsorbed onto the NP surface, the surface charge became more negative [1].

Despite these insights, DLS provides only discrete time point measurements, and centrifugation is time consuming and cannot fully halt ongoing protein–NP interactions on time. Thus, DLS is not suitable for capturing real-time interactions during short incubation periods. To overcome this limitation, the Nanolyze system, which utilizes evanescent field sensing at the single-particle level, was employed to monitor BSA–NP interactions in real time.

In this setup, blank PLGA NPs were first introduced into a microfluidic chip, where some particles were trapped and visualized via light scattering microscopy. Upon injection of the BSA solution, the change in scattering intensity, corresponding to protein adsorption and resulting size increase, was detected in real time. However, due to technical difficulties in instrument setup and operation, clear visualization of BSA–NP interactions was not achieved. Further instrument refinement is required to improve data quality.

In future studies, other proteins such as fibrinogen and various serum glycoproteins (with differing abundances and binding affinities) should be investigated to better understand the complexity of PC–NP interactions, including using whole serum as a more physiologically relevant model.

# 4.3 mRNA/PAMAM-PLGA formulation.

## 4.3.1 PAMAM and Poly-A mRNA

PAMAM G5 is prone to forming hydrogen bonds and aggregating in aqueous solutions, due to the high density of amine groups and strong positive charge. Therefore, to maintain an appropriate NP size, both the choice of buffer and PAMAM concentration must be carefully optimized prior to mRNA complexation.

As shown in Figure 4.8, 0.1 mg/mL PAMAM solutions were prepared in deionized water, HEPES buffer (pH 7.4), and citrate buffer (pH 6.0). Alkaline conditions (pH > 8), which are known to reduce PAMAM particle size, were excluded from this study because mRNA is more susceptible to degradation at higher pH values [65].

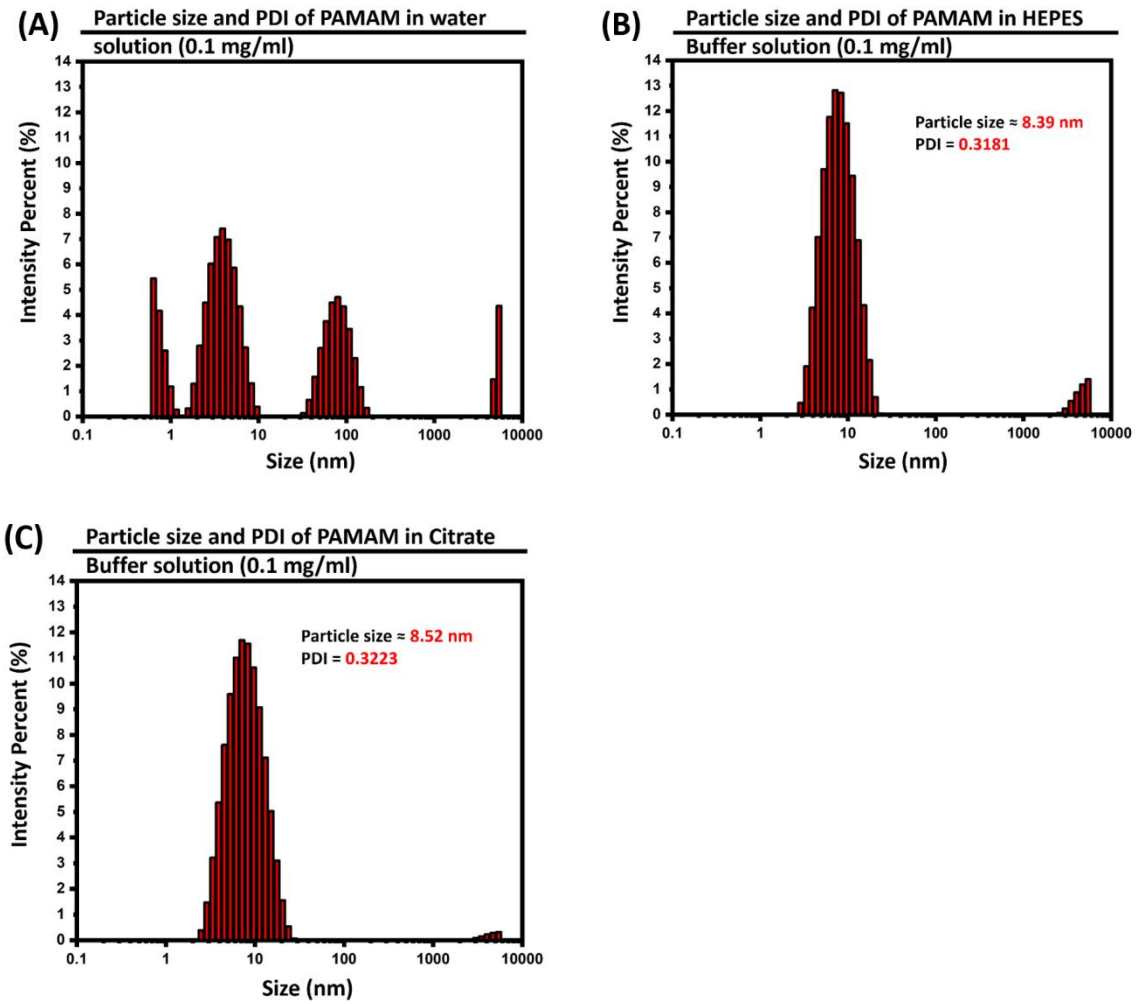


**Figure 4.8:** Behavior of PAMAM G5 in different solvents – (a) 0.1 mg/mL PAMAM G5 in water solution (b) 0.1 mg/mL PAMAM G5 in HEPES buffer pH 7.4. (c) 0.1 mg/mL PAMAM G5 in Citrate buffer pH 6.

The results demonstrated that PAMAM G5 maintained a stable size around 8 nm and showed good colloidal stability in both HEPES and citrate buffers, particularly at concentrations below 0.1 mg/mL. Given the enhanced stability of mRNA under mildly acidic conditions, citrate buffer was selected for use in subsequent formulations. Notably, although PAMAM G5 was dissolved in buffer and the concentration was kept small , it tended to form aggregation gradually and was able to maintain 8 nm for around two weeks. The long-term stability of low concentration PAMAM G5 in buffer solution requires further experiments to evaluate.

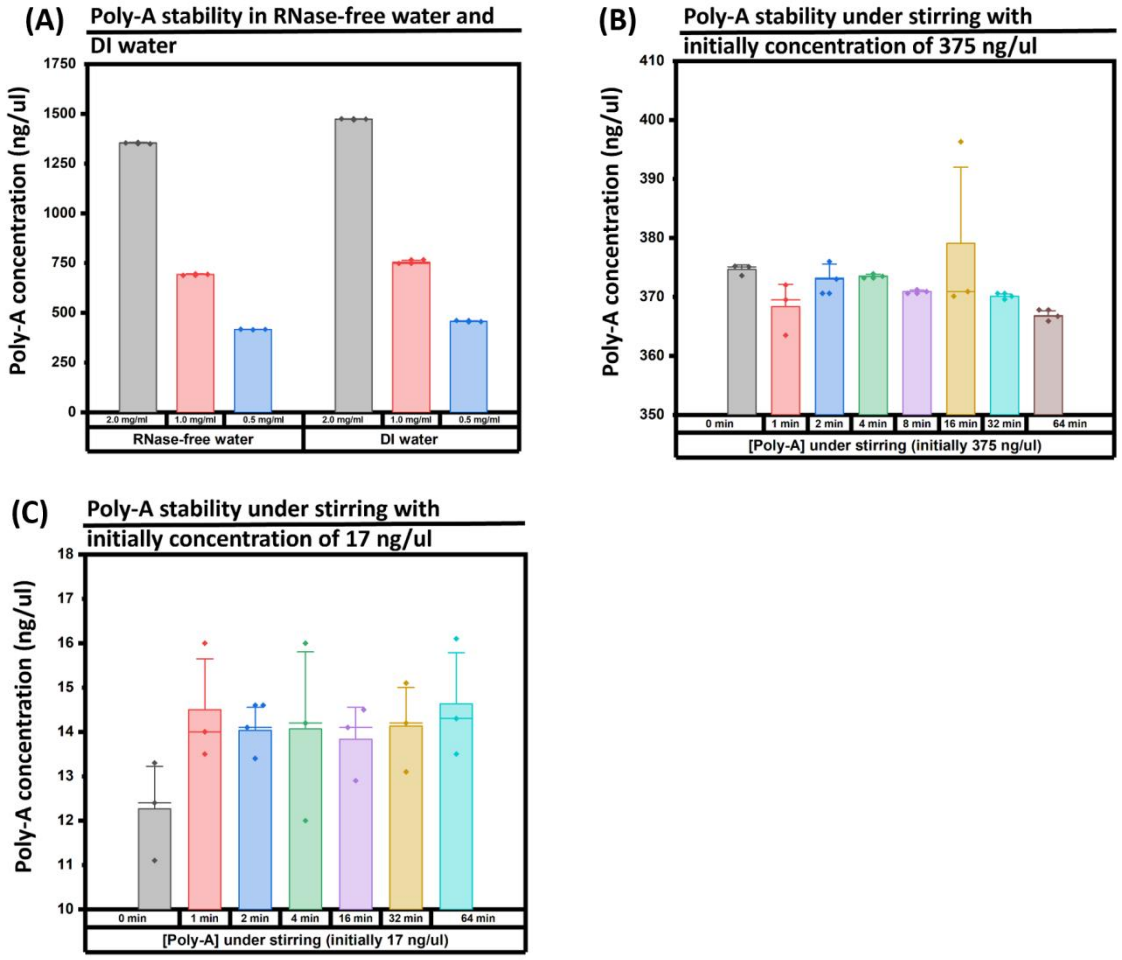


**Figure 4.9:** Poly-A stability test. (a) Poly-A stability in RNase-free water and DI water. (b) Poly-A stability under stirring ar RT within 64 min, in an initial concentration of 375 ng/ul. (c) Poly-A stability under stirring ar RT within 64 min, in an initial concentration of 17 ng/ul.

Before conducting mRNA condensation, the stability of Poly-A RNA was assessed, and the potential loss during the mRNA/PAMAM complexation process was estimated. As shown in Figure 4.9, Poly-A was dissolved in deionized water and RNase-free water at three concentrations (2.0, 1.0, and 0.5 mg/mL). The actual concentrations were measured using NanoDrop spectrophotometry, and the results indicated that the choice of solvent did not significantly affect RNA stability or cause measurable loss.

To further evaluate the impact of stirring, Poly-A solutions were prepared at 375 ng/$\mu$L and 17 ng/$\mu$L, then stirred at 500 rpm for up to 64 minutes. Concentrations were measured at time intervals of 1, 2, 4, 8, 16, 32, and 64 minutes using NanoDrop. The 17 ng/$\mu$L concentration closely reflects conditions during actual mRNA/PAMAM formulation, while 375 ng/$\mu$L was included to reduce measurement variability at low concentrations. The data showed that short-term stirring (within one hour) does not significantly degrade mRNA. However, extended stirring (24–48 hours) resulted in substantial RNA degradation, as illustrated in Table 4.9. Additionally, the functionality of mRNA after stirring was indirectly confirmed in Section 4.6 "Gene Delivery", where GFP expression was successfully observed in macrophages transfected with both GFP/PAMAM and GFP/PAMAM-PLGA complexes. However, NanoDrop measures nucleic acid concentration based on absorbance at 260 nm, detecting all mRNA fragments in solution regardless of their length. As a result, it cannot distinguish between intact and degraded mRNA. Therefore, additional analyses, such as gel electrophoresis, are necessary to assess the integrity and size distribution of mRNA before and after stirring for a more comprehensive comparison.

## 4.3.2 mRNA/PAMAM formulation

### 4.3.2.1 Poly-A/PAMAM formulation

To evaluate the impact of stirring on the colloidal properties of PAMAM G5, a 0.1 mg/mL solution was stirred at 500 rpm for 30 minutes and 30 hours, respectively. The particle sizes were subsequently measured using DLS. As shown in Figure 4.10, both samples exhibited significant aggregation. However, the sample stirred for 30 minutes displayed larger aggregates and a broader size distribution compared to the one stirred for 30 hours.

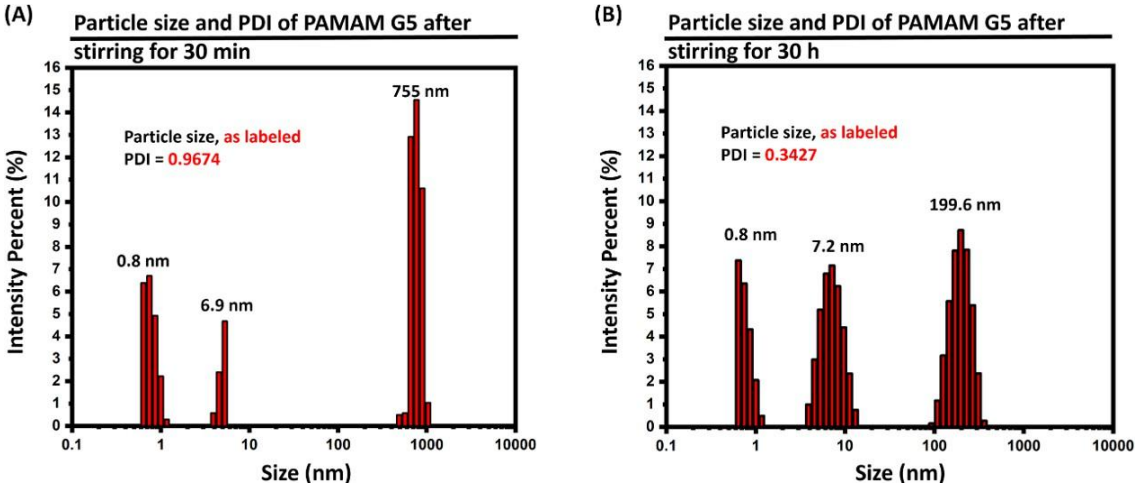


**Figure 4.10:** Size and PDI change of PAMAM G5 (0.1 mg/mL in Citrate buffer pH 6) after stirring at 500 rpm for (a) 30 min and (b) 30 h.

One possible explanation is that stirring increases the likelihood of particle collisions, leading to coagulation and breakdown of the initially stable dispersion. Dur-

ing short-term stirring, this disruption may result in the rapid formation of large aggregates. In contrast, with prolonged stirring, smaller aggregates may gradually form, and a new colloidal equilibrium could be established. It can also be hypothesized that this phenomenon becomes more pronounced at higher PAMAM concentrations. This hypothesis warrants further investigation. For example, a series of samples with increasing PAMAM concentrations could be prepared and stirred for 30 minutes and 30 hours, respectively, followed by analysis using DLS to evaluate changes in particle size and distribution.

To formulate mRNA condensed cargos with appropriate size, different preparation methods, including incubation and stirring, were compared. As shown in Table 4.6, samples prepared by incubation exhibited significant aggregation. While vortexing produced smaller particles, the results were still suboptimal. Inspired by the partial success of vortexing, stirring-based formulation was proposed and tested.

Poly-A/PAMAM complexes were prepared at an N:P molar ratio of 6:1 and stirred at room temperature for 24 and 48 hours, followed by DLS measurements. The stirred samples demonstrated improved size characteristics compared to incubation method (Figure 4.11). This led to a further investigation of stirring parameters, specifically the PAMAM to Poly-A molar ratio and stirring duration. The corresponding particle sizes and distributions are presented in Table 4.6, with detailed size distribution curves shown in Figure 4.12.

| N:P Ratio | Formulation | Temperature | Size (nm) & Percent (%) | PDI | RNA content (ng/$\mu$l, Nanodrop) |
|---|---|---|---|---|---|
| 12:1 | Incubation 15 min | RT | 2300 (32%) | / | 0 |
| 12:1 | Incubation 15 min | RT | 5000 (40%) | / | 0 |
| 12:1 | Vortexing 15 min | RT | 6 (5%); 300 (32%) | / | 0 |
| 12:1 | Vortexing 15 min | RT | 7 (5%); 370 (29%) | / | 0 |
| 6:1 | Stirring 24 h | RT | 6.8 (10%); 100 (1%) | 0.21 | / |
| 6:1 | Stirring 48 h | RT | 7.2 (12%); 100 (1%) | 0.18 | / |
| Only Poly-A | Stirring 30 min | On Ice | / | / | 14.2 |
| Only PAMAM | Stirring 30 min | On Ice | 6.9 (29.3%); 755.8 (50.2%) | 0.97 | / |
| 12:1 | Stirring 30 min | On Ice | 218.3 (100%) | 0.96 | 4.5 |
| 6:1 | Stirring 30 min | On Ice | 281.2 (100%) | 0.68 | 1.95 |
| 3:1 | Stirring 30 min | On Ice | 290.6 (100%) | 1 | 0 |
| Only Poly-A | Stirring 30 h | RT | / | / | 2.86 |
| Only PAMAM | Stirring 30 h | RT | 7.2 (36.8%); 199.6 (42.5%) | 0.34 | / |
| 12:1 | Stirring 30 h | RT | 72 (13.8%); 381 (86.1%) | 0.40 | 1.7 |
| 6:1 | Stirring 30 h | RT | 6.5 (22.1%); 419 (54%) | 0.68 | 0.7 |
| 3:1 | Stirring 30 h | RT | 6.3 (64.6%); 274.2 (13.9%) | 0.22 | 0.5 |

**Table 4.6**: Poly-A/PAMAM cargo particles synthesized under variant formulation methods.

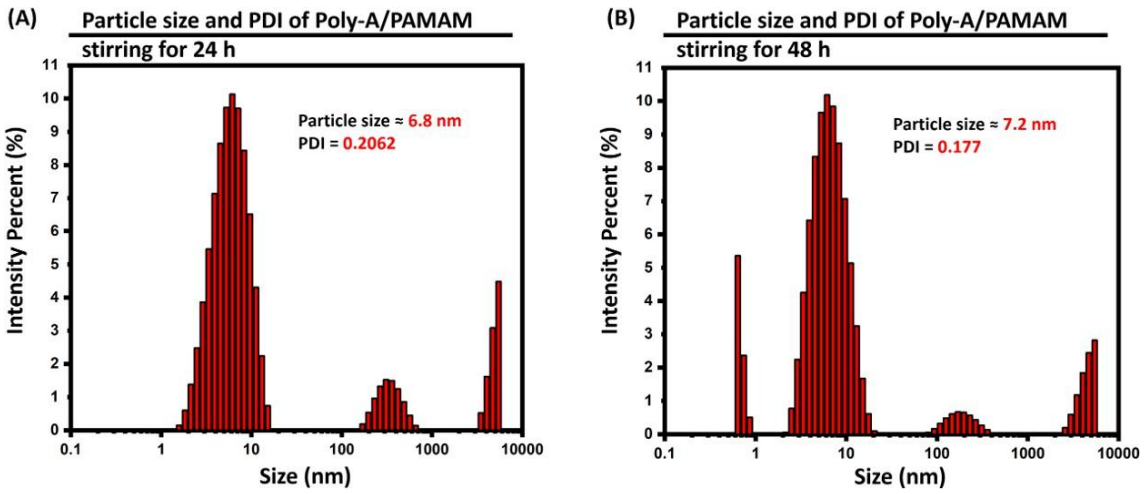


**Figure 4.11:** Poly-A/PAMAM particle size distribution after stirring for (a) 24 h and (b) 48 h during formulation.

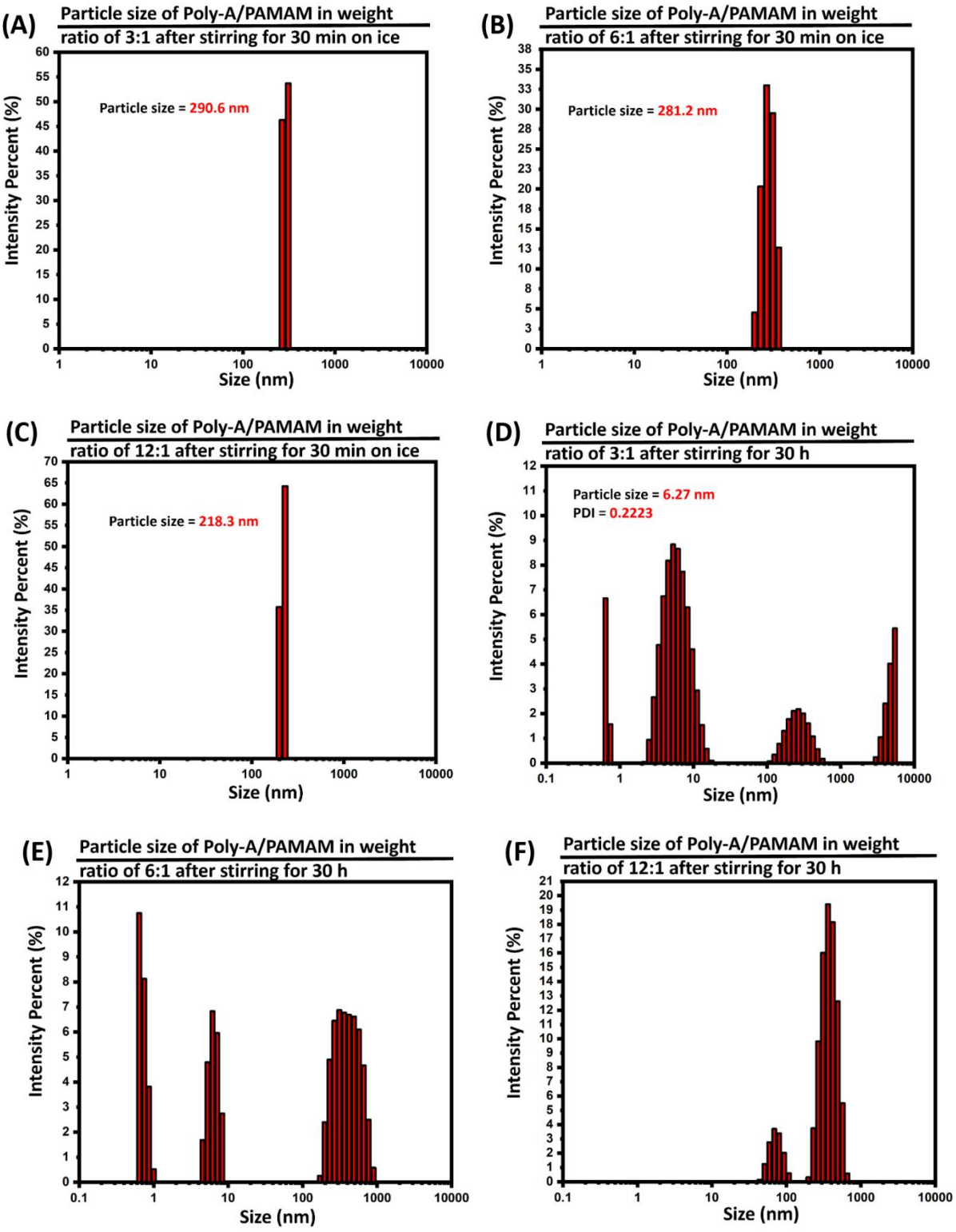


**Figure 4.12:** Poly-A/PAMAM particle size distribution under variant formulation parameters – stirring time and PAMAM : mRNA weight ratio. (a) Particle size of Poly-A/PAMAM in weight ratio of 3 : 1 after stirring for 30 min on ice. (b) Particle size of Poly-A/PAMAM in weight ratio of 6 : 1 after stirring for 30 min on ice. (c) Particle size of Poly-A/PAMAM in weight ratio of 12 : 1 after stirring for 30 min on ice. (d) Particle size of Poly-A PAMAM in weight ratio of 3 : 1 after stirring for 30

h at RT. (e) Particle size of Poly-A PAMAM in weight ratio of 6 : 1 after stirring for 30 h at RT. (f) Particle size of Poly-A PAMAM in weight ratio of 12 : 1 after stirring for 30 h at RT.

The results revealed that regardless of the N:P ratio, samples stirred for only 30 minutes exhibited pronounced aggregation and poor size distribution. In contrast, samples stirred for 30 hours showed generally improved behavior. Interestingly, when the PAMAM to mRNA molar ratio was reduced to 3:1, particle size decreased, and the proportion of particles within the favorable size range increased significantly.

This phenomenon can be explained by considering PAMAM behavior under prolonged stirring as mentioned before. Stirring increases particle collision frequency, and mRNA acts as a linker during the formation process due to electrostatic interactions between the negatively charged mRNA and positively charged PAMAM. In the early stages of stirring (e.g., 30 minutes), this leads to aggregation. However, over longer stirring duration, three mechanisms may contribute to improved size control:

Firstly, complex formation requires time to reach equilibration and stabilize into uniform structures. Secondly, repulsion is enhanced from increased mRNA binding. As the amount of mRNA increases, it binds to more PAMAM surface amines, which raises the electrostatic repulsion between complexes and helps reduce particle size. Thirdly, extended stirring (30 hours) leads to mRNA degradation, reducing free mRNA's ability to act as a "glue" that causes aggregation. This is supported by RNA content measurements in Table 4.6, where oversized complexes retained more intact mRNA, suggesting it contributed to particle aggregation.

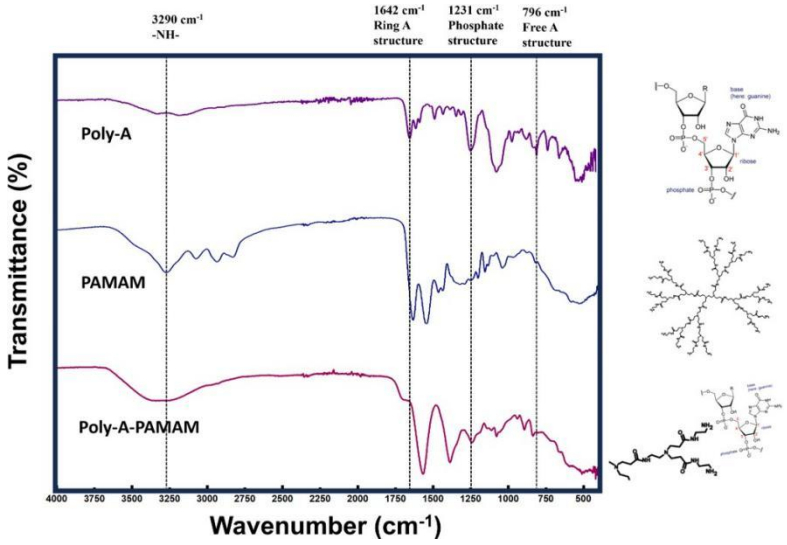


**Figure 4.13:** FTIR of Poly-A, PAMAM and Poly-A/PAMAM for comfirmation of mRNA condensation by PAMAM

The Poly-A/PAMAM sample with a 3:1 molar ratio, stirred for 30 hours, was further characterized by FTIR after freeze-drying to confirm successful mRNA condensation

into PAMAM. As shown in Figure 4.13, characteristic peaks at 1642 $cm^{-1}$, 1231 $cm^{-1}$, and 796 $cm^{-1}$, corresponding to the adenine ring structure, phosphate group, and terminal adenine in mRNA, respectively, were clearly observed in the Poly-A/PAMAM spectrum.

More importantly, the peaks originally observed at 1630 $cm^{-1}$ and 1540 $cm^{-1}$, corresponding to the -C=O- stretch and -N–H- bending in the amide bonds (-CO- NH-) of PAMAM, were shifted to 1566 $cm^{-1}$ and 1387 $cm^{-1}$, respectively. These shifts indicate strong interactions, likely hydrogen bonding and electrostatic attraction, between PAMAM and mRNA. Altogether, the FTIR analysis confirms that Poly-A was successfully condensed with PAMAM after 30 hours of stirring.

#### 4.3.2.2 GFP/PAMAM and mCherry/PAMAM formulation

The formulation of GFP/PAMAM and mCherry/PAMAM followed the same stirring method described in the previous section: using a 3:1 PAMAM-to-RNA molar ratio and stirring at room temperature for 48 hours. As shown in Table 4.7 and Figure 4.14, the resulting cargo particles were consistent with earlier formulations, exhibiting a relatively small size (8 nm) and high proportion (70%) of the desired size range. These results further demonstrate the reproducibility of the mRNA/PAMAM stirring formulation method.

| Sample Types | N:P Ratio | Formulation | Temperature | Size (nm) & Percent (%) | PDI | RNA content (ng/$\mu$l, Nanodrop) |
|---|---|---|---|---|---|---|
| Poly-A/PAMAM | 3:1 | Stirring 48 h | RT | 6.8 (55%); 4110 (15.7%) | 0.2827 | 0.26 |
| GFP/PAMAM | 3:1 | Stirring 48 h | RT | 9.6 (72%); 2598 (14.6%) | 0.3861 | 0.63 |
| mCherry/PAMAM | 3:1 | Stirring 48 h | RT | 6.5 (69.3%); 353.8 (24%) | 0.2708 | 0.76 |

**Table 4.7:** Size, PDI and mRNA contents of Poly-A/PAMAM, GFP/PAMAM and mCherry/PAMAM particles.

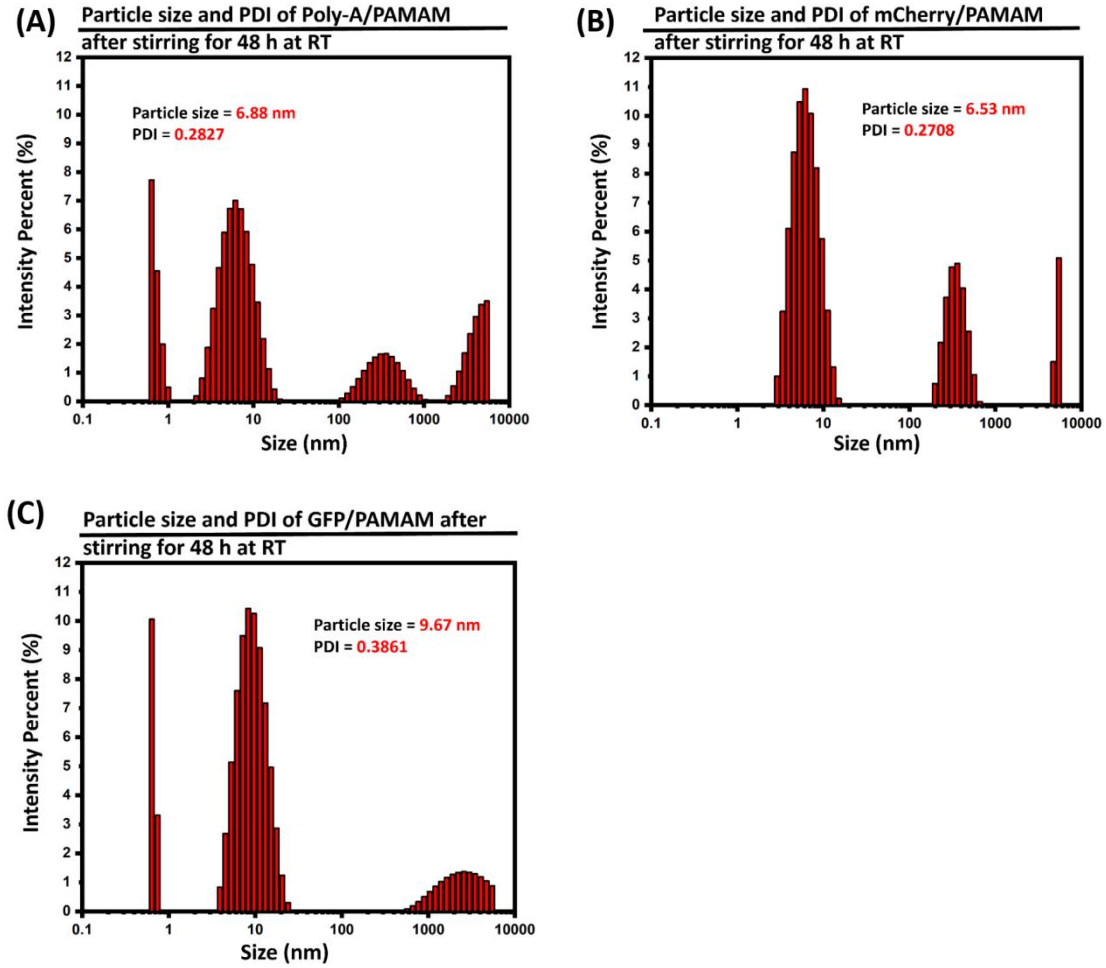


**Figure 4.14:** Particle size and PDI of (a) Poly-A/PAMAM after stirring for 48 h at RT; (b) mCherry/PAMAM after stirring for 48 h at RT; (c) GFP/PAMAM after stirring for 48 h at RT.

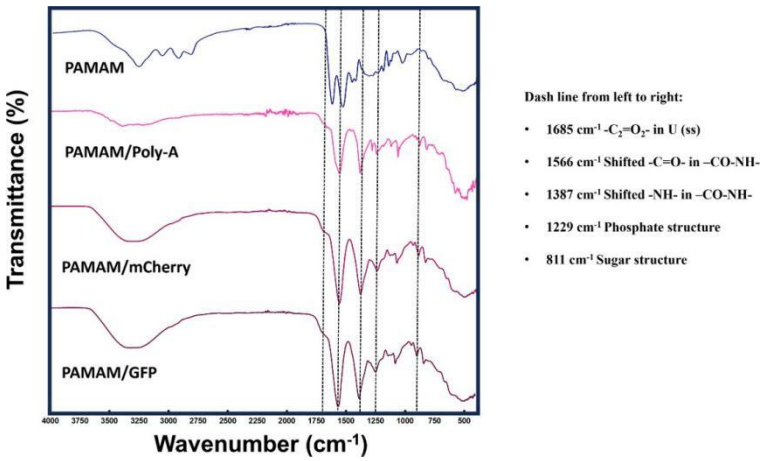


**Figure 4.15:** FTIR for comfirmation of mRNA (Poly-A, mCherry, GFP) condensation by PAMAM

The FTIR spectra of GFP/PAMAM and mCherry/PAMAM also aligned with pre-

vious results, confirming successful mRNA condensation. Specifically, the characteristic PAMAM peaks at 1630 $cm^{-1}$ (-C=O- stretch) and 1540 $cm^{-1}$ (-N–H- bending) were shifted to 1566 $cm^{-1}$ and 1387 $cm^{-1}$, respectively, indicating interaction with mRNA. Additionally, the phosphate peak at 1229 $cm^{-1}$ and the sugar structure peak at 811 $cm^{-1}$, both attributed to RNA, were clearly observed in both formulations.

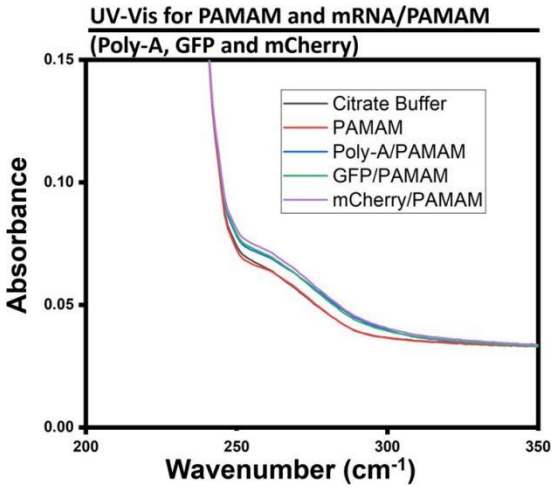


**Figure 4.16:** UV-Vis for PAMAM and mRNA/PAMAM (Poly-A, GFP and mCherry).

To further confirm condensation, UV-Vis spectrometry was performed on GFP/-PAMAM, mCherry/PAMAM, and Poly-A/PAMAM. For comparison, spectra of citrate buffer alone and PAMAM in citrate buffer were also recorded. As shown in Figure 4.16, the absorbance curve of PAMAM without mRNA closely overlapped with that of citrate buffer, indicating no significant absorption. However, in all mRNA-condensed PAMAM samples, a notable increase in absorbance between 250–320 nm was observed. Furthermore, the overlapping absorbance curves of Poly-A/PAMAM, GFP/PAMAM, and mCherry/PAMAM suggest a comparable condensation efficiency among the three formulations. This observation will be further discussed in the mRNA quantification section.

### 4.3.3 mRNA/PAMAM-PLGA NP formulation

Blank PLGA NPs were formulated using a single emulsion method. To encapsulate the hydrophilic mRNA/PAMAM cargo, a water-in-oil-in-water (w/o/w) double emulsion method was employed. For optimization, Poly-A/PAMAM was used as the model cargo. Poly-A/PAMAM-PLGA Prototype 1 was prepared using 35% amplitude for the primary emulsion and 60% for the secondary emulsion, with a formulation containing 50 $\mu$g/mL of Poly-A/PAMAM and 15 mg/mL of PLGA in DCM. In Prototype 2, the emulsion amplitudes were increased to 40% (primary) and 70% (secondary). A slight decrease in particle size was observed with the increased emulsion energy. However, both prototypes exhibited nearly neutral surface charges. This neutrality is likely due to rupture of the primary emulsion droplets and exchange of content between the internal and external aqueous phases,

caused by osmotic pressure differences resulted from the high cargo concentration [31]. To address this, the cargo and PLGA concentrations were reduced to 25 $\mu$g/mL and 5 mg/mL, respectively, in the formulation of Prototype 3. As shown in Table 4.8 and Figure 4.17, Prototype 3 displayed the desired particle size (168.5 nm) and a favorable surface charge (+13.55 mV), making it suitable for immune cell-targeted drug delivery.

| Sample Types | Size (nm) | PDI | Zeta potential (mV) |
|---|---|---|---|
| Blank NP #1 | 100 | 0.21 | 13 |
| Blank NP #2 | 111 | 0.12 | 7.5 |
| Blank NP #3 | 125 | 0.25 | 7.3 |
| Poly-A/PAMAM-PLGA Prototype 1 | 229.8 | 0.2821 | 0 |
| Poly-A/PAMAM-PLGA Prototype 1 (Dried & re-dispersed) | 212.2 | 0.3444 | +0.08 |
| Poly-A/PAMAM-PLGA Prototype 2 | 195 | 0.2229 | +0.29 |
| Poly-A/PAMAM-PLGA Prototype 3 | 168.5 | 0.3029 | +13.55 |
| GFP/PAMAM-PLGA | 217.8 | 0.2990 | +12.45 |
| mCherry/PAMAM-PLGA | 219.3 | 0.2285 | +16.75 |

**Table 4.8:** Blank PLGA NPs and mRNA/PAMAM-PLGA NPs with favorable size (100 - 200 nm), PDI (< 0.35) and zeta potential (around +12 mV).

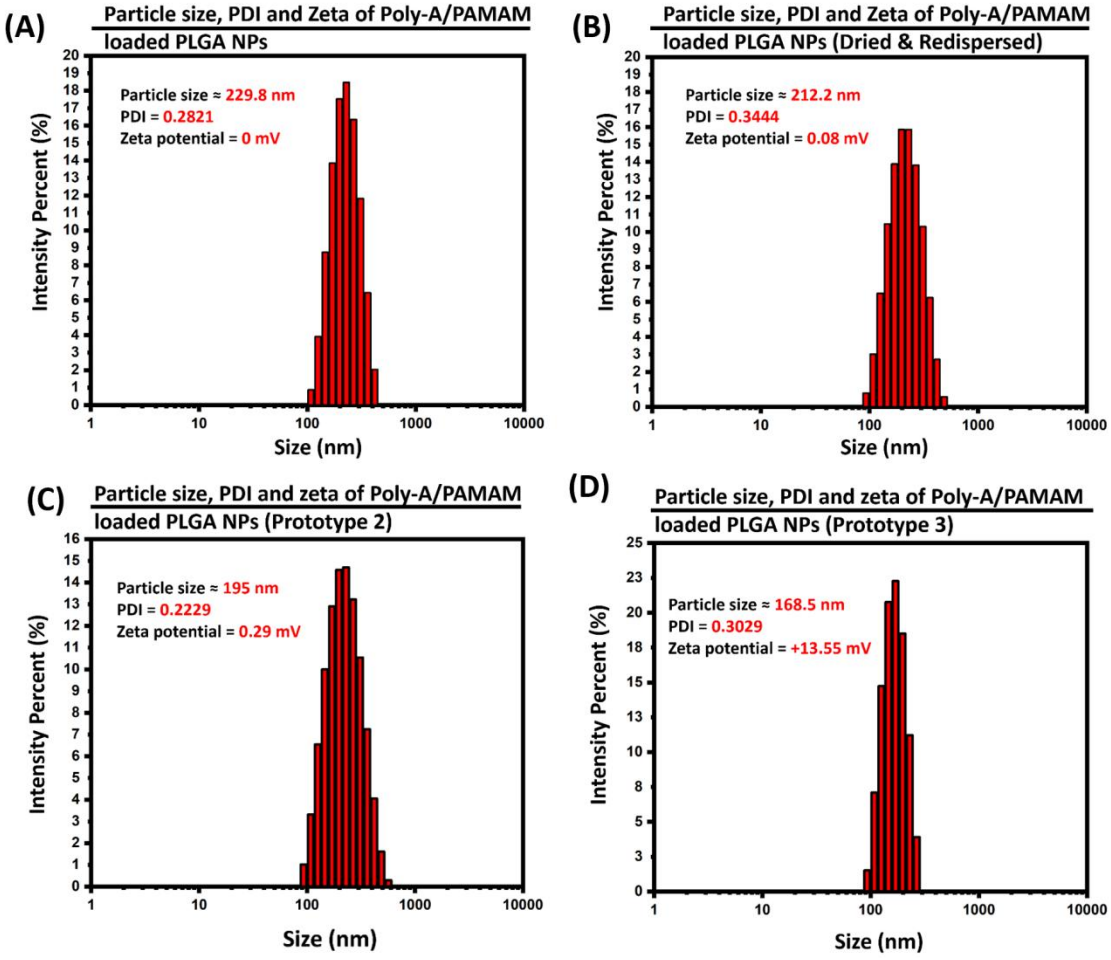

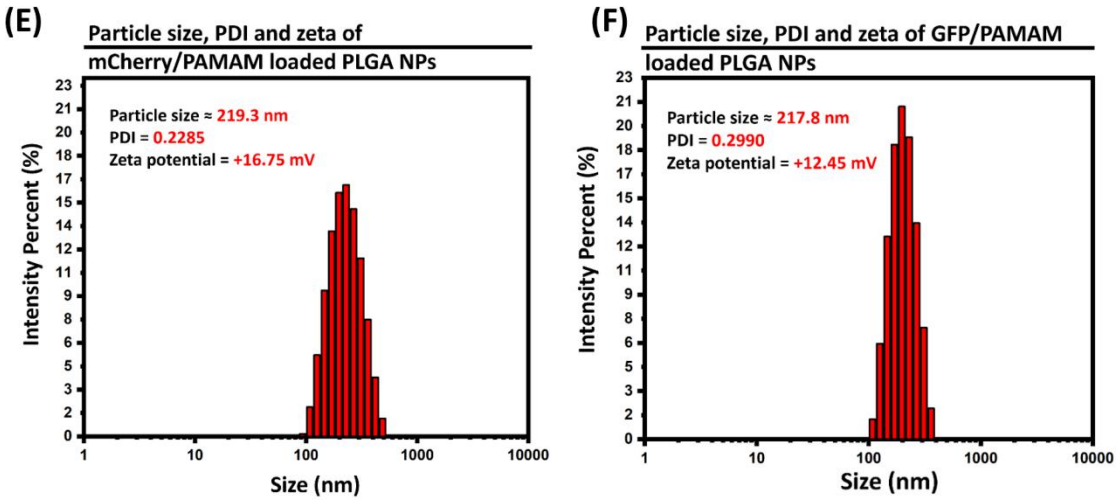


**Figure 4.17:** mRNA/PAMAM-PLGA particle size, PDI and Zeta potential under variant formulation parameters – sonication amplitude, PLGA and cargo concentrations. (a) Poly-A/PAMAM-PLGA: 30%, 5 min for primary emulsion, 60% 12 min for second emulsion, 15 mg/mL PLGA, 50 $\mu$g/mL cargo. (b) Freeze dried and re-dispersed Poly-A/PAMAM-PLGA in dPBS buffer. (c) Poly-A/PAMAM-PLGA (Sonication Amplitude changed): 40%, 5 min for primary emulsion, 75% 12 min for second emulsion, 15 mg/mL PLGA, 50 $\mu$g/mL cargo. (d) Poly-A/PAMAM-PLGA (Cargo and PLGA diluted): 40%, 5 min for primary emulsion, 75% 12 min for second emulsion, 5 mg/mL PLGA, 25 $\mu$g/mL cargo. (e) mCherry/PAMAM-PLGA: 40%, 5 min for primary emulsion, 75% 12 min for second emulsion, 5 mg/mL PLGA, 25 $\mu$g/mL cargo. (f) GFP/PAMAM-PLGA: 40%, 5 min for primary emulsion, 75% 12 min for second emulsion, 5 mg/mL PLGA, 25 $\mu$g/mL cargo.

GFP/PAMAM and mCherry/PAMAM loaded PLGA NPs were formulated using the same conditions as Prototype 3. While their surface charges remained appropriate, which indicated successful encapsulation and no leakage of internal contents, their particle sizes were relatively larger (~216 nm). This increase in size may be attributed to primary emulsion droplet enlargement, which can result from differences in the viscosity of the internal aqueous phase. Such variation could be due to the differences in RNA length between Poly-A (2100-10,000 bp), GFP (711 bp), and mCherry (769 bp), as well as differences in mRNA loading within the PAMAM complexes. However, this hypothesis requires further experimental validation. Future experiments could focus on investigating how mRNA length influences the viscosity of the internal aqueous phase and, in turn, affects the resulting PLGA NP size.

Additionally, future studies may explore the effect of parameters such as primary emulsion ampli- tude, cargo concentration, and PLGA concentration on the particle size of GFP/PAMAM- PLGA and mCherry/PAMAM-PLGA NPs.

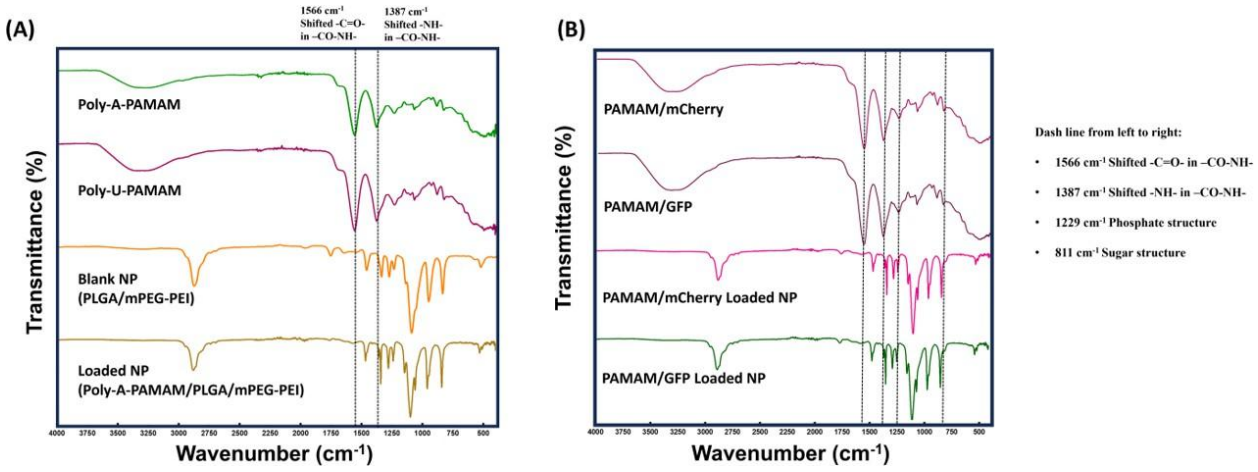


**Figure 4.18:** FTIR for mRNA/PAMAM loaded PLGA NPs. (a) for Poly-A/PAMAM-PLGA NP. (b) for mCherry/PAMAM, GFP/PAMAM loaded PLGA NPs.

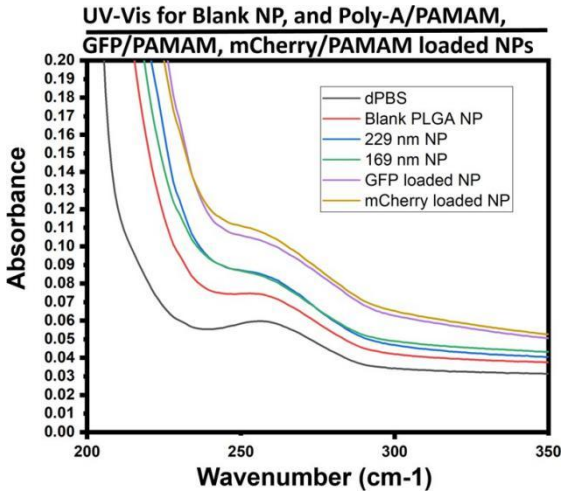


**Figure 4.19:** UV-Vis for Blank NP, and Poly-A PAMAM, GFP PAMAM, mCherry PAMAM loaded NPs

The formulated mRNA loaded NPs (Poly-A, GFP, and mCherry) were characterized using FTIR spectroscopy to confirm successful cargo encapsulation. As shown in Figure 4.18, all NP samples exhibited shifted peaks for the -C=O- stretch and -N–H- bending at 1566 $cm^{-1}$ and 1387 $cm^{-1}$, respectively. In addition, shoulder peaks at 1299 $cm^{-1}$ (phosphate groups from RNA) and 811 $cm^{-1}$ (sugar backbone structure of RNA) were observed in all NP spectra, further indicating the presence of encapsulated RNA.

To reinforce these findings, UV-Vis spectrometry was also performed. As shown in Figure 4.19, all RNA-loaded NP samples exhibited increased absorbance at 260 nm, a characteristic peak for nucleic acids, when compared to blank PLGA NPs. This confirms the successful encapsulation of mRNA/PAMAM cargos (Poly-A/PAMAM,GFP/PAMAM, and mCherry/PAMAM) into the PLGA NPs. Moreover, the higher absorbance at 260 nm from GFP and mCherry loaded NPs compared to

Poly-A loaded NPs (169 and 229 nm NP in Figure 4.19) suggests higher RNA content or greater encapsulation efficiency in these samples. The mRNA content of these NPs is further analyzed in the next section.

## 4.4 Quantification of mRNA Content and Encapsulation Efficiency

To quantify mRNA condensation efficiency by PAMAM, both Nanodrop and UV-Vis spectrometry were employed and compared. As shown in Figure 4.20, absorbance at 260 nm was measured for Poly-A at five different concentrations to construct a calibration curve. Subsequently, mRNA/PAMAM samples and Poly-A solutions were analyzed using both UV-Vis and Nanodrop, with results summarized in Table 4.9. It was found that when the mRNA concentration was below 1 $\mu$g/mL, the calibration curve became unreliable, limiting the accuracy of UV-based quantification at low concentrations. Additionally, gel electrophoresis (Figure 4.21) confirmed the absence of free mRNA in the mRNA/PAMAM complexes, indicating that all detectable absorbance at 260 nm originated from condensed mRNA within the cargo.

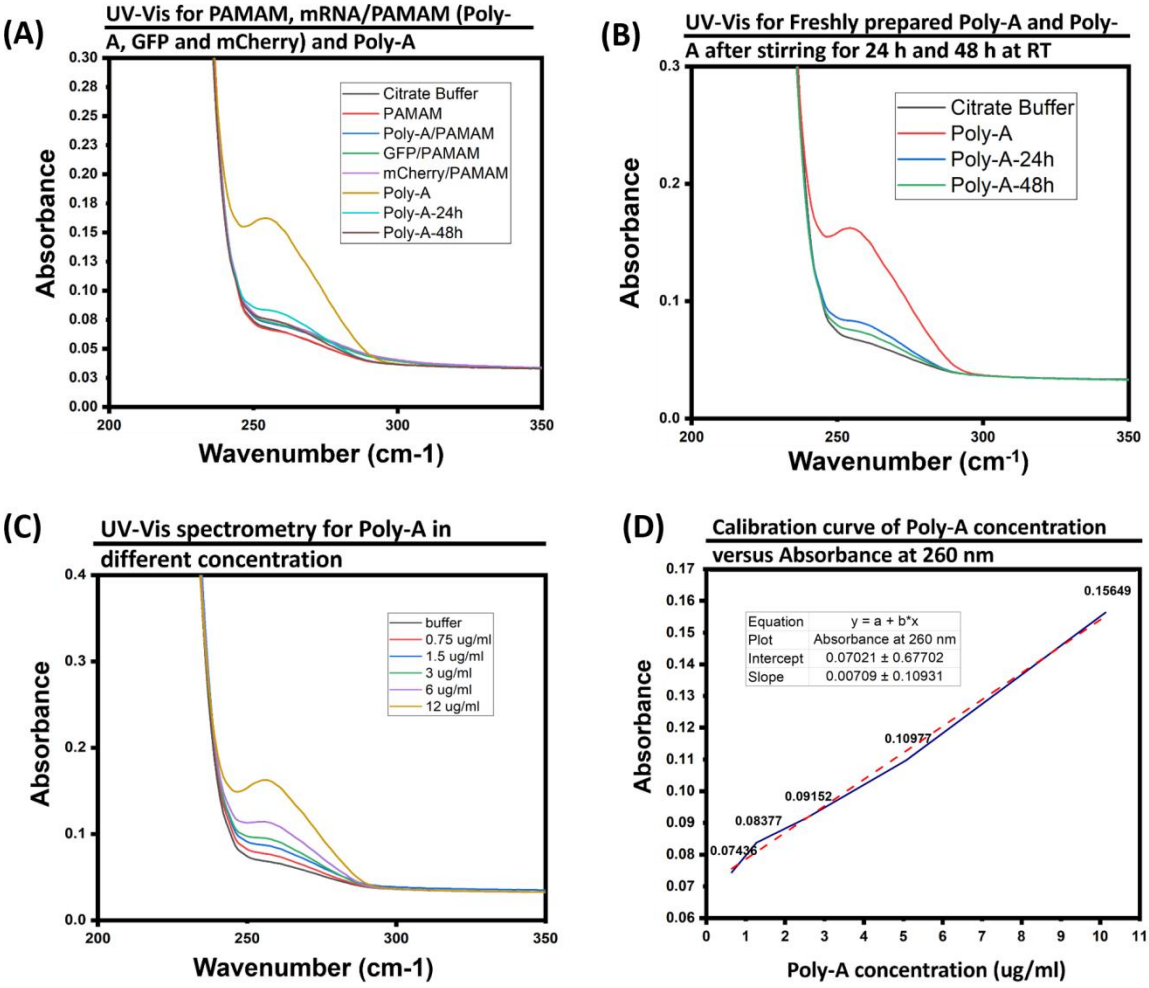


**Figure 4.20:** UV-Vis spectra and Calibration curve of Poly-A. (a) UV-Vis for PAMAM, mRNA/PAMAM (Poly-A, GFP and mCherry) and Poly-A (b) UV-Vis

for Freshly prepared Poly-A and Poly-A after stirring for 24 h and 48 h at RT. (c) UV-Vis spectrometry for Poly-A in different concentration. (b) Calibration curve of Poly-A concentration versus Absorbance at 260 nm.

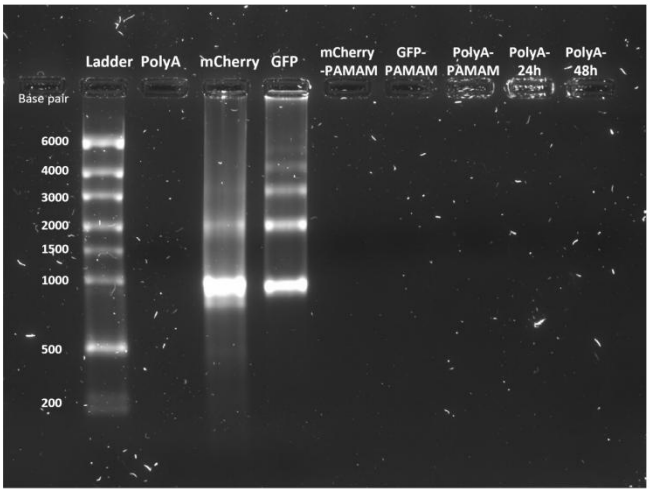


**Figure 4.21:** Agrose gel electophoresis for mRNA/PAMAM (Poly-A, GFP and mCherry) and Poly-A

In the case of Poly-A, it has been reported (as per Thermo Fisher's protocol) that a smear ranging from 6 kb to 0.5 kb typically appears under gel electrophoresis. However, in Figure 4.21, no visible band or smear was observed in the Poly-A lane. A likely explanation, considering procedural differences from the Thermo Fisher protocol, is the absence of formaldehyde in the gel preparation. Formaldehyde acts as a denaturing agent by forming Schiff bases with the amino groups of adenine, thereby preventing RNA base pairing and maintaining RNA in a denatured, linear form [75][76]. Poly-A RNA consists of a heterogeneous mixture of RNA fragments of varying lengths, up to 6,000 bp, with polyadenylated tails. Without denaturation, these RNA strands may form stable secondary structures, making them too large or compact to effectively migrate through the gel. This may explain the absence of visible Poly-A signal. Additionally, this rationale supports the presence of multiple bands in the GFP and mCherry lanes, which likely indicate the formation of base-paired secondary structures, resulting in RNA products longer than 700 bp.

| Samples | Initial mRNA Conc. by Nanodrop | mRNA Conc. after formulation by Nanodrop | Absorbance at 260 nm | mRNA wt% in mRNA/-PAMAM | mRNA Entrapment Efficiency (EE%) |
|---|---|---|---|---|---|
| Fresh prepared Poly-A | 12.3 $\mu$g/ml | / | 0.15298 | / | / |
| Poly-A stirred for 24 h | 13.8 $\mu$g/ml | 2.86 $\mu$g/ml | 0.08027 | / | / |
| Poly-A stirred for 48 h | 14.0 $\mu$g/ml | 0.93 $\mu$g/ml | 0.07244 | / | / |
| Citrate buffer | / | / | 0.06489 | / | / |
| Poly-A/PAMAM | 19.14 $\mu$g/ml | 0.26 $\mu$g/ml | 0.06974 | 0.54% | 1.36% |
| mCherry/PAMAM | 16.19 $\mu$g/ml | 0.76 $\mu$g/ml | 0.07226 | 1.57% | 4.69% |
| GFP/PAMAM | 17.14 $\mu$g/ml | 0.63 $\mu$g/ml | 0.07044 | 1.31% | 3.68% |

**Table 4.9:** mRNA quantification in different mRNA/PAMAM samples, in Nanodrop and UV-Vis

As a result, the concentration values obtained from the Nanodrop measurements were used to calculate the mRNA weight percentage in the mRNA/PAMAM complexes. Based on this analysis, approximately 5% of the input mRNA was successfully condensed by PAMAM, resulting in mRNA contents of 0.54%, 1.57%, and 1.31% in the Poly-A, mCherry, and GFP-loaded complexes, respectively. The mRNA entrapment efficiency (EE%) in PAMAM was calculated as 1.36%, 4.69%, and 3.68% for Poly-A, mCherry, and GFP, respectively.

These entrapment efficiencies were relatively low compared to previous reports. For example, Sharifnia et al. demonstrated over 73.5% mRNA entrapment using PLGA/PEI hybrid NPs [68], while McKenzie et al. reported more than 85% entrapment using ionizable LNPs [77]. However, in the case of PLGA/PEI NPs, mRNA was loaded by incubation with the cationic component in NP, which, while effective for entrapment, resulted in significantly larger particle sizes ( 606 nm), making them less suitable for drug delivery applications [68]. For LNPs, although mRNA was successfully encapsulated in 100 nm particles, the lack of protective structures limited their potential in gene therapy. Moreover, the LNP formulation process required large volumes of concentrated mRNA, leading to significant material loss during the microfluidic nanoprecipitation step [77].

Therefore, future research should focus on improving mRNA entrapment efficiency while maintaining NP sizes within an optimal range for therapeutic delivery. And for more sensitive and precise quantification in future studies, advanced techniques such as $^{31}$P NMR spectroscopy could be employed.

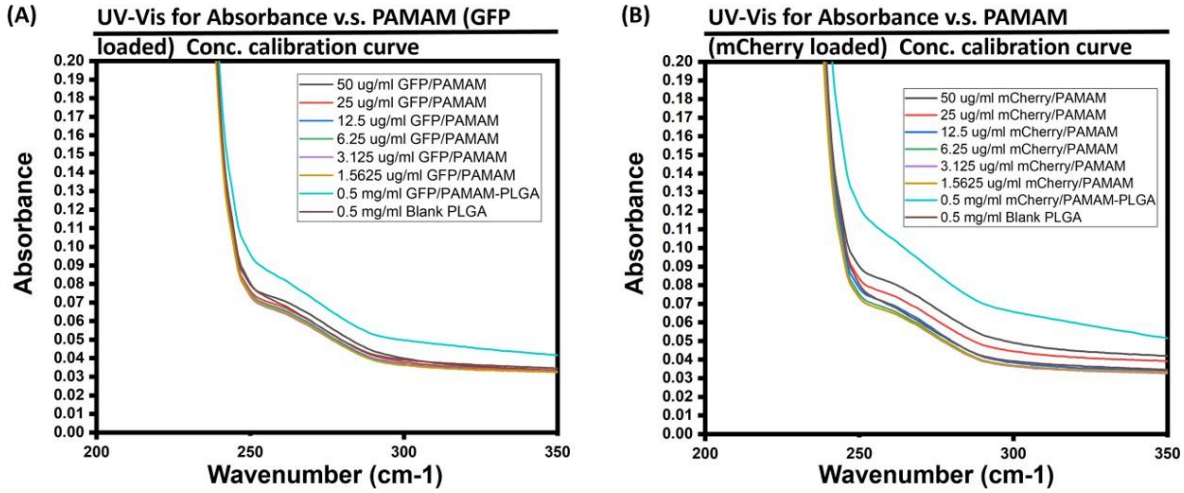


**Figure 4.22:** (a) UV-Vis for Absorbance v.s. PAMAM (GFP loaded) Conc. calibration curve. (b) UV-Vis for Absorbance v.s. PAMAM (mCherry loaded) Conc. calibration curve.

| Cargo Loaded Samples | mRNA/PAMAM Conc. Calculation | mRNA Conc. Calculation | Cargo Loading | mRNA Loading |
|---|---|---|---|---|
| GFP/PAMAM-PLGA | 118.98 $\mu$g/ml | 1.55 $\mu$g/ml | 23.79% | 0.31% |
| mCherry/PAMAM-PLGA | 112.05 $\mu$g/ml | 1.46 $\mu$g/ml | 22.41% | 0.292% |

**Table 4.10:** mRNA quantification – cargo loading and mRNA loading

To quantify cargo loading in PLGA NPs, UV-Vis spectrometry was employed by constructing a calibration curve correlating absorbance at 260 nm with known concentrations of mRNA-loaded PAMAM complexes. As shown in Figure 4.22, a series of mRNA/PAMAM samples at varying concentrations, along with 0.5 mg/mL of both blank PLGA NPs and cargo-loaded PLGA NPs, were measured. The cargo concentration encapsulated within the PLGA matrix was determined by calculating the absorbance difference at 260 nm between the blank and loaded NPs, using the established calibration curve. As summarized in Table 4.10, GFP and mCherry-loaded PLGA NPs exhibited similar overall cargo loading efficiencies of 23.79% and 22.41%, respectively. However, the actual mRNA loading in PLGA remained relatively low, at 0.31% and 0.292%. Although these values provide a preliminary estimate, the mRNA content could be more accurately quantified through mRNA extraction and direct analysis. Due to time constraints, this step was not performed in the current study.

## 4.5 Cytotoxicity Assessment of mRNA/PAMAM-PLGA Nanoparticles

The L929 fibroblast cell line was used in a resazurin assay to assess the cytotoxicity of PLGA NPs. Poly-A-loaded PLGA NPs in two sizes (229 nm and 169 nm) and blank PLGA NPs (100 nm) were prepared at six different concentrations. After 24 hours of incubation, the cell–NP mixtures were treated with resazurin solution and measured using a plate reader. Following background normalization and comparison to a blank control, the resulting cell viability at varying NP concentrations is shown in Figure 4.23.

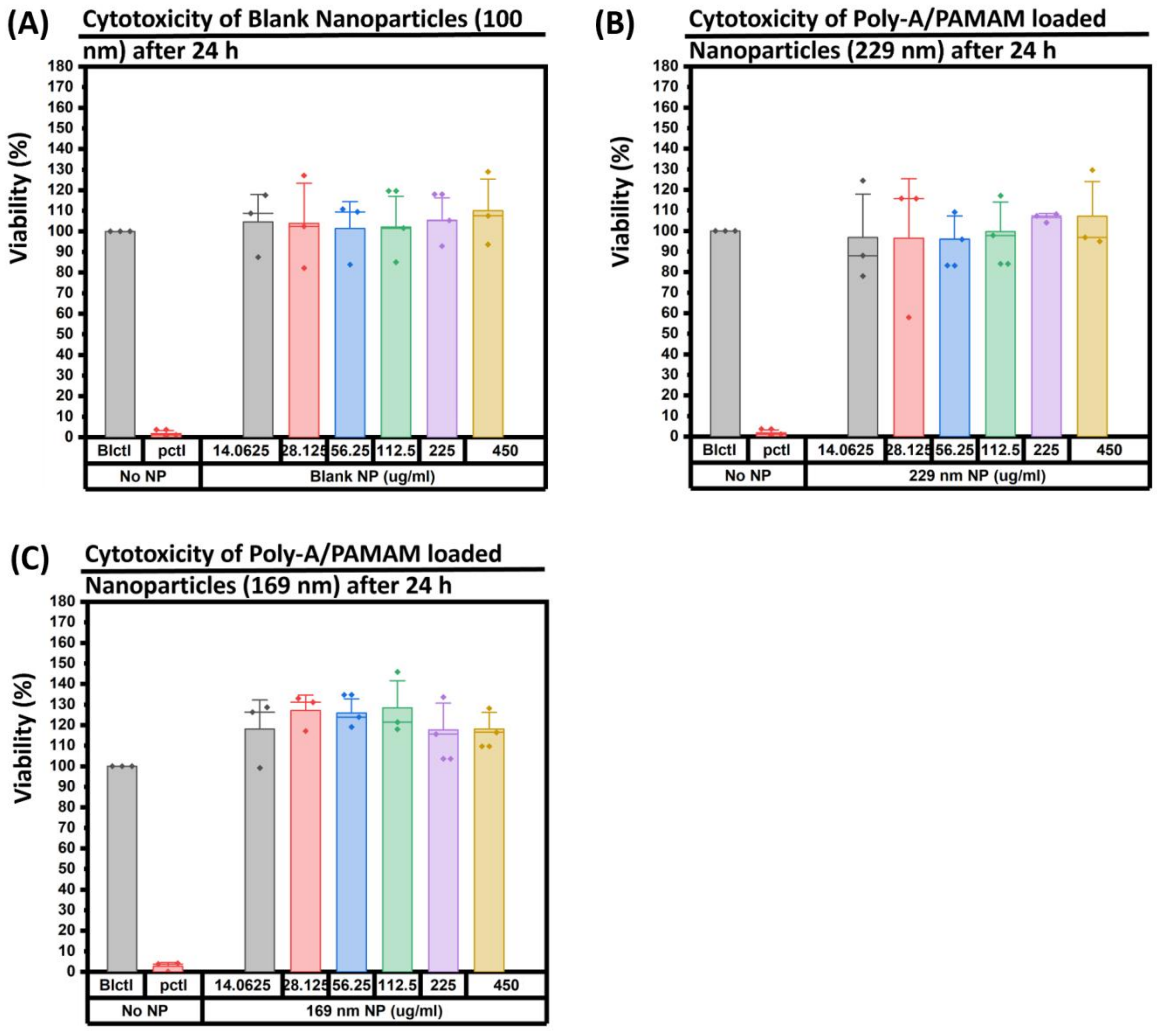


**Figure 4.23:** Cytotoxicity of (a) Blank NPs (100 nm) after 24 h; (b) Poly-A/PAMAM loaded NPs (229 nm) after 24 h; (c) Poly-A/PAMAM loaded NPs (169 nm) after 24 h.

Both the blank NPs and the 229 nm Poly-A NPs exhibited cell viability comparable to the blank control across all concentrations. Interestingly, the 169 nm Poly-A NPs demonstrated a slight enhancement in cell proliferation at all tested concentrations.

These findings confirm the low cytotoxicity and excellent biocompatibility of the formulated mRNA/PAMAM-loaded PLGA NPs toward fibroblast cells.

The cytotoxicity of the cargo and cargo loaded PLGA NPs was evaluated and compared in RAW 264.7 macrophages using the resazurin assay. Cargo samples (GFP and mCherry loaded PAMAM, 2.5 $\mu$g/mL) and cargo loaded PLGA NPs (GFP/PAMAM-PLGA and mCherry/PAMAM-PLGA, 225 $\mu$g/mL) were incubated with macrophages for 72 hours. Additionally, GFP/PAMAM-PLGA NPs were tested at three concentrations (225, 112.5, and 56.25 $\mu$g/mL) under the same incubation conditions. Cell viability was quantified using a plate reader.

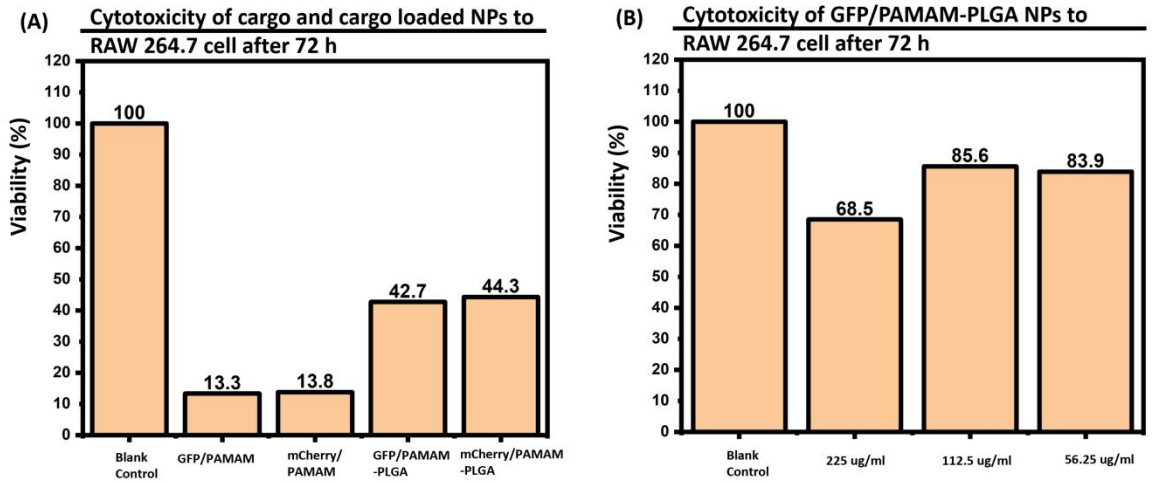


**Figure 4.24:** (a) Cytotoxicity of cargo (2.5 $\mu$g/mL) and cargo loaded NPs (225 $\mu$g/mL) to RAW 264.7 cell after 72 h. (b) Cytotoxicity of different concentration of GFP/PAMAM-PLGA NPs to RAW 264.7 cell after 72 h

As shown in Figure 4.24, macrophages treated with mRNA-PAMAM cargo alone exhibited significantly reduced viability compared to those treated with the encapsulated cargo in PLGA NPs. The PLGA encapsulation resulted in a marked reduction in cytotoxicity, with cell viability improvements ranging from 42% to maximum 85%. Moreover, the cytotoxicity of the cargo-loaded PLGA NPs showed a clear concentration dependence, as illustrated in Figure 4.24 (b).

A slight discrepancy in cell viability between the PLGA NP samples in Figures 4.24 (a) and 4.24 (b), both at 225 $\mu$g/mL, may be attributed to a technical factor: the cell culture plate in (a) was removed from the incubator for approximately 3 hours for confocal microscopy imaging. Overall, the findings are consistent with previous studies [30][31] reporting concentration-dependent cytotoxicity of PAMAM in RAW 264.7 macrophages. Furthermore, the results highlight the protective effect of PLGA encapsulation in mitigating PAMAM induced cytotoxicity.

## 4.6 Cellular Uptake Efficiency of Rhodamine-B Labeled PLGA Nanoparticles

To assess the cellular uptake of PLGA NPs in L929 fibroblasts, rhodamine B-labeled PLGA NPs (RB-NPs) were formulated. A mixture of rhodamine B-labeled PLGA (24–30 kDa) and unlabeled PLGA (7–17 kDa) was prepared at a 1:99 ratio, and the RB-NPs were produced using the same double emulsion method as previously described. The resulting RB-NPs exhibited similar size (169 nm) and surface charge (+13 mV) to those of Poly-A/PAMAM loaded NPs.

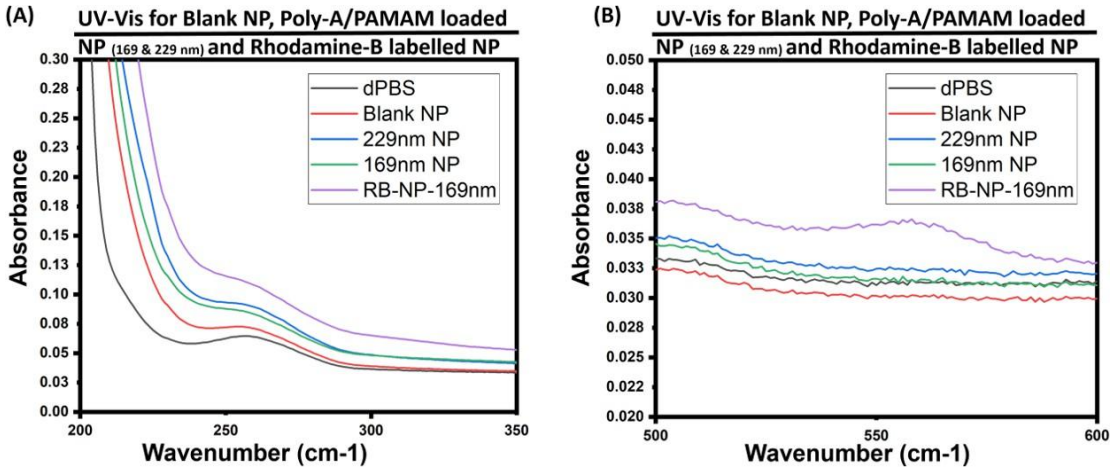


**Figure 4.25:** UV-Vis for Blank NP, Poly-A/PAMAM loaded NP (169 & 229 nm) and Rhodamine-B labelled NPs

To confirm successful labeling, UV-Vis spectrometry was performed to compare the absorbance of blank NPs, Poly-A/PAMAM loaded NPs, and RB-NPs. As shown in Figure 4.25, an absorbance peak at 566 nm was observed for the RB-NPs, confirming the successful incorporation of rhodamine B into the PLGA matrix.

To evaluate the utility of RB-NPs in quantifying cellular uptake, a calibration curve was established by measuring fluorescence intensity from six RB-NP concentrations (225, 112.5, 56.25, 28.125, and 14.0625 $\mu$g/mL) using a plate reader (Figure 4.26 (b)). For the cellular uptake study, L929 fibroblasts were incubated with 225 $\mu$g/mL of RB-NPs for 6, 12, and 24 hours, followed by fluorescence intensity measurement via plate reader.

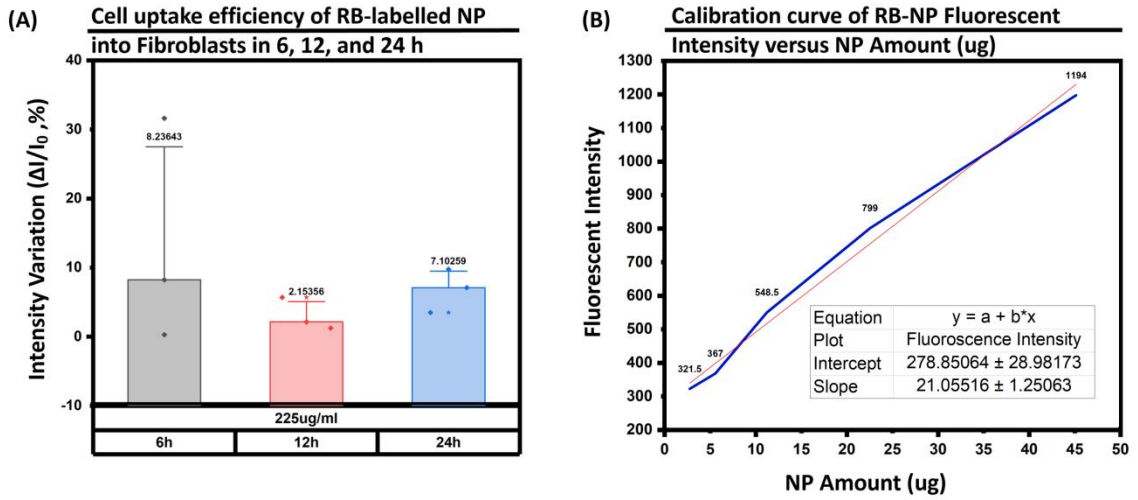


**Figure 4.26:** (a) Cell uptake efficiency of RB-labelled NP into Fibroblasts in 6, 12, and 24 h. And (b) Calibration curve of RB-NP Fluorescent Intensity versus NP Amount ($\mu$g).

As shown in Figure 4.26 (a), cells incubated for 12 and 24 hours exhibited only minor intensity increases compared to the blank control, indicating minimal uptake. Although some fluctuations were observed in the 6-hour group, the overall fluorescence intensity remained low. This may be due to initial NP–cell membrane interactions driven by their opposite surface charges. Since the calculated uptake efficiency was very low, the calibration curve method was deemed inaccurate in quantifying. However, the calibration curve proved the utility of RB-NP in cellular uptake test, though it revealed relatively low peaks at 566 nm.

In summary, the results indicate low cellular uptake of PLGA NPs in fibroblasts, which is consistent with the low cytotoxicity observed in the resazurin assay. Limited uptake likely contributes to the NPs' biocompatibility with fibroblast cells.

## 4.7 Evaluation of Gene Delivery Efficiency

To evaluate the gene delivery efficiency of mRNA-loaded PLGA NPs in immune cells, RAW 264.7 macrophages were incubated with GFP/PAMAM- PLGA NPs and mCherry/PAMAM-PLGA NPs at three concentrations (225, 112.5, and 56.25 $\mu$g/mL) for 24, 48, and 72 hours. Fluorescence intensity was measured using a plate reader to assess expression levels. For comparison, RAW 264.7 cells were also treated with bare mRNA/PAMAM complexes (GFP and mCherry) at three concentrations (2.5, 1.25, and 0.625 $\mu$g/mL) over the same time periods.

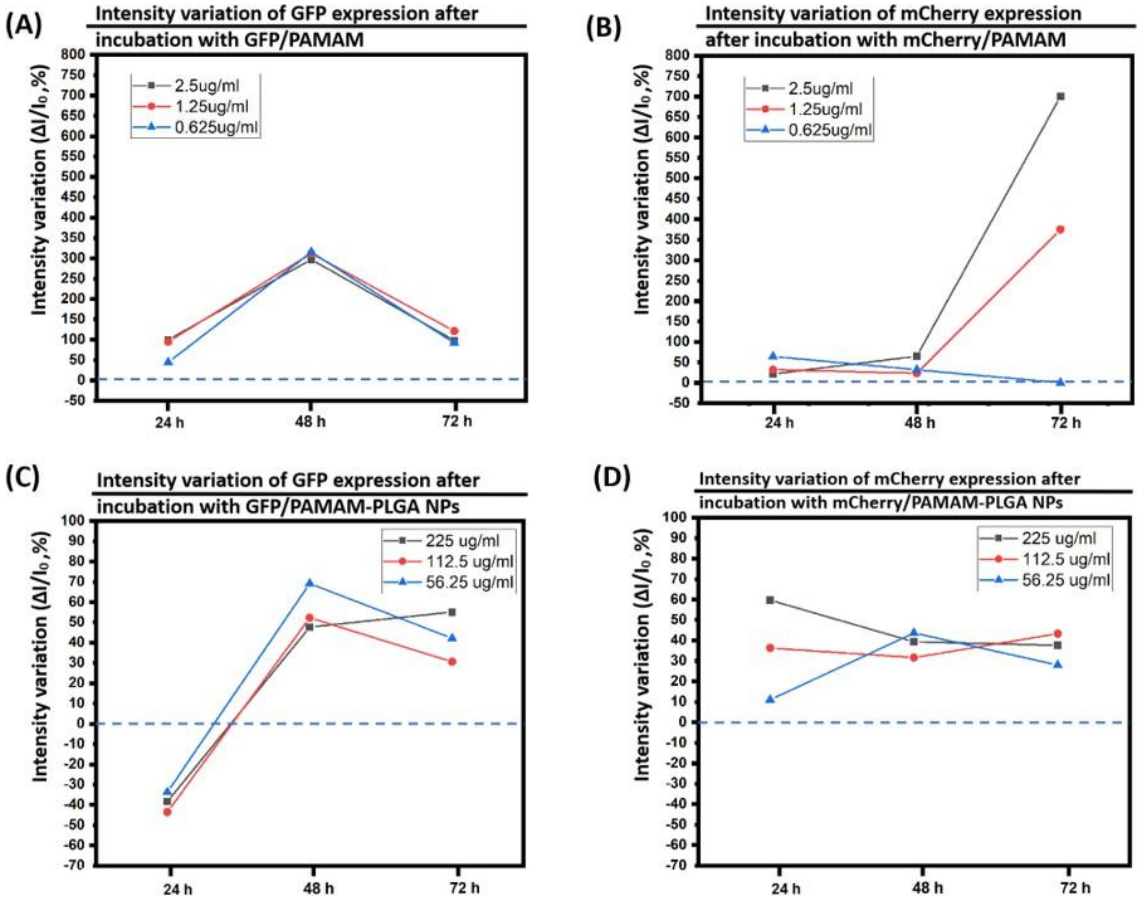


**Figure 4.27:** Gene delivery efficiency among GFP/PAMAM, mCherry/PAMAM, GFP/PAMAM-PLGA NPs and mCherry/PAMAM-PLGA NPs. (a) Intensity variation of GFP expression after incubation with GFP loaded PAMAM. (b) Intensity variation of GFP expression after incubation with mCherry loaded PAMAM. (c) Intensity variation of GFP expression after incubation with GFP/PAMAM-PLGA NPs. (b) Intensity variation of GFP expression after incubation with mCherry/PAMAM-PLGA NPs.

As shown in Figure 4.27, macrophages incubated with GFP/PAMAM exhibited GFP expression at 24, 48, and 72 hours. Notably, peak expression was observed at 48 hours, followed by a decline at 72 hours, suggesting a possible loss of viable cells due to PAMAM cytotoxicity, an effect that has been reported in the literature[30][31]

and warrants further investigation. Interestingly, no clear concentration dependence was observed in GFP/PAMAM samples. In contrast, mCherry/PAMAM showed minimal expression at 24 and 48 hours, but a noticeable, concentration dependent increase in expression was observed after 72 hours. This result aligns with the findings of Vasudevan et al. [79] and Patel et al. [80], where mCherry expression exhibited relatively low fluorescence intensity but peaked at 72 hours, reaching a maximum of approximately 2% when converted to the intensity scale used in this study. Notably, those previous studies utilized capped mCherry mRNA (either with a Cap-1 structure [79][80][81] or modified with N1-methylpseudouridine [82]) to enhance stability and expression [83]. In contrast, the mCherry mRNA used in this project was home-synthesized and uncapped. Therefore, the observation of concentration dependent expression at 72 hours strongly suggests that PAMAM condensation effectively enhanced gene delivery and provided protection for the mRNA.

When mRNA/PAMAM was encapsulated in PLGA NPs (Figure 4.27 (c), (d)), the overall fluorescence intensity was lower compared to the non-encapsulated counterparts. However, expression levels for both GFP and mCherry loaded PLGA NPs were stable and comparable after 48 and 72 hours. mRNA quantification revealed that the amount of mRNA-loaded PAMAM in 225 $\mu$g/mL of PLGA NPs was approximately 0.5 $\mu$g/mL, implying that the actual mRNA content in 112.5 and 56.25 $\mu$g/mL samples was even lower. Despite this, robust expression was still observed, particularly at later time points, indicating effective gene delivery.

Remarkably, bare mCherry/PAMAM at 0.625 $\mu$g/mL did not yield detectable expression even after 72 hours, whereas PLGA-encapsulated mCherry, with less than 0.625 $\mu$g/mL of mRNA and non-capped mCherry, successfully induced expression. This result strongly suggests that PLGA encapsulation enhances the gene delivery efficiency of mRNA/PAMAM complexes, likely by improving stability and intracellular delivery. To validate the proposed mechanism, future studies could assess in vitro mRNA release and stability from NPs. This can be achieved by incubating the NPs in a release buffer for predetermined time intervals, followed by extraction of the released mRNA [68]. The amount of released mRNA can then be quantified using UV-Vis spectrometry, while its integrity and stability can be evaluated through gel electrophoresis.

Notably, to reduce the influence of PC on gene delivery and enhance gene transfection efficacy, most researches incubated gene loaded NPs with cells in serum-free environment. For instance, Oster et al. incubated DNA/PEI-PLGA NPs with L929 fibroblasts in serum-free media, achieving a 9-fold higher transfection efficiency compared to DNA/PEI complexes and a 41,000-fold increase over naked DNA delivery [84]. Similarly, Benfer et al. synthesized siRNA-loaded PVA-PLGA NPs and incubated them with serum-deprived H1299-EGFP cells, resulting in 70% GFP knockdown efficiency [85]. Jo et al. demonstrated that CRISPR plasmid-loaded PLGA NPs incubated with macrophages in plain DMEM led to fluorescence in 95% of 10,000 cells after 24 hours, as observed by imaging cytometry [86]. In contrast, this project incubated mRNA/PAMAM-PLGA NPs with L929 fibroblasts and RAW 264.7 macrophages in complete DMEM containing 10% FBS. Despite the potential interference of serum-induced PC formation and the use of non-capped mCherry mRNA, the successful and sustained expression of both GFP and mCherry

following PLGA encapsulation highlights the enhanced gene delivery capability of the formulated NPs.

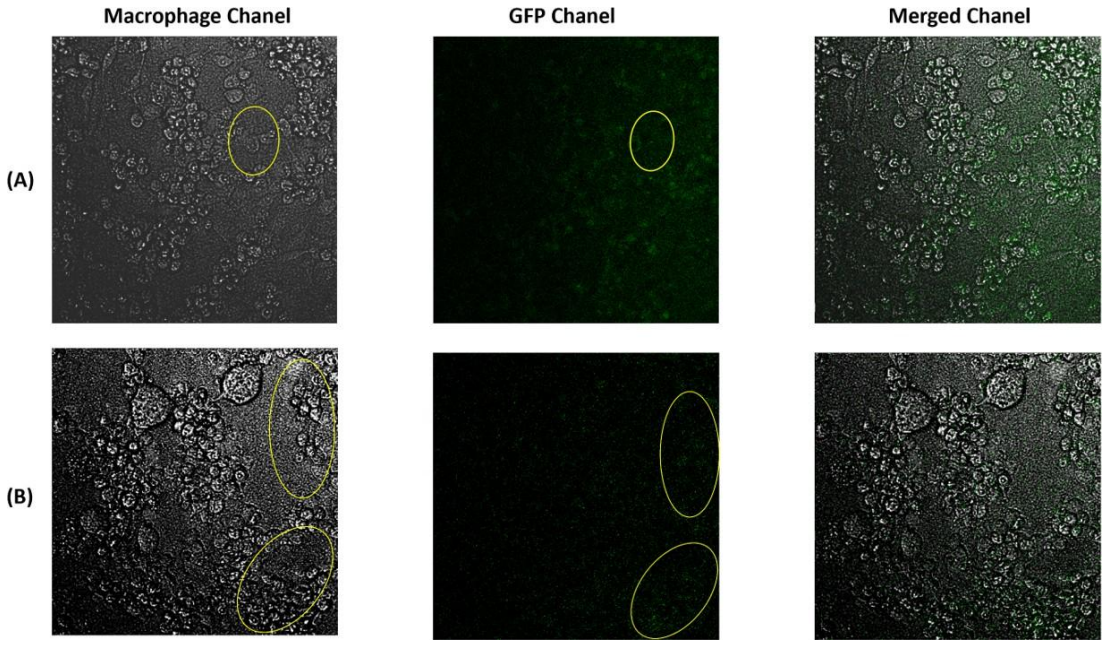


**Figure 4.28:** Confocal microscopy on RAW 264.7 macrophage when incubated with (a) 2.5 $\mu$g/mL mCherry loaded PAMAM and (b) 225 $\mu$g/mL mCherry/PAMAM- PLGA NPs, for 48 hours.

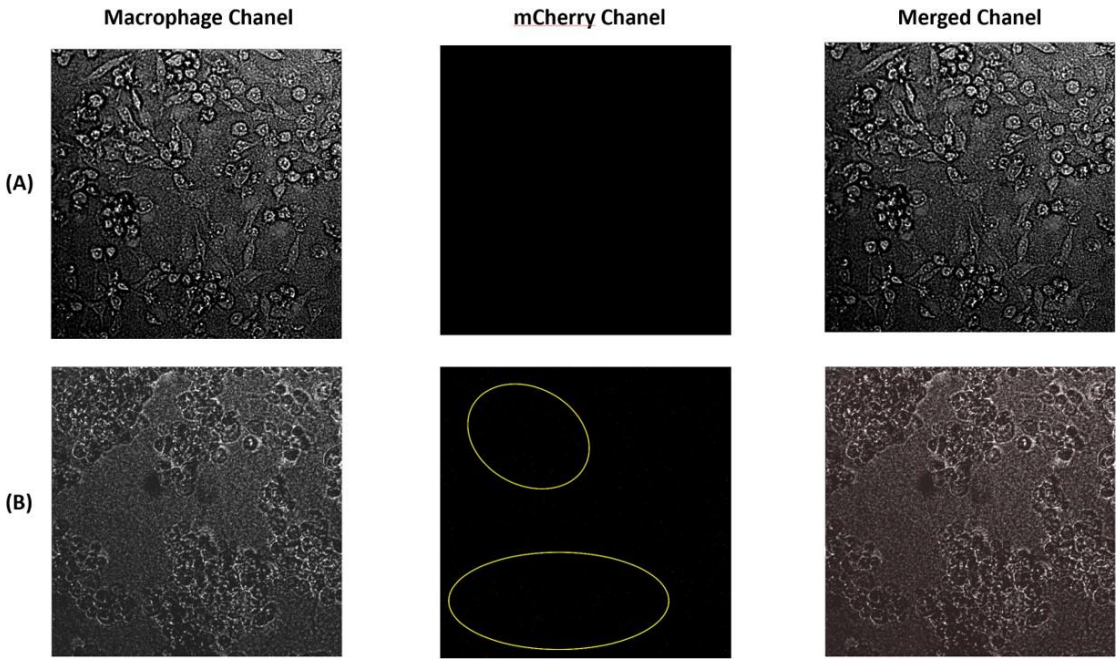


**Figure 4.29:** Confocal microscopy on RAW 264.7 macrophage when incubated with (a) 2.5 $\mu$g/mL GFP loaded PAMAM and (b) 225 $\mu$g/mL GFP/PAMAM-PLGA NPs, for 48 hours.

Moreover, gene delivery efficiency was further assessed using confocal microscopy. RAW 264.7 macrophages were incubated with cargo samples (GFP and mCherry

loaded PAMAM, 2.5 $\mu$g/mL) and cargo loaded PLGA NPs (GFP/PAMAM-PLGA and mCherry/PAMAM-PLGA, 225 $\mu$g/mL) for 72 hours, followed by imaging under both bright field and fluorescence modes. As shown in Figures 4.28 and 4.29, the results were consistent with previous findings: encapsulation of mRNA loaded PAMAM within PLGA NPs enhanced gene delivery efficiency and expression stability. Although the fluorescence intensity of the encapsulated samples was slightly reduced compared to unencapsulated cargo, the overall expression was more stable and sustained. Lastly, the negative fluorescence values observed for GFP/PAMAM-PLGA NPs after 24 hours may be attributed to cell death, potentially caused by early intracellular release of GFP/PAMAM complexes.

# 5

# Conclusion

In this thesis, we explored the development and optimization of PLGA based polymeric NPs for mRNA delivery, with the long-term objective of enabling glycosylation modulation through gene delivery. A series of mRNA loaded NPs were successfully formulated using a PAMAM based condensation strategy and encapsulated within PLGA matrices via a modified emulsion method. Comprehensive characterization revealed that the formulated mRNA/PAMAM-PLGA NPs exhibited favorable size distribution, surface charge, and stability. FTIR and UV–Vis spectroscopy confirmed successful encapsulation of various mRNA cargos (Poly-A, GFP, and mCherry loaded PAMAM), while encapsulation efficiency and cargo loading were quantitatively assessed through absorbance calibration curves and validated using Nanodrop and gel electrophoresis. Although the overall mRNA loading remained low (0.3%), PAMAM effectively condensed 5% of input mRNA, enabling measurable gene delivery performance.

Biocompatibility assessment using L929 fibroblasts demonstrated negligible cytotoxicity across multiple NP concentrations and sizes. Rhodamine-B labeled PLGA NPs were successfully synthesized and utilized to track cellular uptake in fibroblasts. Results revealed limited NPs internalization, consistent with the low cytotoxicity observed.

Encouragingly, in RAW 264.7 macrophages, both GFP and mCherry loaded NPs enabled gene expression over time, with strongest signals observed after 48 hours. Despite the low mRNA content in NPs, expression was detectable and in some cases even exceeded that of bare mRNA/PAMAM complexes, indicating improved stability and delivery efficiency. Notably, encapsulation enhanced transfection consistency and mitigated PAMAM induced cytotoxicity.

To understand biological interface behavior, initial PC studies were conducted using BSA as a model protein. DLS results illustrated dynamic, time dependent protein adsorption on NP surfaces. Although real-time monitoring via evanescent field sensing (Nanolyze) encountered technical difficulties, this approach holds strong potential for future mechanistic studies.

Overall, this work established a reproducible framework for fabricating and characterizing PLGA based mRNA delivery NPs, while demonstrating their potential for gene delivery in immune cells. These findings lay foundational groundwork for future functional studies aiming to modulate cellular glycosylation via mRNA delivery. Further investigations involving targeted mRNA cargos, higher loading efficiency, and glycosylation pathway analysis will be essential to fully realize the therapeutic potential of these polymeric NPs.

# Bibliography


[1] C. C. Fleischer and C. K. Payne, "Nanoparticle–cell interactions: molecular structure of the protein corona and cellular outcomes," *Accounts of chemical research*, vol. 47, no. 8, pp. 2651–2659, 2014.

[2] J. C. Kaczmarek, P. S. Kowalski, and D. G. Anderson, "Advances in the delivery of rna therapeutics: from concept to clinical reality," *Genome medicine*, vol. 9, pp. 1–16, 2017.

[3] M. A. Islam, E. K. Reesor, Y. Xu, H. R. Zope, B. R. Zetter, and J. Shi, "Biomaterials for mrna delivery," *Biomaterials science*, vol. 3, no. 12, pp. 1519–1533, 2015.

[4] C.-H. Wong, "Protein glycosylation: new challenges and opportunities," *The Journal of organic chemistry*, vol. 70, no. 11, pp. 4219–4225, 2005.

[5] A. Albanese, P. S. Tang, and W. C. Chan, "The effect of nanoparticle size, shape, and surface chemistry on biological systems," *Annual review of biomedical engineering*, vol. 14, no. 1, pp. 1–16, 2012.

[6] B. H. Honig, W. L. Hubbell, and R. F. Flewelling, "Electrostatic interactions in membranes and proteins," *Annual review of biophysics and biophysical chemistry*, vol. 15, no. 1, pp. 163–193, 1986.

[7] N. B. Tsui, E. K. Ng, and Y. D. Lo, "Stability of endogenous and added rna in blood specimens, serum, and plasma," *Clinical chemistry*, vol. 48, no. 10, pp. 1647–1653, 2002.

[8] J. Houseley and D. Tollervey, "The many pathways of rna degradation," *Cell*, vol. 136, no. 4, pp. 763–776, 2009.

[9] R. E. McKenzie, J. J. Minnell, M. Ganley, G. F. Painter, and S. L. Draper, "mrna synthesis and encapsulation in ionizable lipid nanoparticles," *Current Protocols*, vol. 3, no. 9, p. e898, 2023.

[10] R. W. Malone, P. L. Felgner, and I. M. Verma, "Cationic liposome-mediated rna transfection." *Proceedings of the National Academy of Sciences*, vol. 86, no. 16, pp. 6077–6081, 1989.

[11] O. S. Fenton, K. J. Kauffman, J. C. Kaczmarek, R. L. McClellan, S. Jhunjhunwala, M. W. Tibbitt, M. D. Zeng, E. A. Appel, J. R. Dorkin, F. F. Mir *et al.*, "Synthesis and biological evaluation of ionizable lipid materials for the in vivo delivery of messenger rna to b lymphocytes," *Advanced Materials*, vol. 29, no. 33, p. 1606944, 2017.

[12] B. Scheel, R. Teufel, J. Probst, J.-P. Carralot, J. Geginat, M. Radsak, D. Jarrossay, H. Wagner, G. Jung, H.-G. Rammensee *et al.*, "Toll-like receptor-dependent activation of several human blood cell types by protamine-condensed mrna," *European journal of immunology*, vol. 35, no. 5, pp. 1557–1566, 2005.

[13] A. Salvati, A. S. Pitek, M. P. Monopoli, K. Prapainop, F. B. Bombelli, D. R. Hristov, P. M. Kelly, C. Åberg, E. Mahon, and K. A. Dawson, "Transferrin-functionalized nanoparticles lose their targeting capabilities when a biomolecule corona adsorbs on the surface," *Nature nanotechnology*, vol. 8, no. 2, pp. 137–143, 2013.

[14] S. Yousefi Adlsadabad, J. W. Hanrahan, and A. Kakkar, "mrna delivery: Challenges and advances through polymeric soft nanoparticles," *International Journal of Molecular Sciences*, vol. 25, no. 3, p. 1739, 2024.

[15] Y. Bae, S. J. Song, J. Y. Mun, K. S. Ko, J. Han, and J. S. Choi, "Apoptin gene delivery by the functionalized polyamidoamine (pamam) dendrimer modified with ornithine induces cell death of hepg2 cells," *Polymers*, vol. 9, no. 6, p. 197, 2017.

[16] F. Joubert, M. J. Munson, A. Sabirsh, R. M. England, M. Hemmerling, C. Alexander, and M. B. Ashford, "Precise and systematic end group chemistry modifications on pamam and poly (l-lysine) dendrimers to improve cytosolic delivery of mrna," *Journal of Controlled Release*, vol. 356, pp. 580–594, 2023.

[17] C.-K. Chen, P.-K. Huang, W.-C. Law, C.-H. Chu, N.-T. Chen, and L.-W. Lo, "Biodegradable polymers for gene-delivery applications," *International journal of nanomedicine*, pp. 2131–2150, 2020.

[18] Y. Chavan, S. Tambe, D. Jain, S. Khairnar, and P. Amin, "Redefining the importance of polylactide-co-glycolide acid (plga) in drug delivery," in *Annales Pharmaceutiques Françaises*, vol. 80, no. 5. Elsevier, 2022, pp. 603–616.

[19] W. Yang, L. Mixich, E. Boonstra, and H. Cabral, "Polymer-based mrna delivery strategies for advanced therapies," *Advanced Healthcare Materials*, vol. 12, no. 15, p. 2202688, 2023.

[20] X. Cai, R. Dou, C. Guo, J. Tang, X. Li, J. Chen, and J. Zhang, "Cationic polymers as transfection reagents

for nucleic acid delivery," *Pharmaceutics*, vol. 15, no. 5, p. 1502, 2023.

[21] Y. Jin, F. Adams, J. Möller, L. Isert, C. M. Zimmermann, D. Keul, and O. M. Merkel, "Synthesis and application of low molecular weight pei-based copolymers for sirna delivery with smart polymer blends," *Macromolecular bioscience*, vol. 23, no. 2, p. 2200409, 2023.

[22] B. A. Smith and C. R. Bertozzi, "The clinical impact of glycobiology: targeting selectins, siglecs and mammalian glycans," *Nature reviews Drug discovery*, vol. 20, no. 3, pp. 217–243, 2021.

[23] M. He, X. Zhou, and X. Wang, "Glycosylation: mechanisms, biological functions and clinical implications," *Signal Transduction and Targeted Therapy*, vol. 9, no. 1, p. 194, 2024.

[24] S. Wan, P. M. Kelly, E. Mahon, H. Stockmann, P. M. Rudd, F. Caruso, K. A. Dawson, Y. Yan, and M. P. Monopoli, "The "sweet" side of the protein corona: effects of glycosylation on nanoparticle–cell interactions," *ACS nano*, vol. 9, no. 2, pp. 2157–2166, 2015.

[25] Y. Miao, L. Li, Y. Wang, J. Wang, Y. Zhou, L. Guo, Y. Zhao, D. Nie, Y. Zhang, X. Zhang *et al.*, "Regulating protein corona on nanovesicles by glycosylated polyhydroxy polymer modification for efficient drug delivery," *Nature Communications*, vol. 15, no. 1, p. 1159, 2024.

[26] S. R. Pardeshi, A. Nikam, P. Chandak, V. Mandale, J. B. Naik, and P. S. Giram, "Recent advances in plga based nanocarriers for drug delivery system: a state of the art review," *International journal of polymeric materials and polymeric biomaterials*, vol. 72, no. 1, pp. 49–78, 2023.

[27] S. Werth, B. Urban-Klein, L. Dai, S. Höbel, M. Grzelinski, U. Bakowsky, F. Czubayko, and A. Aigner, "A low molecular weight fraction of polyethylenimine (pei) displays increased transfection efficiency of dna and sirna in fresh or lyophilized complexes," *Journal of controlled release*, vol. 112, no. 2, pp. 257–270, 2006.

[28] Z. Zhong, J. Feijen, M. C. Lok, W. E. Hennink, L. V. Christensen, J. W. Yockman, Y.-H. Kim, and S. W. Kim, "Low molecular weight linear polyethylenimine-b-poly (ethylene glycol)-b-polyethylenimine triblock copolymers: synthesis, characterization, and in vitro gene transfer properties," *Biomacromolecules*, vol. 6, no. 6, pp. 3440–3448, 2005.

[29] F.-W. Huang, H.-Y. Wang, C. Li, H.-F. Wang, Y.-X. Sun, J. Feng, X.-Z. Zhang, and R.-X. Zhuo, "Pegylated pei-based biodegradable polymers as non-viral gene vectors," *Acta biomaterialia*, vol. 6, no. 11, pp. 4285–4295, 2010.

[30] J.-h. S. Kuo, M.-s. Jan, and H. W. Chiu, "Mechanism of cell death induced by cationic dendrimers in raw 264.7 murine macrophage-like cells," *Journal of pharmacy and pharmacology*, vol. 57, no. 4, pp. 489–495, 2005.

[31] A. Janaszewska, J. Lazniewska, P. Trzepiński, M. Marcinkowska, and B. Klajnert-Maculewicz, "Cytotoxicity of dendrimers," *Biomolecules*, vol. 9, no. 8, p. 330, 2019.

[32] J. Li, S. Li, S. Xia, J. Feng, X. Zhang, Y. Hao, L. Chen, and X. Zhang, "Enhanced transfection efficiency and targeted delivery of self-assembling h-r3-dendriplexes in egfr-overexpressing tumor cells," *oncotarget*, vol. 6, no. 28, p. 26177, 2015.

[33] D. Rajasekaran, J. Srivastava, K. Ebeid, R. Gredler, M. Akiel, N. Jariwala, C. L. Robertson, X.-N. Shen, A. Siddiq, P. B. Fisher *et al.*, "Combination of nanoparticle-delivered sirna for astrocyte elevated gene-1 (aeg-1) and all-trans retinoic acid (atra): an effective therapeutic strategy for hepatocellular carcinoma (hcc)," *Bioconjugate chemistry*, vol. 26, no. 8, pp. 1651–1661, 2015.

[34] J. Li, H. Liang, J. Liu, and Z. Wang, "Poly (amidoamine)(pamam) dendrimer mediated delivery of drug and pdna/sirna for cancer therapy," *International journal of pharmaceutics*, vol. 546, no. 1-2, pp. 215–225, 2018.

[35] M. Sjoberg, M. Mapar, A. Armanious, V. P. Zhdanov, B. Agnarsson, and F. Hook, "Time-resolved and label-free evanescent light-scattering microscopy for mass quantification of protein binding to single lipid vesicles," *Nano Letters*, vol. 21, no. 11, pp. 4622–4628, 2021.

[36] C. J. M. Rivas, M. Tarhini, W. Badri, K. Miladi, H. Greige-Gerges, Q. A. Nazari, S. A. G. Rodríguez, R. Á. Román, H. Fessi, and A. Elaissari, "Nanoprecipitation process: From encapsulation to drug delivery," *International journal of pharmaceutics*, vol. 532, no. 1, pp. 66–81, 2017.

[37] W. Huang and C. Zhang, "Tuning the size of poly (lactic-co-glycolic acid)(plga) nanoparticles fabricated by nanoprecipitation," *Biotechnology journal*, vol. 13, no. 1, p. 1700203, 2018.

[38] K. Y. Hernández-Giottonini, R. J. Rodríguez-Córdova, C. A. Gutiérrez-Valenzuela, O. Peñuñuri-Miranda, P. Zavala-Rivera, P. Guerrero-Germán, and A. Lucero-Acuña, "Plga nanoparticle preparations by emulsification and nanoprecipitation techniques: Effects of formulation parameters," *Rsc Advances*, vol. 10, no. 8, pp. 4218–4231, 2020.

[39] R. M. Mainardes and R. C. Evangelista, "Plga nanoparticles containing praziquantel: effect of formulation variables on size distribution," *International journal of pharmaceutics*, vol. 290, no. 1-2, pp. 137–144, 2005.

[40] S. C. Lee, J. T. Oh, M. H. Jang, and S. I. Chung, "Quantitative analysis of polyvinyl alcohol on the surface of poly (d, l-lactide-co-glycolide) microparticles prepared by solvent evaporation method: effect of particle size and pva concentration," *Journal of Controlled Release*, vol. 59, no. 2, pp. 123–132, 1999.

[41] X. Song, Y. Zhao, W. Wu, Y. Bi, Z. Cai, Q. Chen, Y. Li, and S. Hou, "Plga nanoparticles simultaneously loaded

with vincristine sulfate and verapamil hydrochloride: systematic study of particle size and drug entrapment efficiency," *International journal of pharmaceutics*, vol. 350, no. 1-2, pp. 320–329, 2008.

[42] M. F. Zambaux, F. Bonneaux, R. Gref, P. Maincent, E. Dellacherie, M. Alonso, P. Labrude, and C. Vigneron, "Influence of experimental parameters on the characteristics of poly (lactic acid) nanoparticles prepared by a double emulsion method," *Journal of controlled release*, vol. 50, no. 1-3, pp. 31–40, 1998.

[43] A. Lamprecht, N. Ubrich, M. H. Pérez, C.-M. Lehr, M. Hoffman, and P. Maincent, "Influences of process parameters on nanoparticle preparation performed by a double emulsion pressure homogenization technique," *International journal of pharmaceutics*, vol. 196, no. 2, pp. 177–182, 2000.

[44] M. Iqbal, N. Zafar, H. Fessi, and A. Elaissari, "Double emulsion solvent evaporation techniques used for drug encapsulation," *International journal of pharmaceutics*, vol. 496, no. 2, pp. 173–190, 2015.

[45] N. L. Anderson and N. G. Anderson, "The human plasma proteome: history, character, and diagnostic prospects," *Molecular & cellular proteomics*, vol. 1, no. 11, pp. 845–867, 2002.

[46] T. Cedervall, I. Lynch, M. Foy, T. Berggård, S. C. Donnelly, G. Cagney, S. Linse, and K. A. Dawson, "Detailed identification of plasma proteins adsorbed on copolymer nanoparticles," *Angewandte Chemie International Edition*, vol. 46, no. 30, pp. 5754–5756, 2007.

[47] M. P. Monopoli, D. Walczyk, A. Campbell, G. Elia, I. Lynch, F. Baldelli Bombelli, and K. A. Dawson, "Physical- chemical aspects of protein corona: relevance to in vitro and in vivo biological impacts of nanoparticles," *Journal of the American Chemical Society*, vol. 133, no. 8, pp. 2525–2534, 2011.

[48] F. Pederzoli, G. Tosi, M. A. Vandelli, D. Belletti, F. Forni, and B. Ruozi, "Protein corona and nanoparticles: how can we investigate on?" *Wiley Interdisciplinary Reviews: Nanomedicine and Nanobiotechnology*, vol. 9, no. 6, p. e1467, 2017.

[49] P. Del Pino, B. Pelaz, Q. Zhang, P. Maffre, G. U. Nienhaus, and W. J. Parak, "Protein corona formation around nanoparticles–from the past to the future," *Materials Horizons*, vol. 1, no. 3, pp. 301–313, 2014.

[50] S. Bhattacharjee, "Dls and zeta potential–what they are and what they are not?" *Journal of controlled release*, vol. 235, pp. 337–351, 2016.

[51] C. Berthomieu and R. Hienerwadel, "Fourier transform infrared (ftir) spectroscopy," *Photosynthesis research*, vol. 101, pp. 157–170, 2009.

[52] K. Lundquist, "Proton (1h) nmr spectroscopy," in *Methods in lignin chemistry*. Springer, 1992, pp. 242–249.

[53] M. Picollo, M. Aceto, and T. Vitorino, "Uv-vis spectroscopy," *Physical sciences reviews*, vol. 4, no. 4, p. 20180008, 2019.

[54] D. Zhao, J.-Q. Xu, X.-Q. Yi, Q. Zhang, S.-X. Cheng, R.-X. Zhuo, and F. Li, "ph-activated targeting drug delivery system based on the selective binding of phenylboronic acid," *ACS applied materials & interfaces*, vol. 8, no. 23, pp. 14 845–14 854, 2016.

[55] S. Bai and F. Ahsan, "Synthesis and evaluation of pegylated dendrimeric nanocarrier for pulmonary delivery of low molecular weight heparin," *Pharmaceutical research*, vol. 26, pp. 539–548, 2009.

[56] R. U. Khan, H. Yu, L. Wang, Q. Zhang, W. Xiong, A. Nazir, S. Fahad, X. Chen, and T. Elsharaarani, "Synthesis of polyorganophosphazenes and preparation of their polymersomes for reductive/acidic dual-responsive anticancer drugs release," *Journal of materials science*, vol. 55, no. 19, pp. 8264–8284, 2020.

[57] H. M. Dao, A. R. Pillai, R. Thakkar, S. Parajuli, E. Urena-Benavides, and S. Jo, "Near infrared light-induced disassembly of polymeric micelles based on methylene blue conjugated polyethylene glycol," *Journal of Applied Polymer Science*, vol. 138, no. 2, p. 49665, 2021.

[58] M. N. Ho, L. G. Bach, T. H. Nguyen, M. H. Ho, D. H. Nguyen, C. K. Nguyen, C. H. Nguyen, N. V. Nguyen, and T. T. Hoang Thi, "Pegylated poly (amidoamine) dendrimers-based drug loading vehicles for delivering carboplatin in treatment of various cancerous cells," *Journal of Nanoparticle Research*, vol. 21, pp. 1–12, 2019.

[59] R. Zoqlam, C. J. Morris, M. Akbar, A. M. Alkilany, S. I. Hamdallah, P. Belton, and S. Qi, "Evaluation of the benefits of microfluidic-assisted preparation of polymeric nanoparticles for dna delivery," *Materials Science and Engineering: C*, vol. 127, p. 112243, 2021.

[60] C. Malburet, A. Carboni, S. Guinamand, H. Naik, and S. Fertier-Prizzon, "mrna extraction from lipid nanoparticles," *Journal of Chromatography A*, vol. 1714, p. 464545, 2024.

[61] C. V. Rocha, V. Gonçalves, M. C. da Silva, M. Bañobre-López, and J. Gallo, "Plga-based composites for various biomedical applications," *International Journal of Molecular Sciences*, vol. 23, no. 4, p. 2034, 2022.

[62] M. S. Ehrenberg, A. E. Friedman, J. N. Finkelstein, G. Oberdörster, and J. L. McGrath, "The influence of protein adsorption on nanoparticle association with cultured endothelial cells," *Biomaterials*, vol. 30, no. 4, pp. 603–610, 2009.

[63] M. Mahmoudi, I. Lynch, M. R. Ejtehadi, M. P. Monopoli, F. B. Bombelli, and S. Laurent, "Protein- nanoparticle interactions: opportunities and challenges," *Chemical reviews*, vol. 111, no. 9, pp. 5610–5637, 2011.

[64] A. Kathiravan, R. Renganathan, and S. Anandan, "Interaction of colloidal agtio2 nanoparticles with bovine serum albumin," *Polyhedron*, vol. 28, no. 1, pp. 157–161, 2009.

[65] U. Chheda, S. Pradeepan, E. Esposito, S. Strezsak, O. Fernandez-Delgado, and J. Kranz, "Factors affecting stability of rna–temperature, length, concentration, ph, and buffering species," *Journal of Pharmaceutical Sciences*, vol. 113, no. 2, pp. 377–385, 2024.

[66] T. López-Royo, V. Sebastián, L. Moreno-Martínez, L. Uson, C. Yus, T. Alejo, P. Zaragoza, R. Osta, M. Arruebo, and R. Manzano, "Encapsulation of large-size plasmids in plga nanoparticles for gene editing: comparison of three different synthesis methods," *Nanomaterials*, vol. 11, no. 10, p. 2723, 2021.

[67] P. Pantazis, K. Dimas, J. H. Wyche, S. Anant, C. W. Houchen, J. Panyam, and R. P. Ramanujam, "Preparation of sirna-encapsulated plga nanoparticles for sustained release of sirna and evaluation of encapsulation efficiency," *Nanoparticles in Biology and Medicine: Methods and Protocols*, pp. 311–319, 2012.

[68] Z. Sharifnia, M. Bandehpour, H. Hamishehkar, N. Mosaffa, B. Kazemi, and N. Zarghami, "In-vitro transcribed mrna delivery using plga/pei nanoparticles into human monocyte-derived dendritic cells," *Iranian Journal of Pharmaceutical Research: IJPR*, vol. 18, no. 4, p. 1659, 2019.

[69] D. Cun, D. K. Jensen, M. J. Maltesen, M. Bunker, P. Whiteside, D. Scurr, C. Foged, and H. M. Nielsen, "High loading efficiency and sustained release of sirna encapsulated in plga nanoparticles: quality by design optimization and characterization," *European journal of pharmaceutics and biopharmaceutics*, vol. 77, no. 1, pp. 26–35, 2011.

[70] S. N. Oyaghire, E. Quijano, A. S. Piotrowski-Daspit, W. M. Saltzman, and P. M. Glazer, "Poly (lactic-co-glycolic acid) nanoparticle delivery of peptide nucleic acids in vivo," *Peptide Nucleic Acids: Methods and Protocols*, pp. 261–281, 2020.

[71] H. Van de Ven, M. Vermeersch, A. Matheeussen, J. Vandervoort, W. Weyenberg, S. Apers, P. Cos, L. Maes, and A. Ludwig, "Plga nanoparticles loaded with the antileishmanial saponin $\beta$-aescin: Factor influence study and in vitro efficacy evaluation," *International journal of pharmaceutics*, vol. 420, no. 1, pp. 122–132, 2011.

[72] A. Plugatyr and I. M. Svishchev, "Molecular diffusivity of phenol in sub-and supercritical water: application of the split-flow taylor dispersion technique," *The Journal of Physical Chemistry B*, vol. 115, no. 11, pp. 2555–2562, 2011.

[73] D. Buzatu, F. D. Buzatu, L. Paduano, and R. Sartorio, "Diffusion coefficients for the ternary system water+ chloroform+ acetic acid at 25° c," *Journal of solution chemistry*, vol. 36, pp. 1373–1384, 2007.

[74] M. Tan, Y. Feng, H. Wang, L. Zhang, M. Khan, J. Guo, Q. Chen, and J. Liu, "Immobilized bioactive agents onto polyurethane surface with heparin and phosphorylcholine group," *Macromolecular Research*, vol. 21, pp. 541–549, 2013.

[75] D. Rio, "Denaturation and electrophoresis of rna with formaldehyde. cold spring harb protoc 2015: 219–222," 2015.

[76] F. H. Mansour and D. G. Pestov, "Separation of long rna by agarose–formaldehyde gel electrophoresis," *Analytical biochemistry*, vol. 441, no. 1, pp. 18–20, 2013.

[77] R. E. McKenzie, J. J. Minnell, M. Ganley, G. F. Painter, and S. L. Draper, "mrna synthesis and encapsulation in ionizable lipid nanoparticles," *Current Protocols*, vol. 3, no. 9, p. e898, 2023.

[78] Berényi, S., Mihály, J., Wacha, A., Tőke, O., & Bóta, A. (2014). A mechanistic view of lipid membrane disrupting effect of PAMAM dendrimers. Colloids and Surfaces B: Biointerfaces, 118, 164-171.

[79] Vasudevan, A., Jozić, A., Curtis, A. G., Bodi, E., Ryals, R. C., & Sahay, G. (2025). Lipid nanoparticle-mediated intracameral mRNA delivery facilitates gene expression and editing in the anterior chamber of the eye. Journal of Controlled Release, 379, 1022-1028.

[80] Patel, S., Ryals, R. C., Weller, K. K., Pennesi, M. E., & Sahay, G. (2019). Lipid nanoparticles for delivery of messenger RNA to the back of the eye. Journal of Controlled Release, 303, 91-100.

[81] Ryals, R. C., Patel, S., Acosta, C., McKinney, M., Pennesi, M. E., & Sahay, G. (2020). The effects of PEGylation on LNP based mRNA delivery to the eye. Plos one, 15(10), e0241006.

[82] Gautam, M., Jozic, A., Su, G. L. N., Herrera-Barrera, M., Curtis, A., Arrizabalaga, S., ... & Sahay, G. (2023). Lipid nanoparticles with PEG-variant surface modifications mediate genome editing in the mouse retina. Nature communications, 14(1), 6468.

[83] Ghosh, A., & Lima, C. D. (2010). Enzymology of RNA cap synthesis. Wiley Interdisciplinary Reviews: RNA, 1(1), 152-172.

[84] Oster, C. G., Wittmar, M., Bakowsky, U., & Kissel, T. (2006). DNA nano-carriers from biodegradable cationic branched polyesters are formed by a modified solvent displacement method. Journal of controlled release, 111(3), 371-381.

[85] Benfer, M., & Kissel, T. (2012). Cellular uptake mechanism and knockdown activity of siRNA-loaded biodegradable DEAPA-PVA-g-PLGA nanoparticles. European Journal of Pharmaceutics and Biopharmaceutics, 80(2), 247-256.

[86] Jo, A., Ringel-Scaia, V. M., McDaniel, D. K., Thomas, C. A., Zhang, R., Riffle, J. S., ... & Davis, R. M. (2020). Fabrication and characterization of PLGA nanoparticles encapsulating large CRISPR–Cas9 plasmid. Journal of nanobiotechnology, 18, 1-14.

# A

# Appendix 1

**(Some extra figures and results not shown in the thesis)**

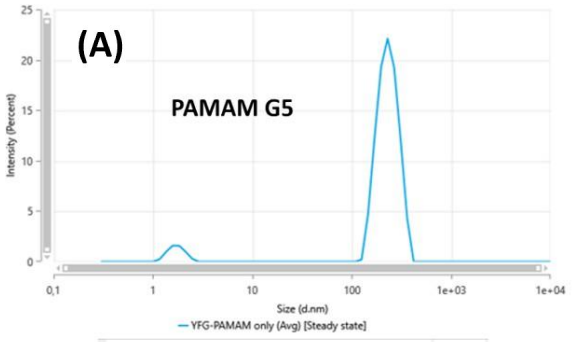


| Name | Mean |
|---|---|
| Z-Average (nm) | 362,7 |
| Polydispersity Index (PI) | 0,3469 |
| Peak 1 Mean by Intensity ordered by area (nm) | 234,9 |
| Peak 1 Area by Intensity ordered by area (%) | 94,32 |
| Peak 2 Mean by Intensity ordered by area (nm) | 1,734 |
| Peak 2 Area by Intensity ordered by area (%) | 5,681 |

**Zeta: +14 mV**

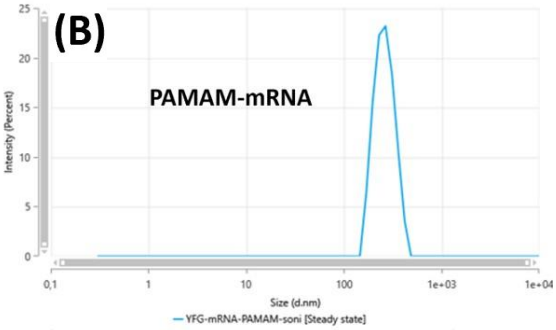


| Name | Mean |
|---|---|
| Z-Average (nm) | 247 |
| Polydispersity Index (PI) | 0,1165 |
| Peak 1 Mean by Intensity ordered by area (nm) | 265,2 |
| Peak 1 Area by Intensity ordered by area (%) | 100 |

**Zeta: +7 mV**

**Figure A.1:** Size, PDI and zeta potential change of 1.0 mg/mL PAMAM in citrate buffer pH 6 before and after incubation with 300 $\mu$g/mL Poly-A

Figure A.1 reveals the size and surface charge change of 1.0 mg/mL PAMAM before and after incubation with Poly-A. Because of the high concentration, PAMAM formed aggregation before mRNA condensation (Panel A). But by adding Poly-A RNA, the size and zeta potential were reduced from 362 nm and +14 mV to 247 nm and +7 mV respectively, indicating successful mRNA condensation. However, due to the large size of mRNA/PAMAM obtained, incubation method was not adopted for following experiments in this project.

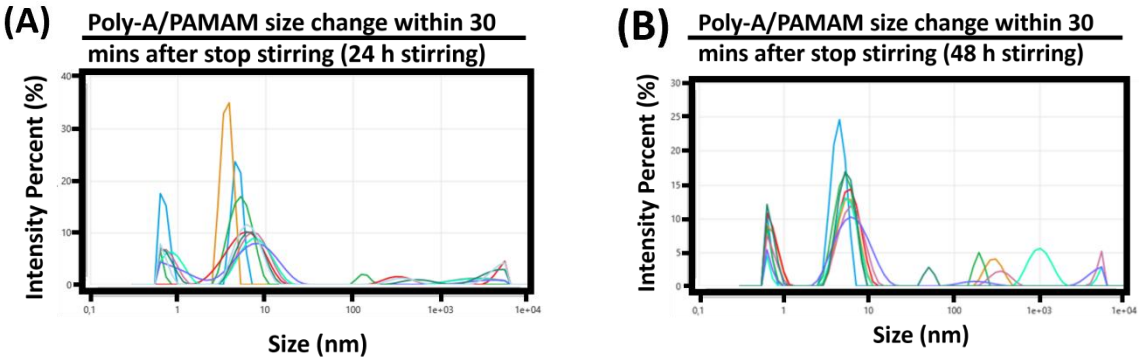


**Figure A.2:** Poly-A-PAMAM size change within 30 mins after stop stirring (a) 24 h stirring; (b) 48 h stirring

Figure A.2 reveals the Poly-A loaded PAMAM size change in 30 min after stirring was stopped. Both of the sample (24 h stirring sample and 48 h stirring sample) exhibited similar tendency that the particle size slightly increased and small amount of aggregation formed. This is consistent to the hypothesis that explained mRNA/PAMAM size change during stirring -- the particle kept small size during stirring, but they collided and formed aggregation when stirring was stopped.

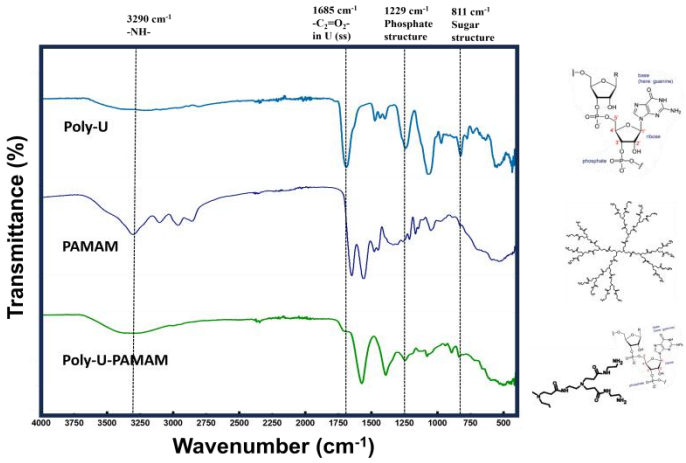


**Figure A.3:** FTIR for Poly-U-PAMAM

Figure A.3 reveals the FTIR spectra of Poly-U RNA, PAMAM and Poly-U loaded PAMAM. Poly-U loaded PAMAM was synthesized at the same time with first batch of stirring formed Poly-A loaded PAMAM, for comparison. Similar to Poly-A loaded PAMAM, the shifted amide groups' peaks and RNA peaks were observed in Poly-U/PAMAM spectra, indicating successful condensation of Poly-U, further proving the applicability of stirring method in mRNA/PAMAM formulation.

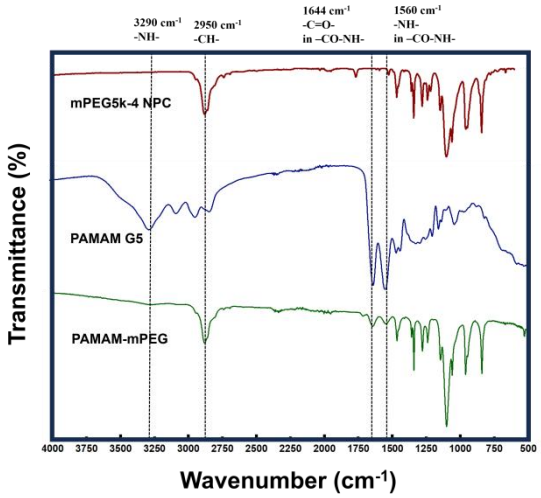


**Figure A.4:** FTIR for PAMAM-mPEG

Figure A.4 reveals the FTIR spectra of PAMAM-mPEG. To reduce the size and aggregation of PAMAM, PAMAM PEGylation was explored. mPEG-4 NPC was added according to the molar quantity of primary amine group in PAMAM, aiming to cover half amount of amine groups. From the FTIR spectra, PAMAM was successfully PEGylated. However, over-PEGylation lead to large particle size and gel-like structure. PEGylated PAMAM was not used in the project, but it provided an idea about reducing the size of PAMAM and further mRNA/PAMAM. Future research can adjust the PAMAM PEGylation by changing the molar ratio of mPEG and PAMAM.

**DEPARTMENT OF CHEMICAL BIOLOGY**
**CHALMERS UNIVERSITY OF TECHNOLOGY**
Gothenburg, Sweden
www.chalmers.se


CHALMERS
UNIVERSITY OF TECHNOLOGY